

SHORT COMMUNICATION

Characterization of contiguous gene deletions in *COL4A6* and *COL4A5* in Alport syndrome-diffuse leiomyomatosis

Kandai Nozu¹, Shogo Minamikawa¹, Shiro Yamada^{2,3}, Masafumi Oka¹, Motoko Yanagita⁴, Naoya Morisada¹, Shuichiro Fujinaga⁵, China Nagano⁶, Yoshimitsu Gotoh⁶, Eihiko Takahashi⁷, Takahiro Morishita⁸, Tomohiko Yamamura¹, Takeshi Ninchoji¹, Hiroshi Kaito¹, Ichiro Morioka¹, Koichi Nakanishi⁹, Igor Vorechovsky¹⁰ and Kazumoto Iijima¹

Alport syndrome-diffuse leiomyomatosis (AS-DL, OMIM: 308940) is a rare variant of the X-linked Alport syndrome that shows overgrowth of visceral smooth muscles in the gastrointestinal, respiratory and female reproductive tracts in addition to renal symptoms. AS-DL results from deletions that encompass the 5' ends of the *COL4A5* and *COL4A6* genes, but deletion breakpoints between *COL4A5* and *COL4A6* have been determined in only four cases. Here, we characterize deletion breakpoints in five AS-DL patients and show a contiguous *COL4A6/COL4A5* deletion in each case. We also demonstrate that eight out of nine deletion alleles involved sequences homologous between *COL4A5* and *COL4A6*. Most breakpoints took place in recognizable transposed elements, including long and short interspersed repeats, DNA transposons and long-terminal repeat retrotransposons. Because deletions involved the bidirectional promoter region in each case, we suggest that the occurrence of leiomyomatosis in AS-DL requires inactivation of both genes. Altogether, our study highlights the importance of homologous recombination involving multiple transposed elements for the development of this continuous gene syndrome and other atypical loss-of-function phenotypes.

Journal of Human Genetics advance online publication, 9 March 2017; doi:10.1038/jhg.2017.28

INTRODUCTION

Alport syndrome (AS) is the most common hereditary nephropathy, characterized by a progressive renal failure, sensorineural deafness and ocular abnormalities. The most common X-linked form of this disease (XLAS, OMIM: 301050) results from mutations in the *COL4A5* gene, which encodes the $\alpha 5$ chain of type IV collagen.¹ Alport syndrome-diffuse leiomyomatosis (AS-DL, OMIM: 308940) occurs as a rare variant of XLAS that shows overgrowth of visceral smooth muscles in the gastrointestinal, respiratory and female reproductive tracts, in addition to renal symptoms.^{1–3} *COL4A5* is located on the long arm of the X chromosome (Xq22) and is head-to-head with the *COL4A6* gene. The *COL4A6* gene encodes the $\alpha 6$ chain of type IV collagen, which is mainly expressed in heart, human esophagus, aorta and bladder smooth muscle basement membrane.^{3–5}

AS-DL patients exhibit contiguous gene deletions at the *COL4A5–COL4A6* locus.⁵ Sixteen AS-DL patients reported so far have been found to have a deletion that encompassed the 5' end of the *COL4A5*

and *COL4A6* genes, and included the bidirectional promoter (the Human Genome Mutation Database). The *COL4A6* deletion breakpoints have been consistently found within intron 2, whereas the *COL4A5* breakpoints usually occur in intron 1.⁶ However, the breakpoints were characterized at a single-nucleotide level only in four cases.^{6–9}

PATIENTS AND METHODS

In our laboratory, we conduct a comprehensive molecular diagnostics of inherited kidney diseases, including AS. So far, 415 suspected AS patients underwent molecular genetic tests, five of them with clinical signs of leiomyomatosis. The pedigrees of the five cases are shown in Supplementary Figure 1.

Genomic DNA was isolated from peripheral blood leukocytes. Screening of contiguous gene deletions was performed with the multiplex ligation probe amplification (MLPA) using the SALSA P191/192 Alport MLPA assay (MRC-Holland, Amsterdam, the Netherlands).^{2,10,11} Long-range PCR amplification and direct sequencing of *COL4A5* and *COL4A6* was

¹Department of Pediatrics, Kobe University Graduate School of Medicine, Kobe, Japan; ²Department of Pediatrics, Tokai University Oiso Hospital, Kanagawa, Japan; ³Division of Human Genetics, National Institute of Genetics, Mishima, Japan; ⁴Department of Nephrology, Kyoto University, Kyoto, Japan; ⁵Division of Nephrology, Saitama Children's Medical Center, Saitama City, Saitama, Japan; ⁶Department of Pediatric Nephrology, Japanese Red Cross Nagoya Daini Hospital, Nagoya, Japan; ⁷Department of Nephrology, Kanagawa Children's Medical Center, Yokohama, Japan; ⁸Department of Pediatrics, University of Occupational and Environmental Health, Fukuoka, Japan; ⁹Department of Pediatrics, Wakayama Medical University, Wakayama, Japan and ¹⁰University of Southampton Faculty of Medicine, Southampton, UK
Correspondence: Dr K Nozu, Department of Pediatrics, Kobe University Graduate School of Medicine, 7-5-1 Kusunoki-cho, Chuo, Kobe, Hyogo 6500017, Japan.
E-mail: nozu@med.kobe-u.ac.jp

Received 6 January 2017; revised 31 January 2017; accepted 31 January 2017

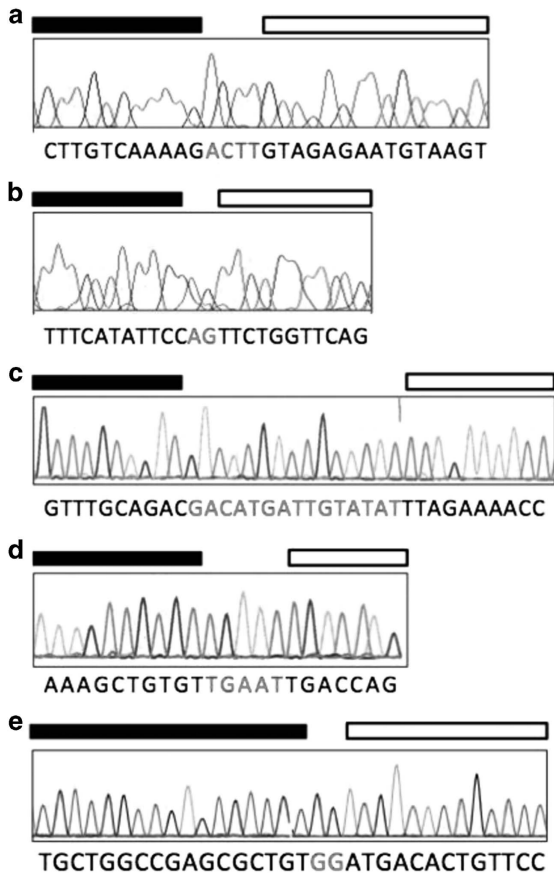


Figure 1 Sequence chromatograms of contiguous gene deletion breakpoints in five AS-DL cases. (a) Case 1 (c.66+5840 of *COL4A6* and c.81+8068 of *COL4A5*). (b) Case 2 (c.66+25107 of *COL4A6* and c.81+18040 of *COL4A5*). (c) Case 3 (c.66+85676 of *COL4A6* and c.276+3257 of *COL4A5*). (d) Case 4 (c.66+119476 of *COL4A6* and c.3246+6706 of *COL4A5*). (e) Case 5 (c.66+84055 of *COL4A6* and c.3246+66915 of *COL4A5*). *COL4A6* and *COL4A5* sequences are shown as black and open rectangles, respectively. Homologous sequence in each case is shown in red. A full color version of this figure is available at the *Journal of Human Genetics* journal online.

conducted to characterize the deletion breakpoints. The human reference sequence of NG_011977.1 and NG_012059.2 for *COL4A5* and *COL4A6* was used, respectively.

To detect a large heterozygous deletion in Case 2, we conducted a semi-quantitative PCR amplification using capillary electrophoresis.^{12,13}

RESULTS

The MLPA analysis of five patients with AS-DL revealed hetero- or hemizygous deletions in each case (Supplementary Figure 2). This analysis was followed by long-range PCRs and direct sequencing to identify each breakpoint (Figures 1a–e, Supplementary Figure 3 and Supplementary Data 1). For a female patient (Case 2, Supplementary Figure 2B), we also conducted a semi-quantitative PCR assay (Supplementary Figure 4).

Deletions are schematically shown in Supplementary Figure 3.^{6–9} To examine the genomic context of deletion breakpoints, we analyzed their flanking sequences using RepeatMasker (Figure 2). Their alignments with Refbase entries¹⁵ revealed the presence of transposed elements (TEs) in 13/18 (72%) breakpoints in nine cases (Figure 2). Cases p2 and p3 showed *COL4A5*-side breakpoints at different positions within the same long interspersed element, family L1. Similarly, Cases c3 and p2 exhibited *COL4A6*-side breakpoints at

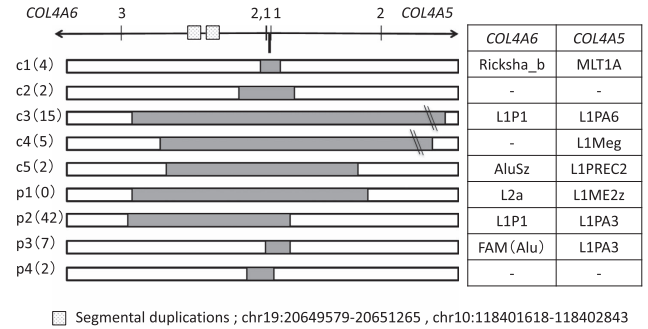


Figure 2 Schematics of novel and previously reported deletions Location of both sides of the breakpoints in the in *COL4A5* and *COL4A6*. Deletions are shown as dark rectangles. Transposable elements in centromeric (*COL4A6*) and telomeric (*COL4A5*) breakpoints are shown to the right. The segmental duplication in intron 2 is marked as a vertical rectangle at the top of the figure. Exons are numbered at the top. c1–c5, our case 1–5, p1 (ref. 4), p2 (ref. 14), p3 (ref. 15), p4 (ref. 13). The number of homologous nucleotides (Figure 1 and Supplementary Data 1) is shown in parentheses.

different positions in the same L1 copy. Homologous sequences at the recombination breakpoints were apparent in eight of nine patients. The length of overlapping sequences varied from 2 to 42 bp (Supplementary Data 1). No breakpoints were located in the annotated duplicated segment (UCSC genome browser) of *COL4A6* intron 2 (Figure 2).

MLPA analysis of maternal samples of Cases 1, 3 and 4 failed to detect any deletion, suggesting that, unlike Cases 2 and 5, these are sporadic cases.

DISCUSSION

This work has more than doubled the number of sequence-characterized *COL4A5* and *COL4A6* breakpoints in AS-DL. Although eight out of nine cases had homologous sequences at the deletion breakpoints, only two cases (c3 and p2) showed relatively long homologous sequences in the L1 family of long interspersed elements, consistent with a well-known L1-mediated recombination mechanism.¹⁶ Almost a half of the human genome is occupied by recognizable TEs, with L1 occupying ~17%.¹⁷ TEs have been shown to provide a source of new exons, genes and regulatory sequences, dramatically influencing evolutionary history, exon–intron structure, speciation and regulation of gene expression. TEs facilitate non-allelic homologous recombination events leading to inherited diseases,¹⁴ including AS-DL (Figure 2).⁸ As compared to c3 and p2, Cases c1, c4, c5, p1 and p3 revealed shorter homologous sequences indicative of the same mechanism. The number of breakpoints in TEs 13/18 (72%) appears to be higher than expected since TEs represent only 40% and 62% of the genomic sequences of *COL4A6* and *COL4A5*, respectively suggesting that TEs might have some roles for causing recombination in this disease.

All deletion breakpoints characterized at the single-nucleotide level in *COL4A6* took place in intron 2.^{6–9} Recently, an AS-DL case was identified with a deletion extending into *COL4A6* beyond this intron,² but the precise breakpoint was not characterized. On the *COL4A5* side, the deletion breakpoint usually maps to intron 1; however, some cases, including two of ours (c3 and c4), showed breakpoints in intron 36 and intron 4, respectively. Recently, Sa *et al.* reported an AS-DL case with a *COL4A5*-only gene deletion, which encompassed exons 1–51 but did not include the common promoter region or exon 1 of *COL4A6*.¹⁸ This report may still be compatible with the requirement for inactivation of both genes in AS-DL, as first proposed by

Zhou *et al.*,⁵ because the authors did not analyze *COL4A6* expression nor did they exclude inactivation of this gene by other mechanisms. Recent studies in yeasts revealed that deletion of many genes were associated with altered mRNA levels of the neighboring genes.¹⁹ These studies are particularly relevant for bidirectional promoters which generate products of two adjacent, often related genes in stoichiometric quantities, ensuring their co-expression in the same or similar biological pathway.

In conclusion, we have more than doubled the number of large contiguous deletions in AS-DL characterized at the single-nucleotide level. Our results show that most deletions were mediated by transposons via homologous recombination events and support the original proposal⁵ that inactivation of both genes is required for the development of leiomyomas in AS-DL.

CONFLICT OF INTEREST

The authors declare no conflict of interest.

ACKNOWLEDGEMENTS

The authors gratefully acknowledge the cooperation of the patients and physicians. This study was supported by a grant from the Ministry of Health, Labour and Welfare of Japan for Research on Rare Intractable Diseases in Kidney and Urinary Tract (H24-nanchitou (nan)-ippan-041 to Kazumoto Iijima) in the 'Research on Measures for Intractable Diseases' Project; a Grant-in-Aid for Scientific Research (KAKENHI) from the Ministry of Education, Culture, Sports, Science and Technology of Japan (Subject ID: 16K19642 to Tomohiko Yamamura, 25893131 to Kandai Nozu and 26293203 to Kazumoto Iijima).

- 1 Kashtan, C. E. Alport syndrome and thin glomerular basement membrane disease. *J. Am. Soc. Nephrol.* **9**, 1736–1750 (1998).
- 2 Uliana, V., Marcocci, E., Mucciolo, M., Meloni, I., Izzi, C., Manno, C. *et al.* Alport syndrome and leiomyomatosis: the first deletion extending beyond COL4A6 intron 2. *Pediatr. Nephrol.* **26**, 717–724 (2011).
- 3 Van Loo, A., Vanholder, R., Buytaert, I., De Paepe, A., Praet, M., Elewaut, A. *et al.* Alport syndrome and diffuse leiomyomatosis with major morbid events presenting at adult age. *Nephrol. Dial. Transplant.* **12**, 776–780 (1997).

- 4 Heidert, L., Cai, Y., Sado, Y., Ninomiya, Y., Thorner, P., Guicharnaud, L. *et al.* Diffuse leiomyomatosis associated with X-linked Alport syndrome: extracellular matrix study using immunohistochemistry and in situ hybridization. *Lab. Invest.* **76**, 233–243 (1997).
- 5 Zhou, J., Mochizuki, T., Smeets, H., Antignac, C., Laurila, P. de Paepe, A. *et al.* Deletion of the paired alpha 5(IV) and alpha 6(IV) collagen genes in inherited smooth muscle tumors. *Science* **261**, 1167–1169 (1993).
- 6 Oohashi, T., Naito, I., Ueki, Y., Yamatsuji, T., Permpoon, R., Tanaka, N. *et al.* Clonal overgrowth of esophageal smooth muscle cells in diffuse leiomyomatosis-Alport syndrome caused by partial deletion in COL4A5 and COL4A6 genes. *Matrix Biol.* **30**, 3–8 (2011).
- 7 Thielen, B. K., Barker, D. F., Nelson, R. D., Zhou, J., Kren, S. M. & Segal, Y. Deletion mapping in Alport syndrome and Alport syndrome-diffuse leiomyomatosis reveals potential mechanisms of visceral smooth muscle overgrowth. *Hum. Mutat.* **22**, 419 (2003).
- 8 Segal, Y., Peissel, B., Renieri, A., de Marchi, M., Ballabio, A., Pei, Y. *et al.* LINE-1 elements at the sites of molecular rearrangements in Alport syndrome-diffuse leiomyomatosis. *Am. J. Hum. Genet.* **64**, 62–69 (1999).
- 9 Ueki, Y., Naito, I., Oohashi, T., Sugimoto, M., Seki, T., Yoshioka, H. *et al.* Topoisomerase I and II consensus sequences in a 17-kb deletion junction of the COL4A5 and COL4A6 genes and immunohistochemical analysis of esophageal leiomyomatosis associated with Alport syndrome. *Am. J. Hum. Genet.* **62**, 253–261 (1998).
- 10 Nozu, K., Krol, R. P., Nakanishi, K., Yoshikawa, N., Nozu, Y., Ohtsuka, Y. *et al.* Detection by multiplex ligation-dependent probe amplification of large deletion mutations in the COL4A5 gene in female patients with Alport syndrome. *Pediatr. Nephrol.* **24**, 1773–1774 (2009).
- 11 Hertz, J. M., Juncker, I. & Marcussen, N. MLPA and cDNA analysis improves COL4A5 mutation detection in X-linked Alport syndrome. *Clin. Genet.* **74**, 522–530 (2008).
- 12 Nozu, K., Przybyslaw Krol, R., Ohtsuka, Y., Nakanishi, K., Yoshikawa, N., Nozu, Y. *et al.* Detection of large deletion mutations in the COL4A5 gene of female Alport syndrome patients. *Pediatr. Nephrol.* **23**, 2085–2090 (2008).
- 13 Nozu, K., Fu, X. J., Nakanishi, K., Yoshikawa, N., Kaito, H., Kanda, K. *et al.* Molecular analysis of patients with type III Bartter syndrome: picking up large heterozygous deletions with semiquantitative PCR. *Pediatr. Res.* **62**, 364–369 (2007).
- 14 Belancio, V. P., Hedges, D. J. & Deininger, P. Mammalian non-LTR retrotransposons: for better or worse, in sickness and in health. *Genome Res.* **18**, 343–358 (2008).
- 15 Tempel, S., Jurka, M. & Jurka, J. VisualRebase: an interface for the study of occurrences of transposable element families. *BMC Bioinformatics* **9**, 345 (2008).
- 16 Gilbert, N., Lutz-Prigge, S. & Moran, J. V. Genomic deletions created upon LINE-1 retrotransposition. *Cell* **110**, 315–325 (2002).
- 17 Lander, E. S., Linton, L. M., Birren, B., Nussbaum, C., Zody, M. C., Baldwin, J. *et al.* Initial sequencing and analysis of the human genome. *Nature* **409**, 860–921 (2001).
- 18 Sa, M. J., Fieremans, N., de Brouwer, A. P., Sousa, R., e Costa, F. T., Brito, M. J. *et al.* Deletion of the 5'exons of COL4A6 is not needed for the development of diffuse leiomyomatosis in patients with Alport syndrome. *J. Med. Genet.* **50**, 745–753 (2013).
- 19 Ben-Shitrit, T., Yosef, N., Shemesh, K., Sharan, R., Ruppim, E. & Kupiec, M. Systematic identification of gene annotation errors in the widely used yeast mutation collections. *Nat. Methods* **9**, 373–378 (2012).

Supplementary Information accompanies the paper on Journal of Human Genetics website (<http://www.nature.com/jhg>)

Diagnostic strategy for inherited hypomagnesemia

Tomoko Horinouchi¹ · Kandai Nozu¹ · Naohiro Kamiyoshi¹ · Koichi Kamei² · Hiroko Togawa³ · Yuko Shima³ · Yoshimichi Urahama⁴ · Tomohiko Yamamura¹ · Shogo Minamikawa¹ · Keita Nakanishi¹ · Junya Fujimura¹ · Ichiro Morioka¹ · Takeshi Ninchoji¹ · Hiroshi Kaito¹ · Koichi Nakanishi³ · Kazumoto Iijima¹

Received: 15 December 2016 / Accepted: 16 February 2017
© Japanese Society of Nephrology 2017

Abstract

Background Hereditary hypomagnesemia is difficult to diagnose accurately because of its rarity and the variety of causative genes. We established a flowchart for identifying responsible genes for hypomagnesemia, and we confirmed its diagnostic efficacy in patients with suspected inherited hypomagnesemia.

Methods We established a flowchart and applied it to five index cases with suspected inherited hypomagnesemia. Direct sequence analysis was used to detect the causative gene variants in four cases, and targeted sequencing analysis using next-generation sequencing (NGS) of all causative genes for hypomagnesemia was used in one.

Results Expected pathogenic variants were detected in the *HNF1B*, *TRPM6*, *CLDN16*, *CASR*, or *SLC12A3* gene in all five cases. The results of all genetic analyses were consistent with the clinical diagnostic results using the flowchart.

Conclusions Accurate genetic diagnosis is crucial for estimating the prognosis, detecting complications in organs other than the kidneys, and for directing genetic counseling. The developed flowchart for identifying responsible genes for hypomagnesemia was useful for diagnosing inherited

hypomagnesemia. In addition, NGS analysis will help to resolve clinical difficulties in making an accurate diagnosis and thus improve the diagnostic strategy for inherited hypomagnesemia.

Keywords Hereditary hypomagnesemia · Diagnostic flowchart · Next-generation sequencing

Introduction

Magnesium (Mg^{2+}) is a cofactor for a group of enzymes and transporters, and it also plays an essential role in the synthesis of nucleic acids and proteins [1]. Hypomagnesemia is defined as a serum Mg^{2+} level <1.7 mg/dL (<0.7 mmol/L) [2]. Patients with hypomagnesemia suffer from nonspecific symptoms such as depression, tiredness, muscle spasms, or muscle weakness [1], while severe Mg^{2+} depletion (<0.4 mmol/L) may lead to cardiac arrhythmias, tetany, or seizures [1]. Hypomagnesemia can be caused by many triggers, including alcohol abuse, chronic diabetes, drugs, or eclamptic seizures [3], while genetic hypomagnesemia can be distinguished from Mg^{2+} deficiency arising from other causes [1]. However, the genetic causes of hypomagnesemia are also heterogeneous and comprise both recessive and dominant disorders (Table 1) [2].

Hereditary hypomagnesemia may be difficult to diagnose, because it is a relatively rare disorder and exhibits a variety of clinical presentations. We established a flowchart for identifying responsible genes for hypomagnesemia (Fig. 1) and demonstrated its efficacy in five index cases.

✉ Kandai Nozu
nozu@med.kobe-u.ac.jp

¹ Department of Pediatrics, Kobe University Graduate School of Medicine, 7-5-1 Kusunoki-cho, Chuo-ku, Kobe 6500017, Japan

² Division of Nephrology and Rheumatology, National Center for Child Health and Development, Tokyo, Japan

³ Department of Pediatrics, Wakayama Medical University, Wakayama, Japan

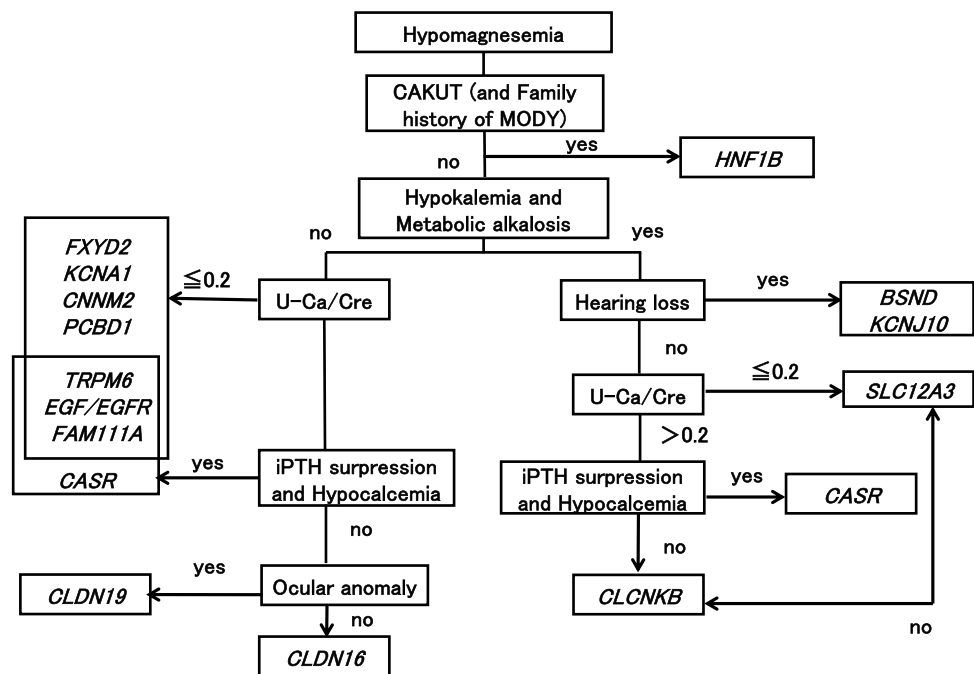
⁴ Department of Nephrology, Komaki City Hospital, Aichi, Japan

Table 1 Genetic causes of hypomagnesemia

| | Gene | Protein | Inheritance |
|---|----------------|--|-------------|
| Familial hypomagnesemia with hypercalciuria and nephrocalcinosis | <i>CLDN16</i> | Claudin-16 | AR |
| Familial Hypomagnesemia with hypercalciuria, nephrocalcinosis, and severe ocular involvement | <i>CLDN19</i> | Claudin-19 | AR |
| Autosomal dominant hypomagnesemia with hypocalciuria | <i>FXYP2</i> | γ -Subunit of the Na-K-ATPase | AD |
| Isolated recessive hypomagnesemia | <i>EGF</i> | pro-EGF | AR |
| Hypomagnesemia with secondary hypocalcemia | <i>TRPM6</i> | TRPM6 | AR |
| Autosomal dominant hypomagnesemia | <i>KCNA1</i> | Voltage gated K channel Kv1.1 | AD |
| Autosomal dominant hypomagnesemia | <i>CNNM2</i> | CNNM2 | AD |
| Autosomal dominant hypomagnesemia with CAKUT | <i>HNF1B</i> | Hepatocyte nuclear factor 1 homeobox B | AD |
| Gitelman syndrome | <i>SLC12A3</i> | NCCT | AR |
| Type3 Bartter syndrome | <i>CLCNKB</i> | ClC-Kb | AR |
| Type4 Bartter syndrome | <i>BSND</i> | Barttin | AR |
| Autosomal dominant hypocalcemia | <i>CASR</i> | Ca sensing receptor | AD |
| Epilepsy, ataxia, sensorineural deafness, and tubulopathy syndrome | <i>KCNJ10</i> | Kir4.1 | AR |
| Hyperphenylalaninemia and primapterinuria/renal cyst and diabetes-like neonatal inflammatory skin and bowel disease-2 | <i>PCBD1</i> | PCBD1 | AR |
| Kenny-Caffey syndrome type 2 | <i>FAM111A</i> | FAM111A | AD |

AR autosomal recessive, AD autosomal dominant, CAKUT congenital anomalies of the kidney and urinary tract

Fig. 1 Flowchart for identifying responsible genes for hypomagnesemia. The flowchart required the following clinical data for identifying responsible genes for hypomagnesemia: (1) congenital anomalies of the kidney and urinary tract (CAKUT) or family history of maturity-onset diabetes of the young (MODY); (2) hypokalemia and metabolic alkalosis (Gitelman-like); (3) hearing loss; (4) hypo or hypercalciuria; (5) hypoparathyroidism and hypocalcemia; and (6) ocular anomalies



Materials and methods

Patients

We investigated five index cases with hypomagnesemia (Table 2). Clinical and laboratory data and pathological findings were obtained from medical records.

Genetic analysis

Genomic DNA was isolated from peripheral blood leukocytes from the patients and their family members using the Quick Gene Mini 80 system (Wako Pure Chemical Industries, Ltd., Tokyo, Japan) according to the manufacturer's instructions. Direct sequencing or next-generation sequencing (NGS) was conducted for

Table 2 Clinical characteristics and results of genetic diagnoses of index cases

| Parameter | Patient 1 | Patient 2 | | Younger Brother | Patient 3 | Elder sister | Patient 4 | Patient 5 |
|--|--|--------------------|-----------------------------|-----------------------------|----------------------------------|-------------------------------|-------------------------------|---------------------|
| Sex and age | Male, 2 years old | Male, 1 month old | Current data (26 years old) | Current data (21 years old) | Female, 6 months old | Female, 4 years old | Female, 33 years old | Female, 8 years old |
| Clinical manifestation | CAKUT | – | – | – | – | – | – | – |
| Serum indices | | | | | | | | |
| K ⁺ , mEq/L | 4.1 | 4.5 | 4.2 | 4 | 5.5 | 4.2 | 3 | 2.2 |
| Ca ²⁺ , mg/dL | 10.2 | 2.9 | 9.2 | 8.9 | 6.3 | 9.3 | 6.2 | 10.1 |
| Mg ²⁺ , mg/dL | 1.5 | 0.3 | 1 | 1.1 | 0.8 | 1.4 | 1.2 | 0.6 |
| HCO ₃ ⁻ , mmol/L | | | | | 14.8 | 25.4 | 30.6 | 30.3 |
| pH | 7.354 | 7.425 | | | 7.369 | 7.385 | 7.568 | 7.459 |
| Creatinine, mg/dL | 0.47 | | 0.85 | 0.69 | 0.3 | 0.41 | 1.54 | 0.26 |
| Intact PTH, pg/mL | N/A | 45.5 | 19 | 35 | 71 | – | Below detectable levels | 73 |
| Urinary indices | | | | | | | | |
| FEMg, % | N/A | | 0.38 | 0.23 | 19 | – | 11.26 | 5.7 |
| Ca ²⁺ /creatinine, g/g cre | Below detectable levels | | 0.02 | 0.007 | 2.1 | 0.15 | 0.33 | 0.01 |
| β2MG, μg/L | 155 | | 168 | <60 | 301 | Below detectable levels | 1220 | 5.7 |
| Echogram | Renal cysts and bilateral renal hypoplasia | Normal | Normal | Normal | Bilateral renal calcification | Bilateral renal calcification | Bilateral renal calcification | Normal |
| Genes | <i>HNF1B</i> | <i>TRPM6</i> | | | <i>CLDN16</i> | | <i>CASR</i> | <i>SLC12A3</i> |
| Nucleotide change | c.1007insC | c.5084-2A>G (Homo) | | | c.414delT | c.715G>T | c.2363T>G | c.1844C>T (Homo) |
| Consequence on protein level | p.(His336HfsX23) | Exon 31 skip? | | | p.(Ala139ArgfsX5) p.(Gly239*) | | p.(Phe-788Cys) | p.(Ser615Leu) |

CAKUT congenital anomalies of the kidney and urinary tract, N/A not analyzed

genes responsible for inherited hypomagnesemia. NGS samples were prepared using a HaloPlex target enrichment system kit (Agilent Technologies, Santa Clara, CA) according to the manufacturer's instructions. The inherited hypomagnesemia-responsible genes *CLCNKB*, *BSND*, *SLC12A3*, *CASR*, *KCNJ10*, *CLDN16*, *CLDN19*, *FXD2*, *EGF*, *TRPM6*, *KCNA1*, *CNNM2*, and *HNF1B* were screened by targeted sequencing.

Ethical considerations

All procedures were approved by the Institutional Review Board (IRB) of Kobe University Graduate School of Medicine and in accordance with the Helsinki Declaration of 1975, as revised in 2000 (IRB number: 301). Informed consent was obtained from all index patients or their parents.

Results

Patients

Patient 1 was a 2-year-old boy who was found to have low serum Mg^{2+} by chance at a regular visit for observation of hypoplastic kidney. He had been born at 36 weeks to unrelated parents after a hydramniotic pregnancy, with a birth weight of 2250 g. His father has an isolated renal cyst and diabetes mellitus, his older sister had died immediately after birth because of Potter's sequence, and his younger brother also had renal hypoplasia. Laboratory test results are shown in Table 2. According to the flowchart, *HNF1B* gene mutation was suspected based on the clinical presentation in this family with CAKUT and diabetes, and direct sequencing of this gene was conducted.

Patient 2 was a 26-year-old man. He had been born at 39 weeks to unrelated parents after an uncomplicated pregnancy, with a birth weight of 2700 g. He presented with recurrent seizures at 1 month old, and although laboratory tests revealed hypomagnesemia and hypocalcemia, no further examination was conducted at that time. His younger brother underwent blood tests at 4 days old because of his family history, which also revealed hypomagnesemia. The results of laboratory tests for the index patient performed at 1 month old are shown in Table 2. He required intravenous Mg^{2+} two or three times a week since the initial diagnosis. This patient had no ocular involvement. His and his brother's current laboratory data are shown in Table 2. We conducted targeted sequencing analysis using NGS, including hereditary hypomagnesemia-causative genes. Based on the clinical presentation of hypomagnesemia and hypocalcemia and intact parathyroid hormone (iPTH) suppression without CAKUT, hypokalemia, or hypercalciuria, this family was suspected to have *TRPM6*, *EGF/EGFR*, or *FAM111A* variants.

Patient 3 was a 6-month-old girl who was born to unrelated parent at 38 weeks after an uncomplicated pregnancy, with a birth weight of 2680 g. Low serum Ca^{2+} and Mg^{2+} were detected by chance during a bout of viral gastroenteritis. Her asymptomatic elder sister was tested after the diagnosis of Patient 3 and was also found to have hypomagnesemia. Laboratory test results for both sisters are shown in Table 2. She had no ocular involvement. The clinical presentation of hypercalciuria without CAKUT, hypokalemia, iPTH suppression, or ocular abnormality suggested *CLDN16* mutation, and direct sequencing of this gene was conducted.

Patient 4 was a 33-year-old woman, whose case has been reported previously [4]. Low serum Ca^{2+} was detected by chance in the absence of any clinical signs, and she was diagnosed with hypocalcemia and hypoparathyroidism at the age of 6 years. She showed hypokalemia, metabolic

alkalosis, and short stature at the age of 12, and was administered growth hormone therapy for 3 years. Hypomagnesemia was detected when she was 25 years old. She developed bilateral renal calcification and mild impairment of kidney function at the age of 33 years. She had been prescribed active vitamin D3 since the age of 6 years, but this was tapered off after a diagnosis of ADH1. The results of laboratory tests performed at her initial visit to our hospital are shown in Table 2. From the clinical presentation of hypokalemia, hypercalciuria, iPTH suppression, and hypocalcemia without CAKUT or hearing loss, she was suspected to be have a *CASR* mutation, and direct sequencing of this gene was conducted.

Patient 5 was an 8-year-old girl who had been born at 40 weeks to unrelated parents after an uncomplicated pregnancy, with a birth weight of 3246 g. She had no remarkable family or past history. However, low serum Mg^{2+} was detected by chance when she was affected by viral gastroenteritis. Her laboratory test results are shown in Table 2. She had no significant inner ear involvement. Based on her clinical presentation of hypokalemia and hypercalciuria, without hearing loss, she was suspected to have an *SLC12A3* mutation.

Flowchart

The flowchart was established according to the following reports of inherited hypomagnesemia. *HNF1B* is a causative gene of CAKUT and early onset diabetes, and *MODY5* that is also caused by *HNF1B* variants is frequently accompanied by hypomagnesemia [5–7]. Patients with *FXRD2*, *KCNA1*, *CNNM2*, or *PCBD1* variants show hereditary hypomagnesemia with hypo- to normocalciuria [8–12]. Hypomagnesemia with secondary hypocalcemia (HSH) caused by *TRPM6* variants is associated with hypo- to normocalciuria with serum iPTH suppression [13–15]. Kenny-Caffey syndrome type 2 is a rare condition caused by *FAM111A* variants. It is characterized by cortical thickening and medullary stenosis of tubular bones, delayed closure of the anterior fontanelle, eye abnormalities, hypoparathyroidism and hypocalcemia accompanied by hypomagnesemia, and hypo- to normocalciuria [16]. ADH1/type V Bartter syndrome caused by *CASR* variants also shows iPTH suppression and hypocalcemia [17–19]. Patients with *EGF* or *EGFR* variants may share similar pathophysiology with HSH, because EGF increases *TRPM6* activity and surface expression [20, 21]. Familial hypomagnesemia with hypocalcemia and nephrocalcinosis (FHHNC) caused by *CLDN16* or *CLDN19* variants is associated with hypercalciuria, while *CLDN19* variants are associated with ocular impairment [22–24]. Hypomagnesemia accompanied by hypokalemia and metabolic alkalosis (Gitelman-like) indicates the possibility of Bartter/

Gitelman syndrome-associated disorders. Both type III Bartter syndrome caused by variants in *CLCNKB* and Gitelman syndrome caused by variants in *SLC12A3* are usually accompanied by hypomagnesemia [25–28]. Pathogenic variants in the *BSND* gene cause type IV Bartter syndrome with sensorineural deafness and occasionally hypomagnesemia [2, 29]. Pathogenic variants in *KCNJ10* also cause hypokalemic and hypomagnesemic tubulopathy with hearing loss (EAST syndrome), and this tubulopathy is identical to that seen in Gitelman syndrome [30].

The flowchart required the following clinical data for identifying responsible genes for hypomagnesemia: (1) congenital anomalies of the kidney and urinary tract (CAKUT) or family history of maturity-onset diabetes of the young (MODY); (2) hypokalemia and metabolic alkalosis (Gitelman-like); (3) hearing loss; (4) hypo- or hypercalciuria; (5) hypoparathyroidism and hypocalcemia; and (6) ocular anomalies (Fig. 1).

Genetic analysis

All genetic test results are shown in Tables 2 and 3. The results of all genetic analyses were consistent with the clinical diagnostic results obtained using the flowchart (Fig. 1). Truncating variants were detected in Patients 1 and 3. A splicing variant was detected in Patient 2. Missense variants were detected in Patients 4 and 5, both of which were predicted as pathogenic by in silico analysis. In addition, variants in Patients 1, 2, 4 and 5 have been reported as pathogenic (Table 3) [31–34].

Discussion

This study demonstrated the validity of our flowchart in five index cases of inherited hypomagnesemia. The flowchart is necessarily complicated because of the genetic heterogeneity of the condition. However, an accurate clinical diagnosis is important in terms of the kidney prognosis, the presence of complications other than hypomagnesemia, and for conducting genetic counseling. Recent developments in genetic techniques mean that it is possible to make a genetic diagnosis using NGS, even in the absence of an accurate clinical diagnosis, as in Patient 2. However, a clinical diagnosis remains important, because NGS is not always available. A diagnostic flowchart thus provides a highly useful tool for clinicians.

Heterozygous variants in *HNF1B* result in multi-system disorders and are the most common monogenic cause of CAKUT, occurring in 10–30% of CAKUT patients in the prenatal period [7]. *HNF1B* is also a causative gene of early onset diabetes, MODY5 [6]. In addition, an initial report showed that hypomagnesemia occurred in up to 50% of affected patients [5]. The presence of CAKUT with hypomagnesemia and a family history of diabetes provided a useful clue to a potential *HNF1B* mutation in Patient 1. Serum Mg^{2+} levels should be monitored in patients with CAKUT as an indicator of potential *HNF1B* mutations, while a family history of early onset diabetes is also a clue for the detection of *HNF1B* variants, as in Patient 1.

Homozygous or compound heterozygous variants in *TRPM6* cause HSH, which is a relatively rare autosomal recessive disease [15]. Affected individuals present in early

Table 3 Results of genetic diagnosis

| Patient | Genes | Inheritance mode | Nucleotide changes | Consequence on protein level | Previous reports | Variant types | SIFT | PolyPhen2 |
|---------|----------------|------------------|-----------------------|----------------------------------|--|--------------------------------|-----------------|--------------------------|
| 1 | <i>HNF1B</i> | AD | c.1006dupC | p.(His336HfsX23) | Mache (2002) Pediatric Nephrol 17, 1021 | Frameshift | – | – |
| 2 | <i>TRPM6</i> | AR | c.5084-2A>G (Homo) | (Exon 31 skip?) | Lainez (2014) Eur J Hum Genet 22, 497 | Splice site variant | – | – |
| 3 | <i>CLDN16</i> | AR | c.414delT c.715G>T | p.(Ala139ArgfsX5) p.(Gly239*) | Novel Novel | Frameshift Nonsense variant | – – | – – |
| 4 | <i>CASR</i> | AD | c.2363T>G | p.(Phe788Cys) | Watanabe (1998) J Clin Endocrinol Metab 83, 2497 | Missense variant | Damaging (0.01) | Probably damaging (1.00) |
| 5 | <i>SLC12A3</i> | AR | c.1844C>T (Homo) | p.(Ser615Leu) | Cruz (2001) Kidney Int 59, 710 | Missense variant | Damaging (0.01) | Probably damaging (1.00) |

infancy with seizures caused by the severe hypocalcemia and hypomagnesemia [15]. HSH is sometimes misdiagnosed as primary hypoparathyroidism because of its initial presenting symptoms of hypocalcemia and concomitant low or inappropriate normal parathyroid hormone (PTH) caused by hypomagnesemia, which blocks the release of PTH and decreases sensitivity to circulating PTH in target organs [13]. Some HSH patients can be managed by Mg^{2+} supplementation without a genetic diagnosis, as in Patient 2. HSH is a relatively rare condition, and the causative mutation in Patient 2 was detected by NGS analysis; however, our flowchart also led to a diagnosis of HSH in this patient.

Loss-of-function mutations in the genes for claudin-16 and its close relative claudin-19 lead to an identical renal phenotype, with combined renal Ca^{2+} and Mg^{2+} wasting and nephrocalcinosis, referred to as FHHNC, inherited in an autosomal dominant mode [23, 24]. FHHNC is frequently complicated by progressive renal failure and the renal prognosis is poor, with progressive chronic kidney disease requiring renal replacement therapy typically occurring in the second or third decades of life [35]. Patients with *CLDN16* and *CLDN19* variants may have different renal prognoses; *CLDN19* mutations are associated with a higher risk of chronic kidney disease and end-stage renal disease, and ocular impairment occurs exclusively in patients with *CLDN19* mutations [22]. Definitive genetic diagnosis may be useful to prediction of prognosis or phenotype in FHHNC patients.

Gain-of-function mutations in *CASR* cause ADH1, which is associated with hypocalcemia, relative hypercalciuria, and inadequate PTH secretion, and occasionally with hypomagnesemia [17]. In some cases, ADH1 is accompanied by hypokalemia, and this combination may be classified as type V Batters syndrome [18, 19]. In addition to HSH, ADH1 may also be misdiagnosed as primary hypoparathyroidism, as in Patient 4.

Loss-of-function mutations in *SLC12A3* cause Gitelman syndrome, which is an autosomal recessive renal tubulopathy characterized by hypokalemic metabolic alkalosis with hypocalciuria and hypomagnesemia [28]. Type III Batters syndrome, which is caused by *CLCNKB* variants, frequently shows phenotypic overlap with Gitelman syndrome [25–27], and some type III Batters syndrome patients may show clinical features of Gitelman syndrome, such as hypomagnesemia and hypocalciuria [25, 26]. It is not possible to make a definite diagnosis in such cases without genetic testing; however, a definitive genetic diagnosis will allow better management of patients and appropriate pathophysiological investigation of the disease.

Our flowchart was useful in the five index cases of inherited hypomagnesemia, and was also validated in the previous cases of inherited hypomagnesemia. However, many

genes are involved in inherited hypomagnesemia, some of which have been reported in too few cases to define their characteristics. For instance, hypomagnesemia associated with variants in *KCNA1* [9] or loss-of-function in the *EGFR* gene [20] has only been reported in one pedigree and one patient, respectively, though there have been some reports of cases with hypomagnesemia treated with cetuximab, a monoclonal antibody directed against EGFR [36]. Phenotypic overlap, such as that between Gitelman syndrome and type III Batters syndrome [25, 26], or diversity of clinical phenotypes associated with gain-of-function mutations in *CASR* causing ADH1 and type V Batters syndrome, will complicate the flowchart [18, 19, 37]. Further studies of inherited hypomagnesemia are, therefore, required to improve the flowchart.

In conclusion, hereditary hypomagnesemia may be difficult to diagnose accurately because of its rarity and the variety of causative genes. Our flowchart for identifying responsible genes for hypomagnesemia provides a useful diagnostic tool, but some kinds of hereditary hypomagnesemia still require genetic testing to reach a definite diagnosis. NGS analysis will help to resolve clinical difficulties and improve the chance of making a definite diagnosis in patients with hereditary hypomagnesemia.

Compliance with ethical standards

All procedures were approved by the Institutional Review Board (IRB) of Kobe University Graduate School of Medicine and in accordance with the Helsinki Declaration of 1975, as revised in 2000 (IRB number: 301). Informed consent was obtained from all index patients or their parents.

This study was supported by a grant from the Ministry of Education, Culture, Sports, Science and Technology of Japan (Subject ID: 15K09691 to Kandai Nozu) and a Health Labour Sciences Research Grant for Research on Measures for Intractable Diseases (H26-nanchitou-ippan-036 to Kazumoto Iijima).

Conflict of interest The authors have nothing to disclose.

References

1. de Baaij JH, Hoenderop JG, Bindels RJ. Magnesium in man: implications for health and disease. *Physiol Rev*. 2015;95(1):1–46.
2. Viering DH, de Baaij JH, Walsh SB, Kleta R, Bockenhauer D. Genetic causes of hypomagnesemia, a clinical overview. *Pediatr Nephrol*. 2016. doi:10.1007/s00467-016-3416-3.
3. Pham PC, Pham PA, Pham SV, Pham PT, Pham PM, Pham PT. Hypomagnesemia: a clinical perspective. *Int J Nephrol Renovasc Dis*. 2014;7:219–30.
4. Kamiyoshi N, Nozu K, Urahama Y, Matsunoshita N, Yamamura T, Minamikawa S, Ninchoji T, Morisada N, Nakanishi K, Kaito H, et al. Pathogenesis of hypokalemia in autosomal dominant hypocalcemia type 1. *Clin Exp Nephrol*. 2016;20(2):253–7.
5. Adalat S, Woolf AS, Johnstone KA, Wirsing A, Harries LW, Long DA, Hennekam RC, Ledermann SE, Rees L, van't Hoff W, et al. HNF1B mutations associate with hypomagnesemia

- and renal magnesium wasting. *J Am Soc Nephrol*. 2009;20(5):1123–31.
6. Horikawa Y, Iwasaki N, Hara M, Furuta H, Hinokio Y, Cockburn BN, Lindner T, Yamagata K, Ogata M, Tomonaga O, et al. Mutation in hepatocyte nuclear factor-1 beta gene (TCF2) associated with MODY. *Nat Genet*. 1997;17(4):384–5.
 7. Vivante A, Kohl S, Hwang DY, Dworschak GC, Hildebrandt F. Single-gene causes of congenital anomalies of the kidney and urinary tract (CAKUT) in humans. *Pediatr Nephrol*. 2014;29(4):695–704.
 8. Meij IC, Koenderink JB, van Bokhoven H, Assink KF, Groenestege WT, de Pont JJ, Bindels RJ, Monnens LA, van den Heuvel LP, Knoers NV. Dominant isolated renal magnesium loss is caused by misrouting of the Na(+),K(+)-ATPase gamma-subunit. *Nat Genet*. 2000;26(3):265–6.
 9. Glaudemans B, van der Wijst J, Scola RH, Lorenzoni PJ, Heister A, van der Kemp AW, Knoers NV, Hoenderop JG, Bindels RJ. A missense mutation in the Kv1.1 voltage-gated potassium channel-encoding gene KCNA1 is linked to human autosomal dominant hypomagnesemia. *J Clin Invest*. 2009;119(4):936–42.
 10. Stuijver M, Lainez S, Will C, Terry S, Gunzel D, Debaix H, Sommer K, Kopplin K, Thumfart J, Kampik NB, et al. CNNM2, encoding a basolateral protein required for renal Mg²⁺ handling, is mutated in dominant hypomagnesemia. *Am J Hum Genet*. 2011;88(3):333–43.
 11. Ferre S, de Baaij JH, Ferreira P, Germann R, de Klerk JB, Lavrijssen M, van Zeeland F, Venselaar H, Kluijtmans LA, Hoenderop JG, et al. Mutations in PCBD1 cause hypomagnesemia and renal magnesium wasting. *J Am Soc Nephrol*. 2014;25(3):574–86.
 12. de Baaij JH, Dorresteijn EM, Hennekam EA, Kamsteeg EJ, Meijer R, Dahan K, Muller M, van den Dorpel MA, Bindels RJ, Hoenderop JG, et al. Recurrent FXD2 p.Gly41Arg mutation in patients with isolated dominant hypomagnesaemia. *Nephrol Dial Transplant*. 2015;30(6):952–7.
 13. Astor MC, Lovas K, Wolff AS, Nedrebo B, Bratland E, Steen-Johnsen J, Husebye ES. Hypomagnesemia and functional hypoparathyroidism due to novel mutations in the Mg-channel TRPM6. *Endocr Connect*. 2015;4(4):215–22.
 14. Groenestege WM, Hoenderop JG, van den Heuvel L, Knoers N, Bindels RJ. The epithelial Mg²⁺ channel transient receptor potential melastatin 6 is regulated by dietary Mg²⁺ content and estrogens. *J Am Soc Nephrol*. 2006;17(4):1035–43.
 15. Schlingmann KP, Weber S, Peters M, Niemann Nejsum L, Vitzthum H, Klingel K, Kratz M, Haddad E, Ristoff E, Dinour D, et al. Hypomagnesemia with secondary hypocalcemia is caused by mutations in TRPM6, a new member of the TRPM gene family. *Nat Genet*. 2002;31(2):166–70.
 16. Unger S, Gorna MW, Le Behec A, Do Vale-Pereira S, Bedeschi MF, Geiberger S, Grigelioniene G, Horemuzova E, Lalatta F, Lausch E, et al. FAM111A mutations result in hypoparathyroidism and impaired skeletal development. *Am J Hum Genet*. 2013;92(6):990–5.
 17. Pearce SH, Williamson C, Kifor O, Bai M, Coulthard MG, Davies M, Lewis-Barned N, McCredie D, Powell H, Kendall-Taylor P, et al. A familial syndrome of hypocalcemia with hypercalciuria due to mutations in the calcium-sensing receptor. *N Engl J Med*. 1996;335(15):1115–22.
 18. Vargas-Poussou R, Huang C, Hulin P, Houillier P, Jeunemaitre X, Paillard M, Planelles G, Dechaux M, Miller RT, Antignac C. Functional characterization of a calcium-sensing receptor mutation in severe autosomal dominant hypocalcemia with a Bartter-like syndrome. *J Am Soc Nephrol*. 2002;13(9):2259–66.
 19. Watanabe S, Fukumoto S, Chang H, Takeuchi Y, Hasegawa Y, Okazaki R, Chikatsu N, Fujita T. Association between activating mutations of calcium-sensing receptor and Bartter's syndrome. *The Lancet*. 2002;360(9334):692–4.
 20. Campbell P, Morton PE, Takeichi T, Salam A, Roberts N, Proudfoot LE, Mellerio JE, Aminu K, Wellington C, Patil SN, et al. Epithelial inflammation resulting from an inherited loss-of-function mutation in EGFR. *J Invest Dermatol*. 2014;134(10):2570–8.
 21. Thebault S, Alexander RT, Tiel Groenestege WM, Hoenderop JG, Bindels RJ. EGF increases TRPM6 activity and surface expression. *J Am Soc Nephrol*. 2009;20(1):78–85.
 22. Godron A, Harambat J, Boccio V, Mensire A, May A, Rigotherier C, Couzi L, Barrou B, Godin M, Chauveau D, et al. Familial hypomagnesemia with hypercalciuria and nephrocalcinosis: phenotype-genotype correlation and outcome in 32 patients with CLDN16 or CLDN19 mutations. *Clin J Am Soc Nephrol*. 2012;7(5):801–9.
 23. Konrad M, Schaller A, Seelow D, Pandey AV, Waldegger S, Leschlauer A, Vitzthum H, Suzuki Y, Luk JM, Becker C, et al. Mutations in the tight-junction gene claudin 19 (CLDN19) are associated with renal magnesium wasting, renal failure, and severe ocular involvement. *Am J Hum Genet*. 2006;79(5):949–57.
 24. Simon DB, Lu Y, Choate KA, Velazquez H, Al-Sabban E, Praga M, Casari G, Bettinelli A, Colussi G, Rodriguez-Soriano J, et al. Paracellin-1, a renal tight junction protein required for paracellular Mg²⁺ resorption. *Science*. 1999;285(5424):103–6.
 25. Matsunoshita N, Nozu K, Shono A, Nozu Y, Fu XJ, Morisada N, Kamiyoshi N, Ohtsubo H, Ninchoji T, Minamikawa S, et al. Differential diagnosis of Bartter syndrome, Gitelman syndrome, and pseudo-Bartter/Gitelman syndrome based on clinical characteristics. *Genet Med*. 2016;18(2):180–8.
 26. Nozu K, Iijima K, Kanda K, Nakanishi K, Yoshikawa N, Satomura K, Kaito H, Hashimura Y, Ninchoji T, Komatsu H, et al. The pharmacological characteristics of molecular-based inherited salt-losing tubulopathies. *J Clin Endocrinol Metab*. 2010;95(12):E511–E518.
 27. Simon DB, Bindra RS, Mansfield TA, Nelson-Williams C, Mendonca E, Stone R, Schurman S, Nayir A, Alpay H, Bakkaloglu A, et al. Mutations in the chloride channel gene, CLCNKB, cause Bartter's syndrome type III. *Nat Genet*. 1997;17(2):171–8.
 28. Simon DB, Nelson-Williams C, Bia MJ, Ellison D, Karet FE, Molina AM, Vaara I, Iwata F, Cushner HM, Koolen M, et al. Gitelman's variant of Bartter's syndrome, inherited hypokalaemic alkalosis, is caused by mutations in the thiazide-sensitive Na–Cl cotransporter. *Nat Genet*. 1996;12(1):24–30.
 29. Birkenhager R, Otto E, Schurmann MJ, Vollmer M, Ruf EM, Maier-Lutz I, Beekmann F, Fekete A, Omran H, Feldmann D, et al. Mutation of BSND causes Bartter syndrome with sensorineural deafness and kidney failure. *Nat Genet*. 2001;29(3):310–4.
 30. Scholl UI, Choi M, Liu T, Ramaekers VT, Hausler MG, Grimmer J, Tobe SW, Farhi A, Nelson-Williams C, Lifton RP. Seizures, sensorineural deafness, ataxia, mental retardation, and electrolyte imbalance (SeSAME syndrome) caused by mutations in KCNJ10. *Proc Natl Acad Sci USA*. 2009;106(14):5842–7.
 31. Cruz DN, Shaer AJ, Bia MJ, Lifton RP, Simon DB, Yale GS, Bartter's Syndrome Collaborative Study G. Gitelman's syndrome revisited: an evaluation of symptoms and health-related quality of life. *Kidney Int*. 2001;59(2):710–7.
 32. Lainez S, Schlingmann KP, van der Wijst J, Dworniczak B, van Zeeland F, Konrad M, Bindels RJ, Hoenderop JG. New TRPM6 missense mutations linked to hypomagnesemia with secondary hypocalcemia. *Eur J Hum Genet*. 2014;22(4):497–504.
 33. Mache CJ, Preisegger KH, Kopp S, Ratschek M, Ring E. De novo HNF-1 beta gene mutation in familial hypoplastic glomerulocystic kidney disease. *Pediatr Nephrol*. 2002;17(12):1021–6.
 34. Watanabe T, Bai M, Lane CR, Matsumoto S, Minamitani K, Minagawa M, Niimi H, Brown EM, Yasuda T. Familial hypoparathyroidism: identification of a novel gain of function mutation in transmembrane domain 5 of the calcium-sensing receptor. *J Clin Endocrinol Metab*. 1998;83(7):2497–502.

35. Weber S, Schneider L, Peters M, Misselwitz J, Ronnefarth G, Boswald M, Bonzel KE, Seeman T, Sulakova T, Kuwertz-Broking E, et al. Novel paracellin-1 mutations in 25 families with familial hypomagnesemia with hypercalciuria and nephrocalcinosis. *J Am Soc Nephrol*. 2001;12(9):1872–81.
36. Schrag D, Chung KY, Flombaum C, Saltz L. Cetuximab therapy and symptomatic hypomagnesemia. *J Natl Cancer Inst*. 2005;97(16):1221–4.
37. Kinoshita Y, Hori M, Taguchi M, Watanabe S, Fukumoto S. Functional activities of mutant calcium-sensing receptors determine clinical presentations in patients with autosomal dominant hypocalcemia. *J Clin Endocrinol Metab*. 2014;99(2):E363–E368.

Restricted nutrition-induced low birth weight, low number of nephrons and glomerular mesangium injury in Japanese quail

H. Nishimura^{1,2*}, E. Yaoita², M. Nameta², K. Yamaguchi³, M. Sato⁴, C. Ihoriya⁴, L. Zhao², H. Kawachi², T. Sasaki⁴, Y. Ikezumi⁵, Y. Ouchi⁶, N. Kashihara⁴ and T. Yamamoto²

¹Department of Physiology, University of Tennessee Health Science Center, Memphis, TN, USA

²Institute of Nephrology and Department of Physiology, Niigata University Graduate School of Medical and Dental Sciences, Niigata, Japan

³Department of Physiology, Niigata University Graduate School of Medical and Dental Sciences, Niigata, Japan

⁴Department of Medicine, Kawasaki Medical School, Okayama, Japan

⁵Department of Pediatrics, Niigata University Graduate School of Medical and Dental Hospital, Niigata, Japan

⁶Department of Geriatric Medicine, Graduate School of Medicine, University of Tokyo, Tokyo, Japan

Insufficient nutrition during the perinatal period causes structural alterations in humans and experimental animals, leading to increased vulnerability to diseases in later life. Japanese quail, *Coturnix japonica*, in which partial (8–10%) egg white was withdrawn (EwW) from eggs before incubation had lower birth weights than controls (CTs). EwW birds also had reduced hatching rates, smaller glomeruli and lower embryo weight. In EwW embryos, the surface condensate area containing mesenchymal cells was larger, suggesting that delayed but active nephrogenesis takes place. In mature EwW quail, the number of glomeruli in the cortical region (mm²) was significantly lower (CT 34.7 ± 1.4, EwW 21.0 ± 1.2); capillary loops showed focal ballooning, and mesangial areas were distinctly expanded. Immunoreactive cell junction proteins, N-cadherin and podocin, and slit diaphragms were clearly seen. With aging, the mesangial area and glomerular size continued to increase and were significantly larger in EwW quail, suggesting compensatory hypertrophy. Furthermore, apoptosis measured by terminal deoxynucleotidyl transferase-mediated dUTP-biotin nick-end labeling analysis was higher in EwWs than in CTs on embryonic day 15 and postnatal day 4 (D4). Similarly, plasma glucocorticoid (corticosterone) was higher ($P < 0.01$) on D4 in EwW quail. These results suggest that although nephrogenic activity is high in low-nutrition quail during the perinatal period, delayed development and increased apoptosis may result in a lower number of mature nephrons. Damaged or incompletely mature mesangium may trigger glomerular injury, leading in later life to nephrosclerosis. The present study shows that birds serve as a model for ‘fetal programming,’ which appears to have evolved phylogenetically early.

Received 1 July 2016; Revised 26 November 2016; Accepted 29 November 2016

Key words: avian kidney, glomerular mesangium injury, fetal programming, low birth weight, nephrosclerosis

Introduction

Increasing evidence suggests that the onset of diseases in adults may originate in adverse events of fetal life, such as reduced nutrient supply and hypoxia.^{1–3} Inadequate nutrition, particularly low protein, in the fetal period results in smaller birth size and may predispose humans and experimental animals to various health problems after maturation, including hypertension, type 2 diabetes, obesity, and cardiovascular and renal disorders.^{4–8} Such developmental programming (developmental plasticity) is the ability of an organism to change its phenotype in response to changes in the environment.^{9,10} Furthermore, in advanced countries, the number of babies with low birth weight (LBW; 2500 g or lower) has been increasing since the 1980s.¹¹ Also, our recent study¹¹ shows that the

incidence of focal segmental glomerulosclerosis (FSGS; diagnosed by renal biopsy) is increasing in children and is associated with enlarged glomeruli and a reduced number of nephrons. Causal relationships among these facts, however, are not completely understood.

Using a unique bird model, we tested the hypothesis that reduced nutrition during the critical time of kidney development retards nephrogenesis, resulting in a low number of nephrons. The remaining nephrons show compensatory enlargement. Increased glomerular pressure damages incompletely mature nephrons, leading to mesangial expansion and nephrosclerosis. Birds provide an ideal model for studying this hypothesis because avian embryos have a predetermined nutrient supply in the egg¹² and their nutrition is free from influence by daily maternal diet. Also, birds show a maturation-dependent increase in blood pressure. We therefore investigated whether Japanese quail in which the nutrient supply was reduced during development: (1) show LBW (low hatch weight) and a decreased number of renal glomeruli; and

*Address for correspondence: Professor H. Nishimura, Department of Health Informatics, Niigata University of Health and Welfare, 1398 Shimamicho, Kitaku, Niigata City 950-3198, Japan.
 (Email nishimura.uthsc@gmail.com)

(2) show renal injury after maturation, particularly in the glomerular mesangium area, possibly leading to nephrosclerosis. Nutrition-reduced quail also provide a good model for studying the phenotype and mechanism of fetal programming and for examining whether 'fetal programming' evolved phylogenetically early.

Materials and methods

Animals, egg incubation and maintenance

Fertilized eggs of *Coturnix japonica* (Ebihara's male/female differentiable strain) were purchased from a commercial hatchery (Ebihara Farm; Tochigi, Japan) and were incubated in a temperature (37.5°C) – and humidity (60%; increased to 80% 3 days before hatching) – controlled incubator with periodic rotation (Ehret Egg Incubator; AFOS, UK).^{13–15} Fertilized quail eggs were hatched on D17–D17.5. Chicks that were hatched after the 18th day were not included. Hatched birds were kept at 37°C for the first 3 days; the temperature was decreased by 2°C every 2 days until it reached 25°C. Thereafter, birds were kept in a temperature (25°C) – and humidity-controlled brooder (JQ-TECH; Toyohashi, Japan) for 3 weeks and then moved to a group pen at room temperature (22–24°C). Chick food (Ebihara Farm, Japan) containing protein (25% minimum), fiber (6%), crude minerals (13.7%), crude fat (3%), calcium (0.9%), phosphorus (0.7%) and crude carbohydrate (rest) was fed to the birds for 2 weeks. The chick food was gradually replaced with adult food containing 24% protein and 2.5–3.0% calcium (the other constituents are similar). Calcium in adult food is higher because females use a large amount of calcium for laying eggs. Drinking water containing multiple vitamins (GQF Manufacturing; Savannah, GA, USA) was given for the first 7 days, followed by tap water *ad libitum*. The photoperiod (12 h light–12 h dark cycle) was controlled. Birds were kept in groups separating control (CT) and experimental [egg white withdrawn (EwW)] quail. Animal protocols were reviewed and approved by the Institutional Animal Care and Use Committee of the Niigata University School of Medical and Dental Sciences, Niigata, Japan and University of Tennessee Health Science Center.

Withdrawal of partial egg white

Before the experiments, intact eggs were boiled to estimate approximate volume of egg white.¹⁵ Egg whites and yolks were separated, and the average percentage of egg white over whole egg weight was calculated ($57.8 \pm 0.6\%$; $n = 7$). In all, 8–10% of estimated egg white was withdrawn before initiation of hatching (referred to as EwW). In preliminary studies, we found that EwW of <5% showed no effect, whereas EwW of >10% reduced the hatching rate from 75–80% to <5%. Fertilized eggs were gently cleaned with warm water. A sterile G19 blunted needle was inserted through a small hole in the steep end of the egg shell, and the egg white was withdrawn into a 1-ml syringe moistened with sterile phosphate-buffered

saline (PBS). The punctured hole was completely sealed by covering it with a small piece of quail egg shell and non-organic adhesive gel. Eggs were discarded when egg white was contaminated with egg yolk, which contains vitamins, calcium, ions and other important materials for egg growth. Analysis of quail eggs¹² indicated that albumen (egg white) comprises 59.2% of the total egg weight.

Animal groups and experimental protocols

Quail incubation and hatches were repeated three times (Series A, B and C). Because of the low hatching rate of EwW groups and limitations in maintenance facilities and sample handling, it was not possible to process all examinations in the same group. We measured birth (hatch) weight in all series, and embryonic weight was measured in Series A and C. Body weight was measured to assess body growth every 2–3 days and then once a week in all groups. The specific aims of the study and protocol differed depending on the series.

Series A: the specific aim of Series A was to determine the morphological development and immunohistochemical properties of glomerular junction proteins in kidneys of embryonic and newborn quail. Kidney specimens were collected at embryonic day 10 (E10), E15, postnatal day 4 (D4) and D21 for examination by electron microscopy (EM) ($n = 2$ each for CT and EwW), histology ($n = 3$ each for CT and EwW), and immunohistochemistry ($n = 3$ each). Trunk blood samples were collected by decapitation at D4 and D21. Series B: this group was used for studying time-dependent structural changes in epithelial cells and mesangium. Specimens for histology ($n = 3$ each) and EM ($n = 2$ each) and for trunk blood samples were collected at 5, 21 and 63 weeks. Series C: the specific aim of this series was to determine the mechanism of reduction of the number of glomeruli in the EwW group. Kidney specimens for measuring apoptosis in CT and EwW quail ($n = 3$ each) were taken at E15, D4 and D16–D18. Histology and EM specimens were also examined ($n = 3$ each) to confirm whether the morphological changes were similar to those in Series A and B. Trunk blood was collected by decapitation at D4 and D16–D18.

In all series examined, small EM specimens were collected from the caudal tip of the lower lobe of the left kidney, whereas the rest of the left lower lobe (largest lobe) was used for histochemical examination. For histology, right and left kidneys (embryonic and neonatal) or whole right kidneys were used. As tissue congestion often occurs due to anesthetic agents and affects a clear microscopic view, we did not use any chemical treatment before decapitation.

Tissue preparation for histology and EM

Kidneys from embryos and chicks were quickly excised and immersed in 4% paraformaldehyde (PFA; pH 7.2) for 3 days, dehydrated in ethanol, and embedded in paraffin. To maintain their gross structure, excised kidneys were placed on filter paper before fixation. Left and right kidneys were collected together

from E10 and E15 embryos and postnatal birds. Tissues were sliced (longitudinal sections) to a thickness of 3–4 μm and stained with hematoxylin-eosin, periodic acid-Schiff (PAS), and periodic acid-methenamine-silver stain (PAM) for morphological examination. Histological examination was conducted with an Olympus Model BX50 microscope (Olympus America; New Hyde Park, NY, USA).

Tissue blocks from quail kidneys for EM examination were fixed in 2.5% glutaraldehyde in 0.1 M phosphate buffer (pH 7.4) at 4°C overnight and postfixed in 1% osmium tetroxide. After dehydration in a graded alcohol series, tissues were embedded in Epon 812 resin. Ultrathin sections were double-stained with uranium acetate and lead citrate for observation by EM (H600A; Hitachi, Tokyo, Japan).¹⁶ For gross examination, thin sections (~2 μm) were stained with 0.1% of toluidine blue and viewed.

Morphometric analysis

Assessment of the number and size of glomeruli was conducted in longitudinally cut slices by (1) counting the number of glomeruli in a designated cortical (superficial) area (0.2 mm², five areas per kidney slice, total 30 areas) and in a deeper zone (1 mm², two areas per kidney slice, total 18 areas) and (2) determining the size of the glomerulus and mesangium areas using a Keyence HS All-in-One Fluorescence Microscope BZ-9000 (Keyence Co.; Osaka, Japan) and Dynamic Cell Count BZ-H1C kit (Keyence). We selected 6–60 glomeruli per kidney slice (depending on protocols; exact numbers are shown in the relevant figures), representing various parts of the kidney from three birds per group; glomeruli containing a vascular pole or a Bowman's capsule transition to a proximal tubule were selected. In avian kidneys, the zonation between cortex and medulla is not as clear as in mammalian kidneys. Hence, 'superficial' and 'deeper' zones are more suitable descriptions.

Measurements of corticosterone

The plasma corticosterone level was measured by radioimmunoassay using a commercially available kit (Coat-A-Count ¹²⁵I RIA kit; Siemens Medical Solutions Diagnostics, Malvern, PA, USA). In birds, corticosterone is the major adrenal steroid that has both gluco- and mineralo-corticoid actions. The structure of avian corticosterone is the same as that of the rat. A rabbit anti-rat corticosterone antibody was used that shows cross-reactivity of <2.9 and 0.9%, respectively, with 11-deoxycorticosterone and cortisol. Incubation for the assay with plasma samples (0.1 ml each) was performed in duplicate for 2 h at 20°C in assay tubes coated with antibody. After decanting solutions (free fraction), radioactivity of the free fraction and that of remaining in the incubation tubes (bound fraction) was counted for 1 min by a gamma counter and the ratio was calculated. The standard curve was obtained by duplicate assay of corticosterone standards ranging from 0 to 500 ng/ml. The minimum detection limit of the assay was 3.0 ng/ml. No sample showed levels of corticosterone exceeding the maximum detection limit.

Immunofluorescent analysis for glomerular cell junction proteins

Glomerular cell junction proteins, podocin and *N*-cadherin, were determined using immunofluorescent techniques.^{17,18} The lower lobes of quail kidneys were embedded in optimum cutting temperature compound, a formulation of water-soluble glycols and resins (Finetek; Sakura, Japan), and were kept at –70°C until being sectioned into 3- μm -thick slices by a cryostat (usually transverse direction). Entire lower lobes were collected from embryonic kidneys (E10 and E15), whereas only the bottom halves of lower lobes from postnatal kidneys were used. The tissue slices were fixed in 2% PFA (10 min), washed with PBS, and then treated with 10% normal goat serum for 30 min. Localization of podocin was investigated by incubating the sliced tissues with the rabbit anti-carboxyl terminus of mouse and human podocin¹⁹ (polyclonal, 1:200 dilution), followed by goat anti-rabbit fluorescein isothiocyanate-conjugated (FITC) (Immunobiological Laboratories, Gunma, Japan) or goat anti-rabbit tetramethylrhodamine isothiocyanate (TRITC) (rhodamine-conjugated; Southern Biotech, Birmingham, AL, USA) labeled immunoglobulin (IgG) (1:200 dilution). *N*-cadherin was determined using mouse monoclonal anti-*N*-cadherin (10 $\mu\text{g}/\text{ml}$; Invitrogen Corp., Camarillo, CA, USA) raised against the intracellular domain of chicken *N*-cadherin, followed by goat anti-mouse FITC- or TRITC-labeled IgG (1:50 dilution). Anti-chicken cadherin reacts with chicken, human, mouse, rat and pig cadherin. Laminin was stained using rabbit anti-mouse EHS (Englebreth Holm-Swarm) sarcoma (1.3 $\mu\text{g}/\text{ml}$; Sigma, St. Louis, MO, USA), followed by goat anti-rabbit TRITC-labeled IgG (1:200 dilution). Zonula occludens-1 (ZO-1) was stained with mouse anti-human recombinant ZO-1 fusion protein (AA334–634, 5 $\mu\text{g}/\text{ml}$; Invitrogen, Life Technologies; Carlsbad, CA, USA), followed by goat anti-mouse FITC-labeled IgG (1:50 dilution). All tissue slices were incubated with the first antibody for 16–20 h at 4°C and the second antibodies for 60 min at ambient temperature (23–24°C).

To delineate the cellular localization of glomerular proteins, double immunofluorescent labeling was performed. Primary antibodies were mixed as follows: (1) rabbit anti-human podocin antibody (as above) and mouse anti-ZO-1 (as above) and (2) anti-chicken cadherin (as above) and rabbit anti-laminin (basement membrane; cross-reacts with avian laminin). After washing with PBS, appropriate FITC- or TRITC-conjugated second antibodies were applied. The tissues were counter-stained by hematoxylin.

Because molecular sequences of avian junction proteins have not been identified, we used antibodies raised against mammalian proteins or a part of their sequences. We chose, however, antibodies that cross-react with proteins from chickens (close species to quail), such as *N*-cadherin, α -smooth muscle actin (SMA), and ZO-1, or confirmed the results with two different sources of antibodies (such as podocin). Also, we

confirmed by Western immunoblot that quail 'podocin' and 'N-cadherin' (glomerular lysate) that bind respectively to anti-human podocin and anti-human N-cadherin showed the bands expected for mammalian podocin and N-cadherin.²⁰ Also, the antibodies for basement membrane constituents such as laminin are very basic antibodies that react with various species.²⁰ α -SMA was measured immunohistochemically using α -SMA antibody raised against mouse clone IA4 (Sigma). α -SMA structure has high homology among species, including birds, and this antibody cross-reacts with chicken α -SMA. We used FITC-labeled goat anti-mouse IgG as second antibody.

To determine whether epithelial cell junction proteins were impaired, the fluorescent intensity of podocin signals was determined using a Keyence fluorescent microscope and cell count program. A total of 30–45 glomeruli was taken from three birds from each CT and EwW group on E15, D4 and D21; glomeruli (longitudinally sliced histological specimens) were selected that showed either urinary poles or vascular poles or both. Intensities were normalized by glomerular areas.

In vivo terminal 2'-deoxyuridine 5'-triphosphate (dUTP) nick-end labeling assay

Apoptosis in glomeruli was assessed using a terminal deoxynucleotidyl transferase-mediated dUTP-biotin nick-end labeling (TUNEL) method for counting DNA fragments.^{21,22} Paraffin-embedded tissue sections (4- μ m thick) were mounted on polylysine-coated glass slides (Matunami Glass, Osaka, Japan) and deparaffinized. TUNEL was carried out using dUTP-FITC according to the manufacturer's instructions (*In Situ* Cell Death Detection Kit Fluorescein; Roche Applied Science, Indianapolis, IN, USA).²¹ The sections were then stained with rhodamine-labeled wheat germ agglutinin lectin (Vector Laboratories, Burlingame, CA, USA) to identify the glomeruli. Nuclei were counter-stained with 4',6-diamidino-2-phenylindole dihydrochloride hydrate (DAPI; Vector Laboratories). In total, 20 glomeruli per section were examined using a fluorescence microscope, and TUNEL-positive cells in the glomeruli were counted. The mean number of positive staining nuclei per glomerulus was designated the glomerular TUNEL score.

Plasma glucose, insulin, creatinine, osmolality and electrolytes

Plasma glucose was measured by the hexokinase method wherein hexokinase plus adenosine triphosphate transforms glucose to glucose 6-phosphate (G-6-P) plus adenosine diphosphate; G-6-P is then reacted with nicotinamide adenine dinucleotide phosphate (NADP) and G-6-P dehydrogenase to form NADPH, which is measured spectrophotometrically.²³ Plasma insulin levels were determined by a chemiluminescent enzyme immunoassay using human insulin antibody.^{24,25} Plasma creatinine was measured by enzymatic analysis of creatininase-HMMPS (*N*-3-sulfopropyl-3-methoxy-5-metylaniline) in albumen (Wako kit; Osaka, Japan) and used as an index for glomerular filtration rate.

Plasma osmolality was measured by freezing-point depression, using Type OM-6030, 6050 and 6060 osmometers (Arkray Inc., Kyoto, Japan). Plasma electrolytes were determined using ionic electrodes and a Hitachi 7180 automated electrolyte analyzer (Hitachi High Technologies Inc., Tokyo, Japan).

Statistical analysis

All the data are shown as means \pm S.E. The effects of time and treatment and their interaction were examined using two-factor analysis of variance (ANOVA; JMP Pro 10 version 10.0.2d1). The difference between control and experimental groups was determined by Student's *t*-test (two-tailed) or the Tukey–Kramer method. The difference was considered significant at a *P* value of <0.05.

Results

Birth weight and body growth

Undernutrition reduced birth (hatch) weight significantly in Series A (15.2%) and in Series B (15.4%) (Fig. 1a). In Series C, the birth weight of EwW quail showed a tendency to be lower than that of CTs, but the difference was not significant. This is presumably because the time lag between hatch and measurement of birth weight in series C was larger in EwW groups and thus some chicks start to grow, whereas all CT birds hatched nearly simultaneously. Embryonic weights on E15, however, were significantly lower in EwW quail in both Series A and C (Fig. 1b). In all series, the hatching rate of EwW groups was low (CT quail 75–80%, EwW quail 5–10%). Interestingly, approximately half of the eggs that did not hatch contained considerably grown embryos, suggesting that reduced nutrition failed to provide a sufficient energy source to proceed with maturation and hatching. The glomerular sizes (areas) of EwW quail were significantly lower on D4 and D16–D18 than those of CTs in the superficial region (Fig. 1c) (considered as more newly developed glomeruli), whereas no significant difference was noted in the deeper regions.

Body growth was similar in both groups except at a few time-points when EwW birds showed slightly lower body mass (Fig. 2a). We measured body mass in all series (showed similar results), and the growth curve of Series B (longest duration) is shown. The body mass of female quail is higher, partly due to holding eggs, than that of male birds. There was no significant difference in kidney weights between CT and EwW quail (Fig. 2b).

Number of glomeruli during development and histological and histochemical observations

In both superficial (equivalent to cortex in mammalian kidney) and deeper regions (equivalent to juxtamedullary areas), the number of glomeruli was significantly lower in kidneys from young mature (3-week-old) EwW quail (Fig. 3a, Series A).

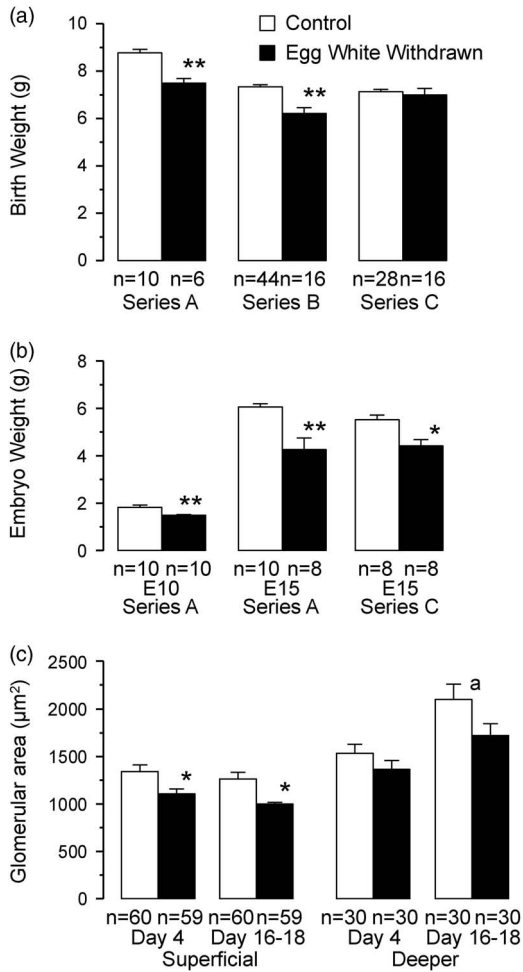


Fig. 1. Effects of reduced nutrition on birth weight (a) and embryo weight (b) of control and egg white withdrawn quail from Series A, B and C. (c) Glomerular size/area during postnatal maturation from Series C. E10 and E15 indicate embryonic day 10 and 15, respectively. * $P < 0.05$; ** $P < 0.01$ from control group; ^a $P < 0.01$ from control postnatal day 4 age group by Tukey–Kramer method.

For comparison, the reduction in the number of glomeruli in an earlier study¹⁵ is shown in Fig. 3b (4.5 weeks). In contrast, the number of glomeruli measured in longitudinally cut sections was similar between CT and EwW kidneys during development (E10, E15 and D2).¹⁵

Histological views of kidneys were similar in all three series examined, and representative views are shown in Fig. 4. In condensate surface areas of E15 kidneys (nephrogenic zone) from intact (Fig. 4a-1) and EwW quail (Fig. 4a-2), ureteric bud-like structures (Fig. 4b), undifferentiated dark-stained mesenchymal cell mass (Fig. 4b), and S-shaped body stage glomeruli (Fig. 4c) were seen in both CT and EwW. More mature glomeruli with clear capillary loops were also seen in E15 and D4 kidneys, and the number further increased with age. In E10 and E15 kidneys, the condensate nephrogenic zone areas were irregular and larger in EwW kidneys than in

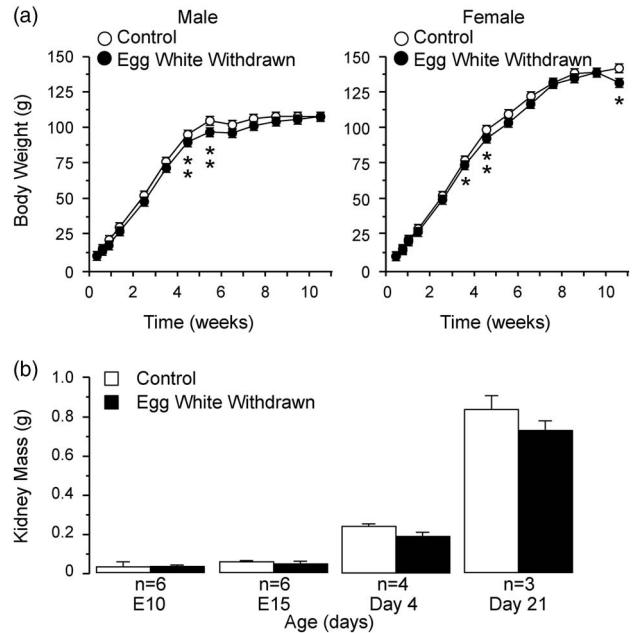


Fig. 2. Body mass of control and egg white withdrawn (EwW) quail (Series B, males and females) as index of body growth (a) and kidney weight (b, Series A). There was no obvious difference in body growth curve between the control and EwW groups except for a few term points when EwW quail showed lower body mass. Numbers of birds used for measurement of body mass are the following. Control: male, $n = 4-15$, female, $n = 19-28$; EwW: male, $n = 4-11$, female, $n = 3-7$. The numbers vary because birds are used for examinations on a periodic schedule. * $P < 0.05$; ** $P < 0.01$ from control group by Student's t -test.

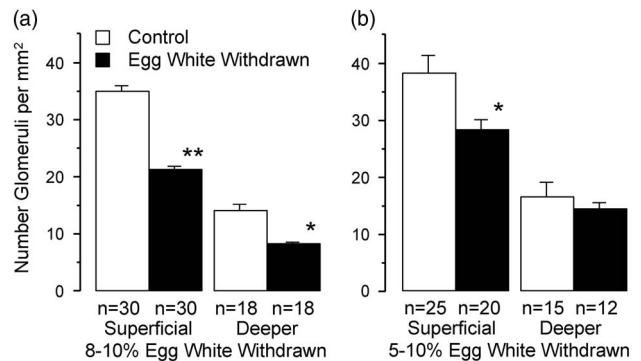
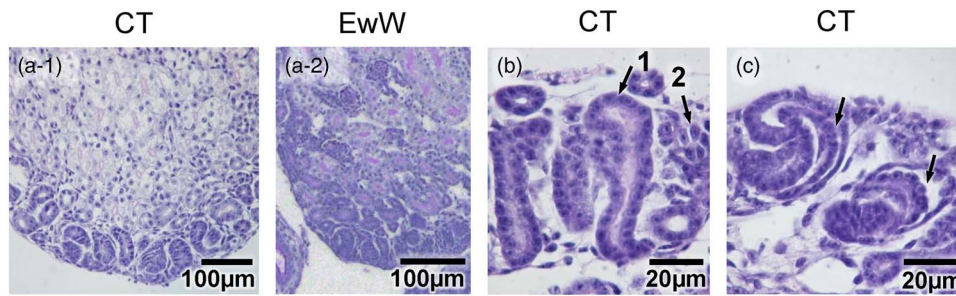


Fig. 3. The number of glomeruli in superficial (equivalent to cortical) and deeper (equivalent to juxtamedullary) regions of mature control and egg white withdrawn (EwW) quail kidneys counted in longitudinal histology sections. See Methods section for details of measurement. (a) The effect of 8–10% of EwW on the number of glomeruli (Series A). (b) For comparison, the result from previous studies¹⁵ done by the same method is shown (4.5 weeks). * $P < 0.05$; ** $P < 0.01$ from control group by Student's t -test.

CT ones (Fig. 4a-2) and mesonephros still remained in E15 and D4 EwW kidneys. Furthermore, the glomeruli were smaller in D4 EwW kidneys, particularly in the superficial area (less mature zone) (Fig. 1c).

E15 (Developing nephron)



5 weeks



10-21 weeks

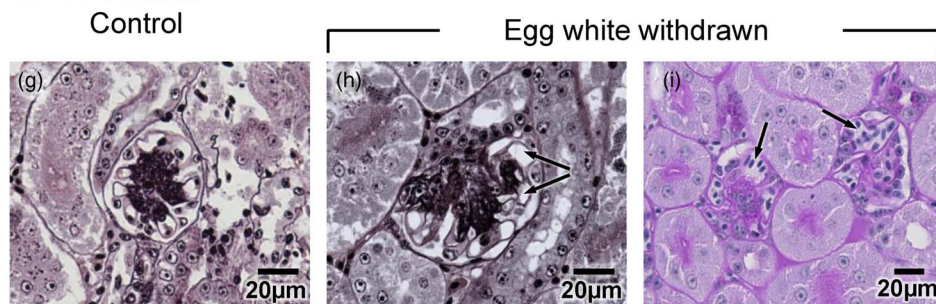
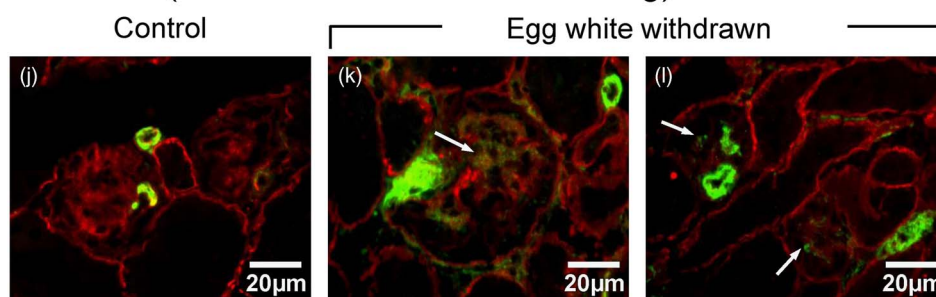
21 weeks (α -Smooth muscle actin staining)

Fig. 4. Histological views of glomeruli from embryonic day 15 (PAS staining), 5-week-old (PAS staining) and 10- to 21-week-old (PAM staining) quail, and immunofluorescent view of α -smooth muscle (SM) actin in 21-week-old quail. (a) Condensate nephrogenic surface area from control (CT, a-1) and egg white withdrawn (EwW, a-2) containing undifferentiated mesenchymal cells. (b) Ureter bud (arrow-1) and mesenchymal mass (arrow-2); (c) S-shaped developing glomerulus; arrow indicates developing podocytes. (d) Mature glomeruli from control quail. (e) Possible glomerulus and tubules that immaturely stopped growing in egg white withdrawn (EwW) quail. (f) Expanded mesangial cells (deeper zone) from EwW quail with accumulation of lightly PAS-stained materials (arrows). (g) Glomerulus from control quail (21 weeks) with well-developed loop structure and Bowman's capsule; PAM staining. (h) Enlarged glomerulus from EwW quail (21 weeks) with enlarged mesangium region; arrows indicate fused capillary loop space. (i) Glomeruli from EwW quail (10 weeks); PAS staining. Capillary loop structures are not clearly seen. Arrows indicate giant fused loops. (j) Immunoreactive α -SM actin staining of control glomeruli. Small arterioles show positive staining. (k and l) Positive α -SM actin staining in arterioles and glomerular mesangium (arrows) in EwW quail.

In 5-week-old CT kidneys, glomeruli showed distinct Bowman's space and capillary loops and PAS-positive mesangium (Fig. 4d). In contrast, 5-week-old EwW kidneys revealed, in superficial regions, cell proliferation areas consisting of undifferentiated cell mass (Fig. 4e). Some of these masses appeared to contain incompletely differentiated glomeruli and renal tubules. Furthermore, after maturation, glomeruli in the deeper zone were larger in EwW kidneys (Fig. 4f), and mesangial cells were frequently expanded and contained substances only lightly stained with PAS (Fig. 4f, arrows). In 10- to 21-week-old or older EwW quail, glomeruli were often irregular in shape and larger than those of CTs in deeper areas (Fig. 5). The mesangial areas contained PAM-positive (also laminin-positive) substance and were larger in EwW kidneys (Fig. 4g and 4h). Fused giant loops were often seen (Fig. 4h and 4i, arrows). Possible adhesion between Bowman's capsule and capillary loops was also seen (Fig. 4i).

We examined α -SMA using an antibody that cross-reacts with avian α -SMA. SMA was clearly seen in the blood vessels from 21-week-old quail kidneys (Fig. 4j, 4k and 4l). In addition, the mesangium from EwW quail, but not from CT quail, showed immunoreactive SMA (Fig. 4k and 4l, arrows).

Size of glomeruli and mesangium

Glomerular size (area, μm^2) and mesangium size (area, μm^2) were measured in longitudinally cut and PAM-stained slices, using a Keyence HS All-in-One Fluorescence Microscope BZ-9000 (Dynamic Cell Count BZ-H1C) (Fig. 5). We selected well-shaped glomeruli showing vascular poles, urinary poles or both. In deeper regions of medullary cones, glomerular size and mesangial areas significantly increased with maturation/aging (5, 21, 63 weeks) (ANOVA, time effect). Also, glomerular size and mesangial areas were significantly larger in the EwW quail than in the CTs (ANOVA, treatment effect). In superficial areas, glomeruli also increased in size with aging, but the treatment effect was not as clear as in deeper regions. In the neonatal to early maturation period (D4 to D17–D18), in contrast, the glomerular size was smaller in EwW quail (Fig. 1c).

EM observations

In the developing stage of CT glomeruli, the basal membrane was thin or irregular (Fig. 6a and 6b). Glomeruli from the EwW group also showed similar findings. Podocyte foot processes (FPs) often had irregular width (Fig. 6d–6h), and the cell junction complex was seen away from the basal membrane (Fig. 6a–6d) (arrows). In glomeruli that had distinct capillary loops, podocytes with well-developed FPs and slit diaphragms (Fig. 6e, 6f and 6j) and mesangium in the center area were seen (Fig. 6g and 6m). The regularity of the FPs increased with maturation in both CT and EwW kidneys. In EwW kidneys, vacuoles in the mesangium and podocytes (Fig. 6g), thin tall podocyte FPs (Fig. 6h and 6l), and basal membranes with irregular width (Fig. 6h) were seen. In EwW quail glomeruli, capillary loops were sometimes disrupted (Fig. 6k) or merged and showed ballooning. Mesangial areas

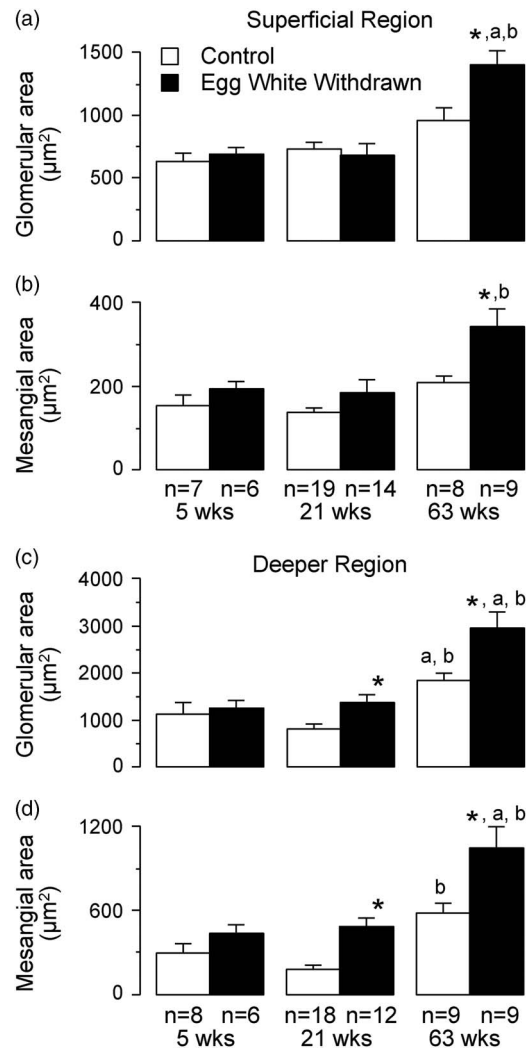


Fig. 5. Glomerular area (size) and mesangial area of superficial (a, b) and deeper (c, d) regions from 5-, 21-, and 63-week-old quail kidneys [n = number of glomeruli from three birds per age per each control (CT) and egg white withdrawn (EwW) group] (Series B). Areas were measured using a Keyence fluorescent microscope and cell count program in longitudinally cut histology specimens (PAM staining) using well-shaped glomeruli with either vascular poles or urinary poles or both. In deeper regions, glomerular size and mesangial areas showed significant time- and treatment-dependent effects (ANOVA), whereas in superficial regions the difference between CT and EwW groups is clear only in 63-week-old quail kidneys. * $P < 0.05$ from control group. Significantly higher ($P < 0.05$) than 5 weeks (a) and 21 weeks (b) controls.

were enlarged and contained cellular constituents with apparently complex interdigitation between mesangial processes and matrix and endoplasmic reticulum (Fig. 6n and 6o).

Junction protein markers

Immunoreactive podocin during kidney development (E10), double-staining of immunoreactive *N*-cadherin and laminin,

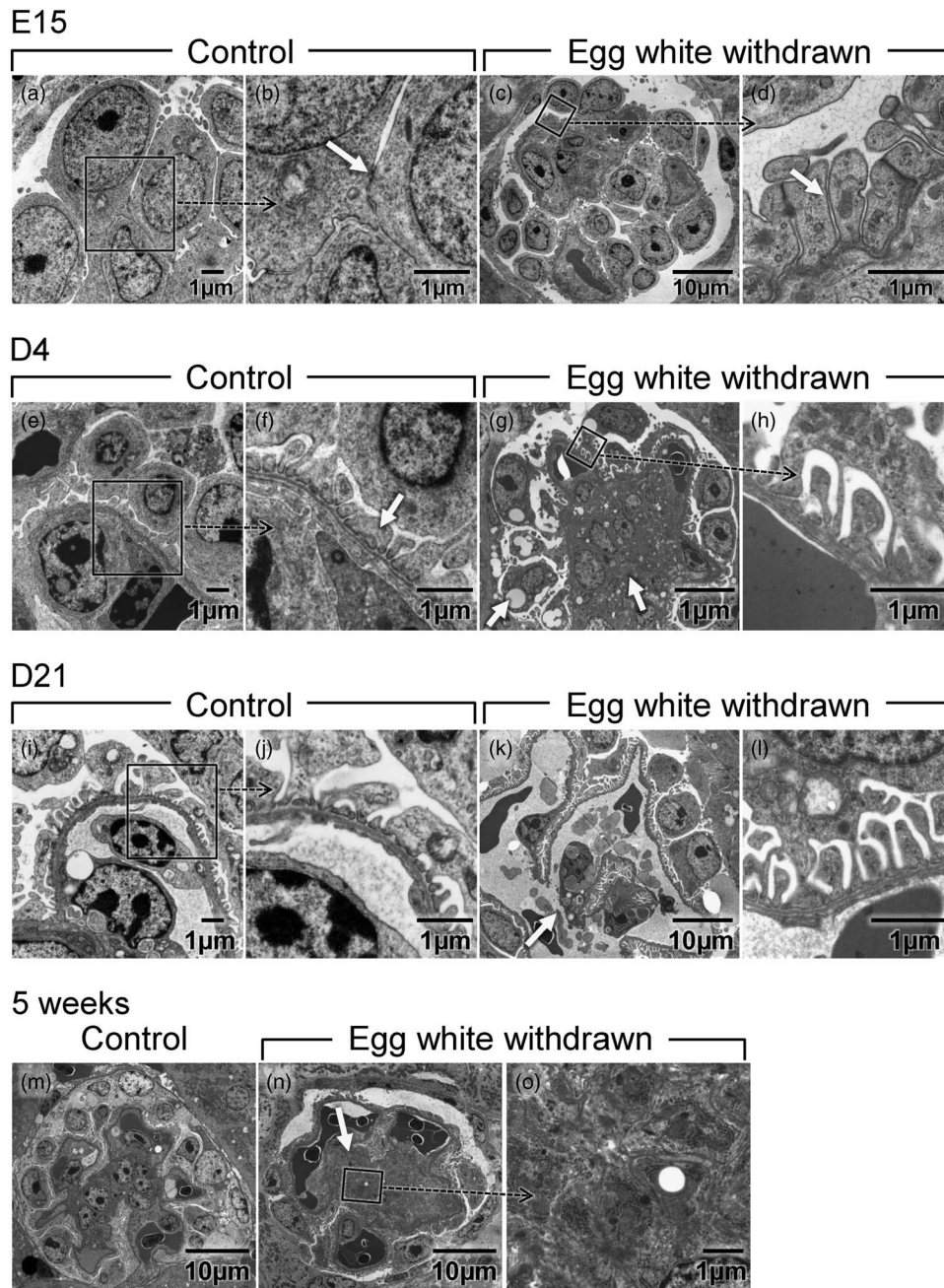


Fig. 6. Electronmicroscopic views of glomeruli from embryonic day 15, postnatal day 4 (D4), D21, and 5-week-old quail from control and egg white withdrawn (EwW) groups. (b) is enlarged framed area from (a). Arrow in (b) shows cell junction apart from basement membrane. (d) is enlarged from (c) (framed) and shows well-developed foot processes (FPs) of podocytes with attachment to adjacent FP (arrow). Similarly, (f) and (h) are expanded areas from (e) and (g), respectively. (f) shows irregularly sized and fused FPs (arrow). In (g), numerous vacuoles are seen in the mesangial area (arrow) and some in podocytes. (i) and (j) [Enlarged from (i)] show well-developed FPs. In (k), arrow shows disrupted capillary loop and thin FPs in (l). (n) and (o) (expanded) indicate enlarged mesangium in EwW quail as compared to that of controls (m). For detailed observations, see Results section.

and podocin and ZO-1 of young adult quail are shown in Fig. 7. Glomeruli of mesonephric kidneys were large in CT (Fig. 7a) and EwW kidneys (not shown), and podocin staining was seen along the capillary loops (Fig. 7a). In metanephric kidneys from E15 quail, podocin was expressed in glomeruli

of the S-shaped body stage from both CT (Fig. 7b) and EwW groups. In mature glomeruli double-stained with podocin and ZO-1, immunoreactive podocin signals were seen as a continuous spot along capillary loops beneath the glomerular capsule outside the ZO-1 staining that is presumably

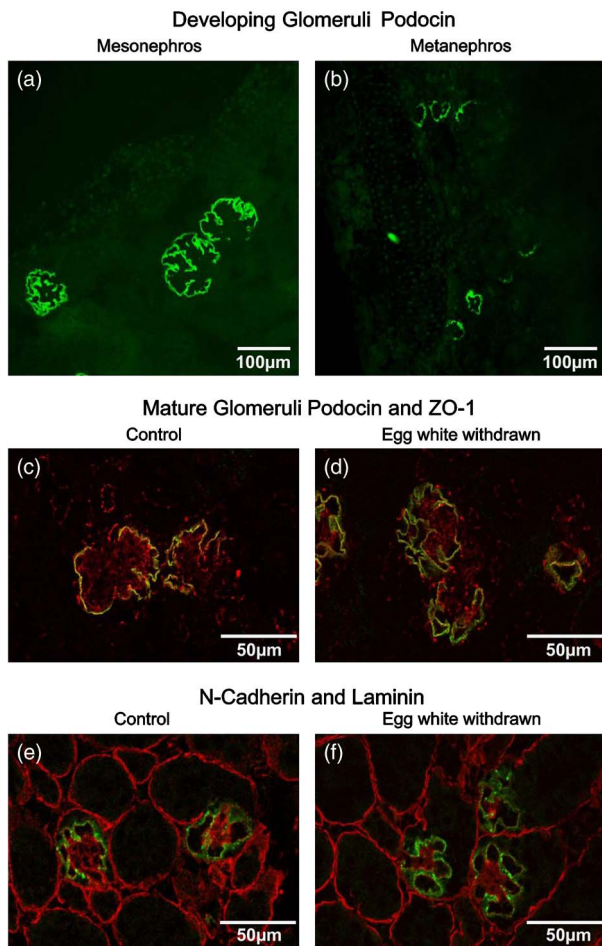


Fig. 7. Immunofluorescent views of junction proteins. Podocin staining (FITC green) of large mesonephric (a) and developing metanephric (b) glomeruli from embryonic day 15 kidney from control (CT) group. (c) (CT) and (d) [egg white withdrawn (EwW)] are podocin (FITC green) and ZO-1 (TRITC red) double-staining of mature glomeruli from young adult quail. (e) (CT) and (f) (EwW) show *N*-cadherin (FITC) and laminin (TRITC) double-staining examined by confocal microscope (A1Rsi; Nikon; Tokyo, Japan). See Methods section for antibodies and staining conditions. For detailed observation, see Results section.

basement membrane. There were no apparent differences in location and intensity of podocin staining between CT and EwW kidneys (Fig. 7c and 7d). In both groups, *N*-cadherin was strongly expressed in the superficial mesenchymal cell area (nephrogenic zone) and in the podocytes of S-shaped glomeruli and early capillary stage of metanephric glomeruli. *N*-cadherin staining was restricted to the capillary loop (podocytes) membrane immediately outside the basement membrane stained by laminin (Fig. 7e and 7f). There was no obvious difference between CT and EwW birds in terms of distribution and staining of *N*-cadherin. Clear laminin staining was seen in the mesangial area.

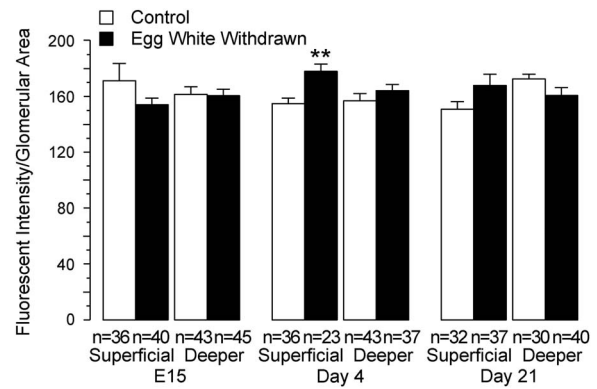


Fig. 8. Fluorescent intensity of podocin signals determined by Keyence fluorescent microscope and cell count program in a total of 30–45 glomeruli from three birds from each control and egg white withdrawn group at embryonic day 15, postnatal day 4 (D4), and D21. Intensity was normalized by glomerular area in each glomerulus. ** $P < 0.01$ from control group by Student's *t*-test.

The fluorescent intensity of podocin signals determined by using a Keyence fluorescent microscope and cell count program is summarized in Fig. 8. There were no significant differences in intensity between CT and EwW groups in the superficial and deeper zones in three age groups (E15, D4 and D21) except in the D4 superficial area.

Apoptosis

Apoptotic cells identified by TUNEL analysis are shown in Fig. 9a (upper panel). In all, 20 glomeruli were randomly selected from each CT and EwW group at three stages (E15, D4, D17–D18). The number of TUNEL signals (DNA fragment) per glomerulus was significantly higher in EwW than in CT groups on E15 (Fig. 9a, upper and lower panels) and D4 (Fig. 9a). The apoptosis level became lower with maturation in both groups, and no difference was noted between CT and EwW groups on Day 17–18.

Plasma corticosterone, glucose, insulin, creatinine, osmolarity and electrolytes

Plasma levels of corticosterone (major glucocorticoid in birds) determined by radioimmunoassay are shown in Fig. 9b. Data from Series A, B and C were combined. On D4, the glucocorticoid level was significantly higher in EwW quail. The level became lower on D17–D18, and no difference was noted between groups on D17–D18. Plasma levels of glucose (mg/dl) were high, but no significant differences were noted between CT and EwW groups on D4 (CT: 299.6 ± 12.9 , $n = 7$; EwW: 269.3 ± 20.3 , $n = 7$), on D17–D18 (CT: 331.6 ± 9.1 , $n = 10$; EwW: 370.9 ± 8.6 , $n = 8$), or at 63 weeks (CT: 319.8 ± 8.2 , $n = 4$; EwW: 337.8 ± 14.4 , $n = 4$) of age. Plasma levels of immunoreactive insulin (μ IU/ml) on D4 (CT: 1.96 ± 0.30 , $n = 5$; EwW: 2.80 ± 0.79 , $n = 3$) were higher than those on D17–D18 (CT: 1.19 ± 0.19 , $n = 10$, $P < 0.01$;

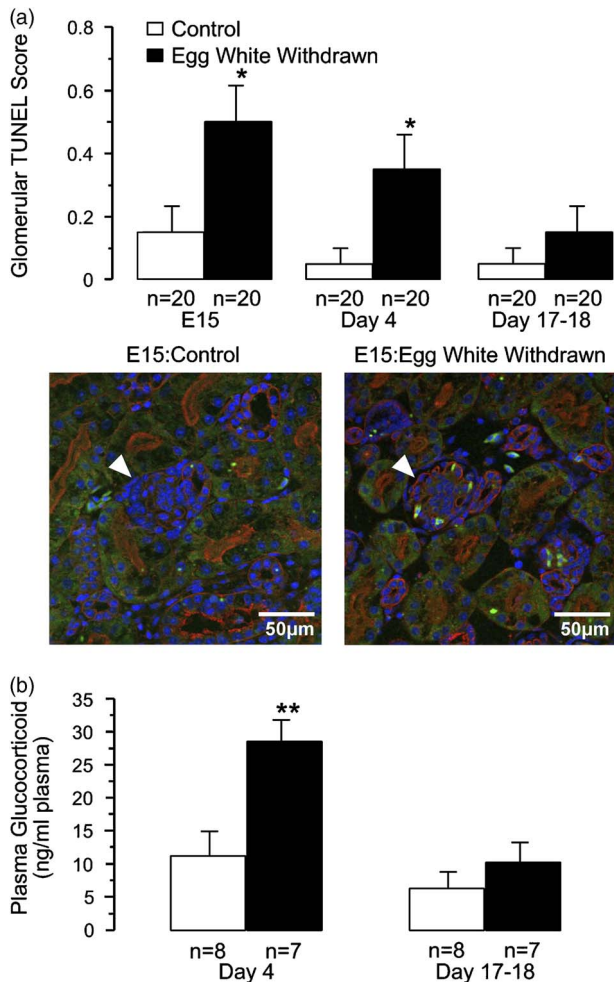


Fig. 9. (a) Glomeruli with positive terminal deoxynucleotidyl transferase-mediated dUTP-biotin nick-end labeling (TUNEL) marker that indicates possible apoptotic changes. In total, 20 glomeruli were randomly selected from control (CT) and egg white withdrawn (EwW) quail kidneys in three age groups each. Positive TUNEL signals (DNA fragments) in each glomerulus was counted, and the mean number of positive stainings per glomerulus is shown as the glomerular TUNEL score. Examples of TUNEL signals from embryonic day 15 CT and EwW kidneys are shown. Arrow head: glomerulus; bright green: TUNEL staining; red: wheat germ agglutinin lectin staining; blue: 4',6-diamidino-2-phenylindole dihydrochloride hydrate staining for nuclei. (b) Plasma glucocorticoid (corticosterone) determined by radioimmunoassay in developing quail at days 4 and 17–18. The minimum detection limit of the assay, defined as the apparent concentration at 95% B/B0 in the standard curve, was 3.0 ng/ml. No sample showed levels of corticosterone exceeding the maximum detection limit. * $P < 0.05$; ** $P < 0.01$ from control group, Tukey–Kramer method.

EwW: 0.92 ± 0.09 , $n = 7$, $P < 0.05$), but no significant difference was noted between CT and EwW groups. Likewise, no differences in levels of plasma electrolytes, osmolality or creatinine were seen between CT and EwW groups at 3, 5, 10, 21 and 63 weeks of age (Table 1).

Discussion

Kidney development

The current study agrees with the general view of the avian kidney developmental stages of pro-, meso- and metanephric kidneys.²⁶ We also noted the developmental process of avian glomeruli, including a ureteric buds stage, S-shaped body stage and capillary loop stage.²⁶ The lower embryonic weights, smaller glomeruli and longer retention of mesonephric kidney seen in developing EwW groups indicate that EwW birds developed more slowly than CT birds. We reported previously¹⁵ that nephrogenesis continues after birth in the superficial condensate area consisting of mesenchymal cells; this nephrogenic zone was reduced in time-dependent fashion for ~3 weeks in CT quail. Also, at E10, embryos from the EwW group had wider nephrogenic zones ($20.4 \pm 1.3\%$ of medullary cone) than the CT group did ($10.1 \pm 2.4\%$, $P < 0.01$)¹⁵ (also, Fig. 4a-1 and 4a-2 in the present study); this difference was gone after hatch (D2), suggesting that in spite of delayed development, nephrogenesis was active in EwW birds. As we reported previously, surface glomeruli are smaller; and more mature, larger glomeruli are seen toward the deeper regions.¹⁵

Effects of reduced nutrition during development and possible evidence of programming

Studies by Barker *et al.*^{27,28} and numerous other epidemiological studies have indicated a strong inverse relationship between birth weight and the risk of coronary heart disease, hypertension, type 2 diabetes and other diseases in adulthood.^{1–3} It is postulated that insufficient nutrient availability during gestation may lead to developmental adaptations and that a number of organ structures and functions undergo programming during embryonic and fetal life via hormonal influences.^{29–30} These adaptive measures have short-term benefits to the embryo and fetus, but subsequent catch-up growth may create metabolic conflicts that predispose the adult to increased risks of adult disease susceptibility, including obesity.^{29–30} Also, catch-up growth immediately after early malnutrition may program postprandial hyperleptinemia.³¹ A kidney with a reduced number of nephrons would have less renal reserve to adapt to dietary excesses or to compensate for renal injury.³ Impairment of nephrogenesis, renal sodium transport, the renin–angiotensin system, glucocorticoid levels (excessive increase) and the sympathetic nervous system appear to play a critical role in this fetal programming of adult diseases.^{32,4–6}

We used a bird model because embryonic growth during incubation for hatching occurs with a predetermined nutrition source devoid of direct influence from maternal nutrition or circulation. In rodents and other mammals,^{1,33} reduced fetal nutrition is induced by decreasing the mother's nutrition. The fetus is accordingly exposed to the metabolic and hormonal changes of the mother in addition to the effect of low nutrition. Also in birds, environmental factors such as temperature and humidity are well controlled during incubation.

Table 1. Plasma osmolality, electrolytes and creatinine in control and egg white withdrawn

| Groups | Age | Osmolality (mOsm/l) | Na (mEq/l) | K (mEq/l) | Cl (mEq/l) | Creatinine (mg/dl) |
|---------------------|------------------------|---------------------|-------------|-----------|-------------|--------------------|
| Control | 3 weeks, <i>n</i> = 4 | | | | | 0.12 ± 0.01 |
| Egg white withdrawn | | | | | | |
| Control | 5 weeks, <i>n</i> = 3 | 324.0 ± 2.3 | 146.5 | 7.0 | 116.0 | 0.21 ± 0.04 |
| Egg white withdrawn | 5 weeks, <i>n</i> = 3 | 313.0 ± 8.2 | 140.5 | 5.8 | 109.0 | 0.26 ± 0.04 |
| Control | 10 weeks, <i>n</i> = 3 | 351.3 ± 28.8 | 151.3 ± 2.3 | 7.4 ± 0.6 | 122.0 ± 1.2 | 0.13 ± 0.05 |
| Egg white withdrawn | 10 weeks, <i>n</i> = 3 | 330.0 | 149.0 | 5.40 | 119.0 | 0.20 ± 0.09 |
| Control | 21 weeks, <i>n</i> = 3 | 339.3 ± 10.1 | 146.7 ± 1.2 | 6.4 ± 0.7 | 113.7 ± 1.7 | 0.14 ± 0.003 |
| Egg white withdrawn | 21 weeks, <i>n</i> = 3 | 325.3 ± 2.7 | 148.7 ± 1.3 | 6.1 ± 0.6 | 112.7 ± 1.5 | 0.14 ± 0.03 |
| Control | 63 weeks, <i>n</i> = 4 | 318.8 ± 6.8 | 148.5 ± 2.2 | 5.7 ± 0.3 | 114.8 ± 2.8 | 0.16 ± 0.01 |
| Egg white withdrawn | 63 weeks, <i>n</i> = 4 | 325.5 ± 3.8 | 151.8 ± 3.6 | 5.9 ± 0.5 | 120.3 ± 4.1 | 0.13 ± 0.01 |

Values are means ± S.E. Those without S.E. indicate mean of *n* = 2.

Furthermore, the present study indicates that so-called 'fetal programming' is not limited to mammalian species, but may be a phylogenetically important biological process.

The current study suggests that reduced nutrition during incubation causes delayed maturation and structural alteration of the quail kidney that are likely to program nephron disorders such as nephrosclerosis. The evidence includes (1) embryos were smaller and showed delayed embryonic growth and a lower hatching rate. The possible delay in kidney development agrees with the inhibition of ureteric bud branching in rats whose mothers had restricted nutrition.³⁴ (2) The size of glomeruli in developing kidneys in the superficial area of EwW quail was smaller than that in CT kidneys. Birth (hatch) weight was smaller in most birds, but body growth soon caught up, as seen in the 'catch-up growth' of mammals.^{29–31,35} (3) The number of glomeruli was lower in the mature EwW group, particularly in the superficial region, agreeing with our previous results¹⁵ and with studies in mammals.^{4,5} In contrast, the number of glomeruli was similar in the two groups during development,¹⁵ but the nephrogenic zone area was larger in low-nutrition quail. (4) The number of TUNEL signals in glomeruli was higher in EwW than in CT groups during the perinatal period, suggesting that more apoptosis takes place in nutrition-reduced kidneys. Therefore, although nephrogenesis actively occurs, apoptosis in glomeruli may exceed development/maturation in EwW quail, resulting in the reduced number of glomeruli after maturation by programming. (5) At 5 weeks of age (young adult), but not earlier, the mesangial cells of some EwW glomeruli frequently contain lightly PAS-positive edematous substance; and the capillary loops merge, forming giant loops partly similar to those seen in human nephrosclerosis.¹¹ Furthermore, undifferentiated cell masses are seen in 5-week-old EwW quail kidney (Fig. 4e); we hypothesize that the biological clock for terminating nephrogenesis remains the same in growth-retarded kidneys as in CT kidneys. Immature glomeruli may lead to fibrotic degeneration in later life. The glomeruli of EwW quail became significantly larger with aging, suggesting hypertrophy compensating for the reduced number of glomeruli. This agrees with mammalian

studies showing that overloading of the remaining nephrons causes compensatory enlargement and hyperfiltration.³

Role of mesangium in reduced nutrition-induced renal injury

In the nutrition-reduced group, we noted changes in the mesangium, such as vacuoles, edematous appearance, positive α -SMA, and proliferation/enlargement. It has been shown that glomerular cell death and accumulation of extracellular matrix correlate with the progress of nephrosclerosis and deterioration of renal function.²² Extracellular matrix supports mesangial cell function and survival, and alteration in its constituents increases the susceptibility of mesangial cells to micro-environmental changes that lead to mesangial cell apoptosis and glomerular scarring. Also, the glomerular basement membrane and contractile mesangial cells establish a biomechanical unit that develops wall tension in the glomerular capillaries.^{36,37} It is thus possible that incomplete mesangial-basement membrane structure due to insufficient development in EwW quail may lead to the failure of the biomechanical unit, particularly in young birds, when blood pressure and thus glomerular hydrostatic pressure rapidly increase.³⁸ It has been reported that mesangial flow (interstitial fluid in glomerulus) plays a role in the maintenance of mesangial structure and that function and flow disruption induced by occlusion of renal lymphatic and/or venous flow lead to mesangial and glomerular injury³⁹ and aging.⁴⁰

In human nephrosclerosis, detachment of podocytes from the glomerular basement membrane seems to be the major mechanism of podocyte loss.⁴¹ In the present study, histological or EM examination of EwW quail kidneys showed no clear morphological changes in podocytes, whereas ballooning or deformation of capillary loops was seen in EwW kidneys. Podocin and *N*-cadherin signals were expressed in mesonephros and metanephros, but no clear difference was noted in fluorescent visualization of signals between CT and EwW quail. Fluorescent intensity of podocin showed no difference between CT and experimental groups or among age groups,

suggesting that cell junction proteins are unlikely to be impaired in the quail model of renal injury due to reduced nutrition. Immunoreactive podocin in quail kidneys was also confirmed using rabbit anti-podocin antibody (kindly provided by Dr. H. Tsukaguchi; Kansai Medical University; Osaka, Japan) raised against a synthetic peptide comprising the 17 carboxy-terminal amino acids of human podocin.²⁰ Expression and distribution were similar to those in the present study. Genomic analysis revealed that the developing chick genome lacks nephrin and nephroproteins, whereas the structure of the slit diaphragms of podocyte FPs is maintained.⁴²

In the present study, plasma levels of creatinine (measured as an index for glomerular filtration rate), electrolytes and osmolality are similar between CT and EwW quail, suggesting that renal function is not impaired at this stage in spite of morphological injury of glomerular mesangium.

Mechanism of fetal programming

Two primary processes that drive programming are structural alteration and epigenetic changes in gene expression. Structural alteration includes low numbers of nephrons due to retarded development or to increased apoptosis, low numbers of cardiomyocytes and low deposition of elastin, leading to weak vascular walls.^{32,43} Intrauterine environmental changes (some may be permanent) trigger epigenetic changes⁴⁴ that lead to modification of gene expression rather than changes in the DNA sequence or genetic code. DNA methylation can affect genome stability, viability, expression and imprinting. Several factors that trigger such changes include impaired maternal–fetal nutrition (deficit or excess), hypoxia, exposure to excess glucocorticoid and impaired placental function, such as reduced blood flow and low nitric oxide level.^{4,32,33,43} Such epigenetic modifications remain to be studied in the quail model.

We noted that neonatal EwW quail plasma corticosterone (major adrenocorticoid in birds that has both gluco- and mineralocorticoid actions) levels are also higher. It is possible that the impaired nutrition and low-energy source may be compensated by increased adrenocorticoid hormones. In humans, plasma cortisol levels were found to be higher; and the levels increased more in response to adrenocorticotrophic hormone stimulation in the LBW group compared with the normal birth weight group, suggesting that prenatal programming of the hypothalamic–pituitary–adrenal (HPA) axis may be a fundamental mechanism underlying the development of metabolic syndrome in populations with LBW.^{3,45,46} Elevation of adrenal steroid hormones may also be a fetal response to stressful conditions such as insufficient nutrition or hypoxia. Prenatal stress and maternal exposure to glucocorticoid may lead to permanent modification of the HPA axis, possibly due to an impaired negative feedback mechanism,⁴⁷ possibly via effects on the epigenome.^{45,46} Prenatal exposure to increased glucocorticoid affects development of the fetal brain, neurotransmitter system and behavior.⁴⁸

Plasma levels of glucose in birds are in general higher than in other vertebrates of similar body size.⁴⁹ In the present study, we

also noted that plasma glucose levels are over 300 mg/dl in both CT and EwW quail, whereas immunoreactive insulin levels are low in both the neonatal and maturing periods. We anticipated that plasma glucose levels would be higher in nutrition-reduced quail for energy supplementation, as shown in mammals.^{1,8} No differences in plasma glucose or insulin levels were seen, however, between the CT and EwW groups. It has been reported⁴⁹ that plasma insulin levels in birds are about one-tenth of those in rats, supporting the observation of lower numbers of β -cells in the avian pancreas; the reported levels agree with our current observation.

Recent studies show that an increased incidence of non-diabetic obesity in children is often associated with glomerulopathy, including glomerular hyperfiltration and renal injury, such as glomerulomegaly, mesangial expansion and nephrosclerosis.⁵⁰ It is not clear, however, whether these findings or the increase in FSGS is linked to the increased incidence of LBW or prematurely born babies. Niigata University Pediatric Department's Nephrology Group, with which the authors collaborate, reported¹¹ that of 16 children diagnosed with secondary FSGS by renal biopsy, 37.5% had LBW; LBW may be deemed a risk factor for FSGS and also a means of its early discovery. The results from the present animal experiments support these clinical observations.

Summary and perspectives

Major findings in Japanese quail include (1) undernutrition delayed embryonic growth and reduced the birth weight; (2) young adults exposed to reduced nutrition during development had a lower number of glomeruli due in part to increased apoptosis; and (3) glomeruli, specifically mesangium from undernutrition quail, were expanded with accumulation of laminin-positive substance, whereas podocyte junction proteins remained positive. This suggests that undernutrition may initially trigger the structural changes in the glomerular mesangium, possibly leading to nephrosclerosis. It remains to be determined whether hyperfiltration and increased glomerular pressure due to progressively rising blood pressure during maturation³⁸ cause mesangial injury and subsequent inflammatory responses in incompletely developed glomeruli or in those that have developmental defects such as lack of normal mesangial constituent substances. Particular attention may be needed to examine injury at the mesangial angles^{37,51} of the glomerular capillary loop where the capillary wall directly faces the mesangium without a glomerular basement membrane and podocyte FPs. Our attempt to measure glomerular filtration rate by inserting a fine catheter chronically in aortae and veins of quail to see whether a low number of glomeruli affects renal function⁵² was halted due to considerable distress of the birds such as weight loss, limping and restricted movement. In a previous study,¹⁵ we reported that EwW quail lost significantly more body mass by water restriction, suggesting impaired water homeostasis.

Although the current study does not show a difference in blood glucose and insulin levels between CT and EwW quail,

further time-course study of catch-up growth^{30,35} is necessary. Indeed, preterm birth is a global problem that needs greater attention from policymakers, researchers, health care providers, the media, donor organizations and other stakeholders.

Acknowledgments

The authors thank Michiko Igashima and Harumi Kogami for excellent technical assistance in histology, Dr. Toshio Shimada for help in measurement of plasma corticosterone. Preliminary studies were presented at the Council for High Blood Pressure Research, Orlando, FL, 2011. The authors are entirely responsible for the scientific content of the manuscript.

Financial Support

This work was supported by the Ministry of Education, Culture, Sports, Science and Technology, Japan (H.N., Grant-in-Aid for Scientific Research No. 21390307).

Conflicts of Interest

None.

Ethical Standards

The authors assert that all procedures contributing to this work comply with the ethical standard of the relevant national guides of the care and use of laboratory animals (Japanese quail, *Coturnix Japonica*). Animal protocols were reviewed and approved by the Institutional Animal Care and Use Committee of the Niigata University Graduate School of Medical and Dental Sciences, Niigata, Japan and University of Tennessee Health Science Center.

References

- Fowden AL, Giussani DA, Forhead AJ. Intrauterine programming of physiological systems: causes and consequences. *Physiology*. 2006; 21, 29–37.
- Ingelfinger JR, Woods LL. Perinatal programming, renal development, and adult renal function. *Am J Hypertens*. 2002; 15, 46S–49S.
- Luyckx VA, Brenner BM. Low birth weight, nephron number, and kidney disease. *Kidney Int Suppl*. 2005; 68, S68–S77.
- Baum M. Role of the kidney in the prenatal and early postnatal programming of hypertension. *Am J Physiol Renal Physiol*. 2010; 298, F235–F247.
- Manning J, Vehaskari VM. Postnatal modulation of prenatally programmed hypertension by dietary Na and ACE inhibition. *Am J Physiol Regul Integr Comp Physiol*. 2005; 288, R80–R84.
- Moritz KM, Dodic M, Wintour EM. Kidney development and the fetal programming of adult disease. *BioEssays*. 2003; 25, 212–220.
- Ojeda NB, Grigore D, Alexander BT. Intrauterine growth restriction: fetal programming of hypertension and kidney disease. *Adv Chronic Kidney Dis*. 2008; 15, 101–106.
- Portha B, Chavey A, Movassat J. Early-life origins of type 2 diabetes: fetal programming of the beta-cell mass. *Exp Diabetes Res*. 2011; article ID 105076, 16 pages.
- Burdge GC, Lillycrop KA. Nutrition, epigenetics and developmental plasticity: implications for understanding human disease. *Annu Rev Nutr*. 2010; 30, 315–339.
- Gluckman PD, Hanson MA, Buklijas T, Low FM, Beedle AS. Epigenetic mechanisms that underpin metabolic and cardiovascular diseases. *Nat Rev Endocrinol*. 2009; 5, 401–408.
- Ikezumi Y, Suzuki T, Karasawa T, et al. Low birthweight and premature birth are risk factors for podocytopenia and focal segmental glomerulosclerosis. *Am J Nephrol*. 2013; 38, 149–157.
- Prelipcean A (Teusan), Prelipcean AA, Teusan V. Investigations on the structure, chemical composition and calorificity of the quail eggs, deposited at the plateau phase of the laying period. *Lucrari Stiintifice Seria Zootehnie*. 2014; 57, 113–120.
- Miwa T, Nishimura H. Diluting segment in avian kidney. II. Water and chloride transport. *Am J Physiol Regul Integr Comp Physiol*. 1986; 250, R341–R347.
- Nishimura H, Koseki C, Imai M, Braun EJ. Sodium chloride and water transport in the thin descending limb of Henle of the quail. *Am J Physiol Renal Fluid Electrolyte Physiol*. 1989; 257, F994–F1002.
- Nishimura H, Yang Y, Lau K, et al. Aquaporin-2 water channel in developing quail kidney: possible role in programming adult fluid homeostasis. *Am J Physiol*. 2007; 293, R2147–R2158.
- Kihara I, Yaoita E, Kawasaki K, et al. Origin of hyperplastic epithelial cells in idiopathic collapsing glomerulopathy. *Histopathology*. 1999; 34, 537–547.
- Koda R, Zhao L, Yaoita E, et al. Novel expression of claudin-5 in glomerular podocytes. *Cell Tissue Res*. 2011; 343, 637–648.
- Yaoita E, Yao J, Yoshida Y, et al. Up-regulation of connexin43 in glomerular podocytes in response to injury. *Am J Pathol*. 2002; 161, 1597–1606.
- Nakatsue T, Koike H, Han GD, et al. Nephron and podocin dissociate at the onset of proteinuria in experimental membranous nephropathy. *Kidney Int*. 2005; 67, 2239–2254.
- Yaoita E, Nishimura H, Nameta M, et al. Adherens junction proteins in glomerular podocytes of quail kidney. *J Histochem Cytochem*. 2016; 64, 67–76.
- Satoh M, Matter CM, Ogita H, et al. Inhibition of apoptosis-regulated signaling kinase-1 and prevention of congestive heart failure by estrogen. *Circulation*. 2007; 115, 3197–3204.
- Sugiyama H, Kashihara N, Makino H, Yamasaki Y, Ota Z. Apoptosis in glomerular sclerosis. *Kidney Int*. 1996; 49, 103–111.
- Neese JW, Duncan P, Bayse D, et al. Development and evaluation of a hexokinase/glucose-6-phosphate dehydrogenase procedure for use as a national glucose reference method. *HEW Publication No. (CDC) 77-8330*. 1976. Center for Disease Control: Atlanta, GA.
- Dupont J, Dagou C, Derouet M, Simon J, Taouis M. Early steps of insulin receptor signaling in chicken and rat: apparent refractoriness in chicken muscle. *Domest Anim Endocrinol*. 2004; 26, 127–142.
- Nishizono I, Iida S, Suzuki N, et al. Rapid and sensitive chemiluminescent enzyme immunoassay for measuring tumor markers. *Clin Chem*. 1991; 37, 1639–1644.
- Davey MG, Tickle C. The chicken as a model for embryonic development. *Cytogenet Genome Res*. 2007; 117, 231–239.
- Barker DJP, Eriksson JG, Forsen T, Osmond C. Fetal origins of adult disease: strength of effects and biological basis. *Int J Epidemiol*. 2002; 31, 1235–1239.

28. Barker DJ, Winter PD, Osmond C, Margetts B, Simmonds SJ. Weight in infancy and death from ischaemic heart disease. *Lancet*. 1989; 2, 577–580.
29. Lau C, Rogers JM. Embryonic and fetal programming of physiological disorders in adulthood. *Birth Defects Res C Embryo Today*. 2004; 72, 300–312.
30. Taylor PD, Poston L. Developmental programming of obesity in mammals. *Exp Physiol*. 2007; 92.2, 287–298.
31. Coupe' B, Grit I, Darmaun D, Parnet P. The timing of 'catch-up growth' affects metabolism and appetite regulation in male rats born with intrauterine growth restriction. *Am J Physiol Regul Integr Comp Physiol*. 2009; 297, R813–R824.
32. Alexander B, Dasinger JH, Intapad S. Fetal programming and cardiovascular pathology. *Comp Physiol*. 2015; 5, 997–1025.
33. Wu G, Bazer FW, Cudd TA, Meininger CJ, Spencer TE. Maternal nutrition and fetal development. *J Nutr*. 2004; 134, 2169–2172.
34. Awazu M, Hida M. Maternal nutrient restriction inhibits ureteric bud branching but does not affect the duration of nephrogenesis in rats. *Pediatr Res*. 2015; 77, 633–639.
35. Ibáñez L, Suárez L, Lopez-Bermejo A, et al. Early development of visceral fat excess after spontaneous catch-up growth in children with low birth weight. *J Clin Endocrinol Metab*. 2008; 93, 925–928.
36. Sakai T, Kriz W. The structural relationship between mesangial cells and basement membrane of the renal glomerulus. *Anat Embryol*. 1987; 176, 373–386.
37. Sakai T, Lemley KV, Hackenthal E, et al. Changes in glomerular structure following acute mesangial failure in the isolated perfused kidney. *Kidney Int*. 1992; 41, 533–541.
38. Nishimura H, Xi Z, Zhang L, et al. Maturation dependent neointima formation in fowl aorta. *Comp Biochem Physiol A Mol Integr Physiol*. 2001; 30, 39–54.
39. Sugizawa Y. Mesangial injury associated with renal lymph stasis and blood congestion. *Nihon Jinzo Gakkai Shi*. 1987; 29, 39–49.
40. Romano LA, Ferder L, Inserra F, et al. Intraglomerular expression of alpha-smooth muscle actin in aging mice. *Hypertension*. 1994; 23(Pt 2), 889–893.
41. Kriz W, Lemley KV. A potential role for mechanical forces in the detachment of podocytes and the progression of CKD. *J Am Soc Nephrol*. 2015; 26, 258–269.
42. Miner JH. Life without nephrin: It's for the birds. *J Am Soc Nephrol*. 2012; 23, 369–371.
43. Thornburg KL, O'Tierney PF, Louey S. The placenta is a programming agent for cardiovascular disease. *Placenta*. 2010; 31, S54–S59.
44. Ingelfinger JR, Schnaper HW. Renal endowment: developmental origins of adult disease. *J Am Soc Nephrol*. 2005; 16, 2533–2536.
45. Moisiadis VG, Matthews SG. Glucocorticoids and fetal programming part 1: outcomes. *Nat Rev Endocrinol*. 2014a; 10, 391–402.
46. Moisiadis VG, Matthews SG. Glucocorticoids and fetal programming part 2: mechanisms. *Nat Rev Endocrinol*. 2014b; 10, 403–411.
47. Kapoor A, Dunn E, Kostaki A, Andrews MH, Matthews SG. Fetal programming of hypothalamo-pituitary-adrenal function: prenatal stress and glucocorticoids. *J Physiol*. 2006; 572, 31–44.
48. Weinstock M. The potential influence of maternal stress hormone on development and mental health of the offspring. *Brain Behav Immun*. 2005; 19, 296–308.
49. Braun EJ, Sweazea KL. Glucose regulation in birds. *Comp Biochem Physiol B Biochem Mol Biol*. 2008; 151, 1–9.
50. Srivastava T. Nondiabetic consequences of obesity on kidney. *Pediatr Nephrol*. 2006; 21, 463–470.
51. Kriz W, Schiller A, Kaissling B, Taugner R. Comparative and functional aspects of thin loop limb ultrastructure. In *Functional Ultrastructure of the Kidney* (eds. Maunsbach AB, Olsen TS, Christensen EI), 1980; pp. 241–250. Academic Press, New York.
52. Bailey JR, Nishimura H. Renal response of fowl to hypertonic saline infusion into the renal portal system. *Am J Physiol*. 1984; 246, R624–R632.



Clinical Notes

Acute kidney injury in type 3 Bartter syndrome: Angiotensin-converting enzyme inhibitors as a cause

Ryuhei Nagao,¹ Shinzi Suzuki,¹ Hisashi Kawashima,¹ Kandai Nozu² and Kazumoto Iijima²¹Department of Pediatrics, Tokyo Medical University, Shinjuku, Tokyo and ²Department of Pediatrics, Kobe University Graduate School of Medicine, Chuo, Kobe, Japan**Key words** acute kidney injury, angiotensin-converting enzyme inhibitor, Bartter syndrome, genetic test, infant.

Bartter syndrome (BS) is a renal tubular disorder characterized by hyperactivity of the renin-angiotensin-aldosterone system (RAAS). Angiotensin-converting enzyme inhibitors (ACEI) may be used to treat BS. We present a patient with type 3 BS with acute kidney injury (AKI) as a result of ACEI treatment. Although ACEI have been reported as a cause of renal dysfunction in other kidney diseases, this is the first report on the association of ACEI with BS.

The patient was a female infant vaginally delivered at 39 weeks of gestation with birthweight 2816 g. At 3 months of age, her weight was 4150 g, and she was diagnosed with failure to thrive and was admitted to hospital.

Blood testing indicated hypokalemia (serum potassium, 2.5 mEq/L), metabolic alkalosis, and hyperreninemia (blood renin activity >20 ng/mL/h); because the blood pressure was normal, BS was suspected. On day 7 of hospitalization, treatment was initiated with potassium supplementation (2.5 mEq/kg/day), an aldosterone antagonist (spironolactone, 1.7 mg/kg/day), and an ACEI (captopril, 0.9 mg/kg/day). As a result, serum potassium increased to 4.5 mEq/L on day 15 of hospitalization. Although serum potassium stabilized, serum creatinine gradually began to rise at this point. On day 29 of hospitalization, serum creatinine had increased to 0.7 mg/dL. According to the Kidney Disease: Improving Global Outcomes (KDIGO) classification, the patient was classified into stage 3 (cut-off serum creatinine, 0.2 mg/dL), and the pediatric-modified Risk, Injury, Failure, Loss, End-Stage Renal Disease (p-RIFLE) score indicated renal injury (glomerular filtration rate [GFR] decrease, 51%). Drug-induced AKI was suspected; captopril was discontinued, and serum creatinine decreased to 0.2 mg/dL, but hypokalemia reappeared. On day 50 of hospitalization, another ACEI, lisinopril (0.06 mg/kg/day), was initiated. Five days later, serum creatinine had increased to 0.4 mg/dL, and the patient was now at stage 2 according to the KDIGO classification and at renal risk according to the p-

RIFLE classification (GFR decrease, 35%). Lisinopril was discontinued, and serum creatinine decreased again. Ultimately, captopril at a dose of 0.075 mg/kg caused no elevation in serum creatinine, and serum potassium was stabilized at 4.0–4.5 mEq/L.

On genetic testing a mutation was identified in the chloride channel gene, *CLCNKB*, the causative gene of type 3 BS (Fig. 1). The father was already known to be a carrier of the c.1830G>A p.W610X mutation,¹ and duplication of exons 15–19 was detected in the mother. This compound heterozygote mutation involving W610X and exon 15–19 duplication, which was detected in the patient, has not been reported previously. Type 3 BS is reported to be the most common variant among BS patients in Japan. This may be because many Japanese people are carriers of the Japanese founder effect mutation (c.1830G>A p.W610X).²

The concept of normotensive ischemic AKI has been proposed for AKI that develops without clear hypotension. Usually, when there is a decreased circulating plasma volume, the self-regulatory function of the kidney works so that prostaglandin E2 causes afferent arterioles to dilate and angiotensin II causes efferent arterioles to contract. When angiotensin II is suppressed by ACEI, however, the afferent arterioles dilate; thus, intraglomerular pressure can no longer be maintained, leading to decreased GFR. This breakdown in self-regulatory function is believed to induce vulnerability to blood flow changes in the kidneys, making it impossible to maintain GFR even with blood pressure variations within the normal range.³ The present patient had decreased blood pressure variations within the normal range, but there was no clear hypotension. In addition, dehydration was suspected due to decreased suckling and urine. This suggested that normotensive ischemic AKI had occurred.

Bartter syndrome often presents as dehydration, indicating that the patients are constantly at risk of AKI. Countermeasures to prevent normotensive ischemic AKI include prevention of dehydration by providing adequate fluids, and inhibition of excessive RAAS activity while maintaining self-regulatory function on careful drug treatment, starting from below the minimum dose. Genetic testing was done after the parents consent.

Correspondence: Ryuhei Nagao, MD PhD, Department of Pediatrics, Tokyo Medical University, 6-7-1, Nishishinjuku, Shinjuku-ku, Tokyo 160-0023, Japan. Email: ryuhei@tokyo-med.ac.jp

Received 2 March 2016; revised 2 June 2016; accepted 21 July 2016.

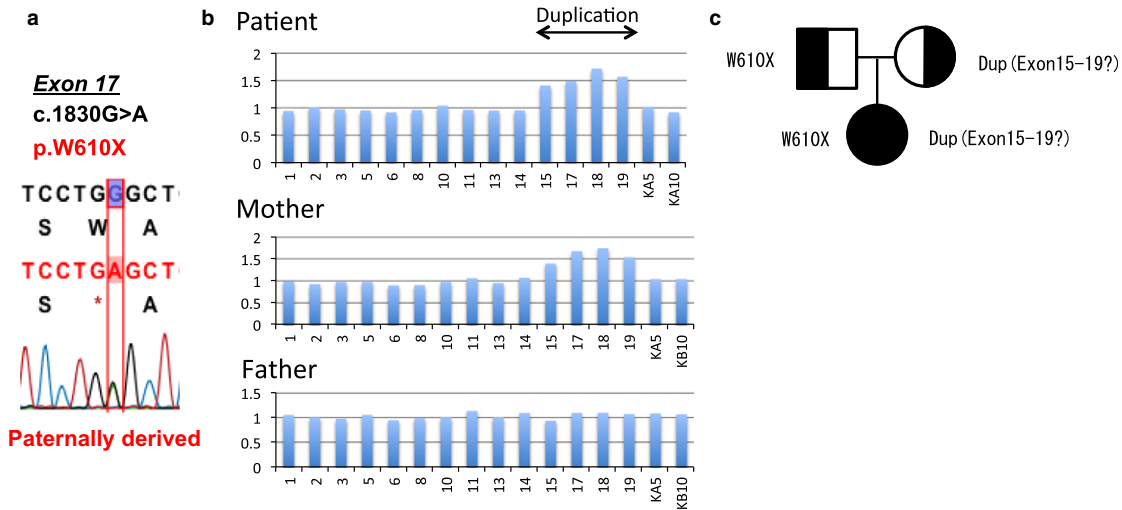


Fig. 1 Abnormality in (a) the chloride channel gene, *CLCNKB*, causative of type 3 BS, detected on genetic testing during hospitalization, facilitating definitive diagnosis. (b) Multiplex ligation-dependent probe amplification. The patient’s father was already known to be a carrier of the c.1830G>A p.W610X mutation, and duplication of exons 15–19 was detected in the patient’s mother. This compound heterozygote mutation, involving (c) W610X and exon 15–19 duplication, detected in the patient, has not been previously reported.

Disclosure

The authors declare no conflict of interest.

Author contributions

N.R., S.S. and K.H. carried out treatment; N.R. and S.S. collected and analyzed data; N.R. wrote the manuscript; K.H. critically reviewed the manuscript; N.K. and I.K. performed genetic testing; S.S., N.K. and I.K. gave conceptual advice. All authors read and approved the final manuscript.

References

- 1 Fukuyama S, Hiramatsu M, Akagi M, Ohta T. Novel mutations of the chloride channel Kb (ClC-Kb) gene in two Japanese patients clinically diagnosed as Bartter syndrome with hypocalciuria. *J. Clin. Endocrinol. Metab.* 2004; **89**: 5847–50.
- 2 Nozu K, Fu XJ, Nakanishi K *et al.* Molecular analysis of patients with type III Bartter syndrome: Picking up large heterozygous deletions with semiquantitative PCR. *Pediatr. Res.* 2007; **62**: 364–9.
- 3 Abuelo JG. Normotensive ischemic acute renal failure. *N. Engl. J. Med.* 2007; **357**: 797–805.

Altered expression of *Crb2* in podocytes expands a variation of *CRB2* mutations in steroid-resistant nephrotic syndrome

Tomohiro Udagawa¹ · Tohaku Jo² · Takeshi Yanagihara² · Akira Shimizu³ · Jun Mitsui⁴ · Shoji Tsuji⁴ · Shinichi Morishita⁵ · Reiko Onai¹ · Kenichiro Miura¹ · Shoichiro Kanda¹ · Yuko Kajiho¹ · Haruko Tsurumi¹ · Akira Oka¹ · Motoshi Hattori⁶ · Yutaka Harita¹

Received: 22 August 2016 / Revised: 2 November 2016 / Accepted: 8 November 2016 / Published online: 10 December 2016
© IPNA 2016

Abstract

Background Steroid-resistant nephrotic syndrome (SRNS) is a genetically heterogeneous disorder for which more than 25 single-gene hereditary causes have been identified.

Methods Whole exome sequencing was performed in a 3-year-old girl with SRNS. We analyzed the expression of *Crb2* and slit diaphragm molecules in the patient's glomeruli, and compared it with that of controls or other nephrotic patients.

Results Whole-exome analysis identified novel compound heterozygous mutations in exons 10 and 12 of *CRB2* (p.Trp1086ArgfsX64 and p.Asn1184Thr, each from different parents; Asn1184 within extracellular 15th EGF repeat domain). Renal pathology showed focal segmental glomerulosclerosis with effaced podocyte foot processes in a small area, with significantly decreased *Crb2* expression.

Molecules critical for slit diaphragm were well-expressed in this patient's podocytes. *Crb2* expression was not altered in the other patients with congenital nephrotic syndrome with *NPHS1* mutations.

Conclusions These findings demonstrate that *Crb2* abnormalities caused by these mutations are the mechanism of steroid-resistant NS. Although *CRB2* mutations previously found in SRNS patients have been clustered within the extracellular tenth EGF-like domain of this protein, the present results expand the variation of *CRB2* mutations that cause SRNS.

Keywords Steroid-resistant nephrotic syndrome · *Crb2* · Podocyte · Slit diaphragm

Introduction

Idiopathic nephrotic syndrome (NS) is the most common form of NS in children [1]. Some 80–90 % of patients with childhood-onset NS are steroid-sensitive; this is called minimal change disease, and its renal biopsy findings show only diffuse foot process effacement on electron microscopy. Steroid-resistant NS (SRNS) is the second most common chronic kidney disease in the first three decades of life, and renal prognosis is generally poor with end-stage renal failure (ESRF) occurring in 30–40 % of patients [2]. The etiology and pathogenesis of SRNS have been a conundrum for decades; however, the single-gene cause can be found in some SRNS patients. To date, more than 25 single-gene causes of hereditary NS have been identified; they can display either dominant or recessive inheritance [3]. Very recently, next-generation sequencing technology discovered that a causative mutation can be detected in 30 % of all individuals who develop SRNS before 25 years of age [4]. As genetic alterations are associated with a poor response to immunosuppressive agents in

Tomohiro Udagawa and Tohaku Jo contributed equally to this work

✉ Yutaka Harita
haritay-ped@h.u-tokyo.ac.jp

- ¹ Department of Pediatrics, Graduate School of Medicine, The University of Tokyo, 7-3-1 Hongo, Bunkyo-ku, Tokyo 113-8655, Japan
- ² Department of Pediatrics, Nippon Medical School, Tokyo, Japan
- ³ Department of Analytic Human Pathology, Nippon Medical School, Bunkyo-ku, Tokyo, Japan
- ⁴ Department of Neurology, Graduate School of Medicine, The University of Tokyo, Bunkyo-ku, Tokyo, Japan
- ⁵ Department of Computational Biology and Medical Sciences, Graduate School of Frontier Sciences, The University of Tokyo, Chiba, Japan
- ⁶ Department of Pediatric Nephrology, Tokyo Women's Medical University, Shinjuku-ku, Tokyo, Japan

children with SRNS [5, 6], genetic diagnosis of SRNS can offer a cause-based diagnosis and permit personalized treatment options for SRNS.

The family of Crumbs proteins, homologous to *Drosophila* Crumbs (Crb), contain large extracellular domains, including epidermal growth factor (EGF)-like and laminin G-like domains, a single transmembrane domain, and a cytoplasmic tail that contains single FERM and PDZ protein-binding motifs. The longest transcript of *CRB2* (RefSeq NM_173689 [MIM 609720]) has 13 coding exons. In 2015, several *CRB2* mutations were found in patients with SRNS [7]. Three of the four missense mutations (p.Cys620Ser, p.Arg628Cys, and p.Cys629Ser) identified in SRNS occur within exon 7 of *CRB2*, which encodes the extracellular tenth EGF-like domain of this protein [7]. Biallelic *CRB2* mutations consistent with autosomal-recessive inheritance were also found in families who shared a phenotype comprising cerebral ventriculomegaly and echogenic kidneys with histopathological findings of congenital nephrosis [8].

Recent data resulting from morpholino-induced knock-down of zebrafish *crb2b* demonstrated some of the possible mechanisms of Crb2 in glomerular filtration. The *crb2b*^{-/-} homozygotes resulted in the disappearance of slit diaphragms and decreased ZO-1 expression, which suggests that differentiation and protein trafficking of slit components are affected in *crb2b* mutants [7, 9]. However, pathological analysis of the morphological changes of podocytes or the expression pattern of Crb2 in patients with *CRB2* mutations has not been reported, and the effect of pathogenic *CRB2* mutations on the expression of other molecules in human podocytes is undetermined.

Here, we report a Japanese girl who presented with pneumococcal meningitis and SRNS in whom we found novel compound heterozygosity for two deleterious sequence variants in *CRB2*: a frameshift mutation and a missense mutation that predicted p.Asn1184Thr. Here we analyzed *Crb2* expression and molecules at podocyte filtration slits in normal kidneys and the patient's kidney. The data showed that Crb2 expression is specifically affected in these patients, indicating the pathogenicity of the mutations.

Materials and methods

Whole exome analysis and *CRB2* gene analysis

Genomic DNA was extracted from peripheral white blood cells of the patient and parents using a QIAamp DNA Blood Midi Kit (Qiagen, Hilden, Germany). Exome sequences were enriched using a SureSelect v5+UTRs Kit (Agilent Technologies, Santa Clara, CA, USA) from 3 µg of genomic DNA, according to the manufacturer's instructions. The

captured DNA samples were subjected to massively parallel sequencing (100-bp paired-end reads) on an Illumina HiSeq2000 sequencing system (Illumina, Santiago, CA, USA). Short reads were aligned to the reference genome (hg19) using Burrows–Wheeler alignment (BWA) [10] with default parameter settings. Single-nucleotide variants and short insertions/deletions were called using SAMtools [11] with default parameter settings. Sanger sequencing was performed to detect *CRB2* and to validate the presence of each variant detected by exome sequencing in the patient and her Japanese parents. The entire coding region and exon–intron boundaries of exons 10 and 12 of the *CRB2* gene were amplified from the genomic DNA using polymerase chain reaction (PCR). The primers for exon 10 were 5'-GAGA ACTTCACCGGCTGCTTG-3' and 5'-GACT TCTCTGCCCCACCATA-3'. The primers for exon 12 were 5'-GGGACAGTGGATGGATAAGC -3' and 5'-ATGACAGAGTGGCCCAGGAAC -3'.

Histological analysis

Tissue for light microscopy was collected and processed routinely whereas tissue for direct immunofluorescence was stained, utilizing fluorescein-tagged antibodies against immunoglobulin G (IgG), IgA, and IgM, and complement proteins C1q, C3, and C4. Biopsy tissue for electron microscopy was routinely fixed. Immunohistological analysis of podocyte protein expression was performed as follows. Paraffin-embedded samples from human renal biopsy samples were deparaffinized in xylene and rehydrated through an ethanol–H₂O gradient, followed by heat-induced epitope retrieval by incubating in a target retrieval solution (S1699; Dako, Carpinteria, CA, USA) for 20 min at 121 °C. Sections were cooled to room temperature and incubated with the primary antibodies, followed by incubation with Alexa Fluor conjugated secondary antibodies (Invitrogen, Carlsbad, CA, USA). Images were obtained using a confocal microscope (model FV300; Olympus, Tokyo, Japan) and were processed using Adobe Photoshop CS6. The following antibodies were obtained commercially: rabbit polyclonal anti-*CRB2* (Sigma-Aldrich, St Louis, MO, USA), mouse monoclonal anti-zonula occludens-1 (ZO-1; 33–9100; Invitrogen, Carlsbad, CA, USA), and rabbit polyclonal anti-synaptopodin (Meridian Life Science, Memphis, TN, USA). Rabbit polyclonal anti-nephrin IgG and rabbit polyclonal anti-podocin have been described previously [12, 13]. Control samples (donor kidney or biopsy samples from patients with minimal change disease obtained during remission periods) were stained at the same time. Kidney samples from patients with congenital nephrotic syndrome have also been described previously [13].

Preabsorption of Crb2 antibody

HEK293T cells were purchased from the ATCC (Manassas, VA, USA) and maintained in DMEM containing 10 % fetal bovine serum. Transfections were performed using Polyethylene-imine Max (PEI-Max) reagent (Polysciences, Warrington, PA, USA) following the manufacturer’s instructions. Cells were lysed in a lysis buffer (20 mM Tris–HCl [pH 7.5], 150 mM NaCl, 1 mM EDTA, and 1 % NP-40) containing a protease inhibitor cocktail (Roche, Germany) for 15 min on ice. Lysates were clarified by centrifugation and incubated with agarose beads conjugated with anti-FLAG M2 antibody for 1 h at 4 °C. The diluted primary antibody for Crb2 was incubated with the immunoprecipitates from cells transfected with control vector or flag-Crb2 for antibody absorption.

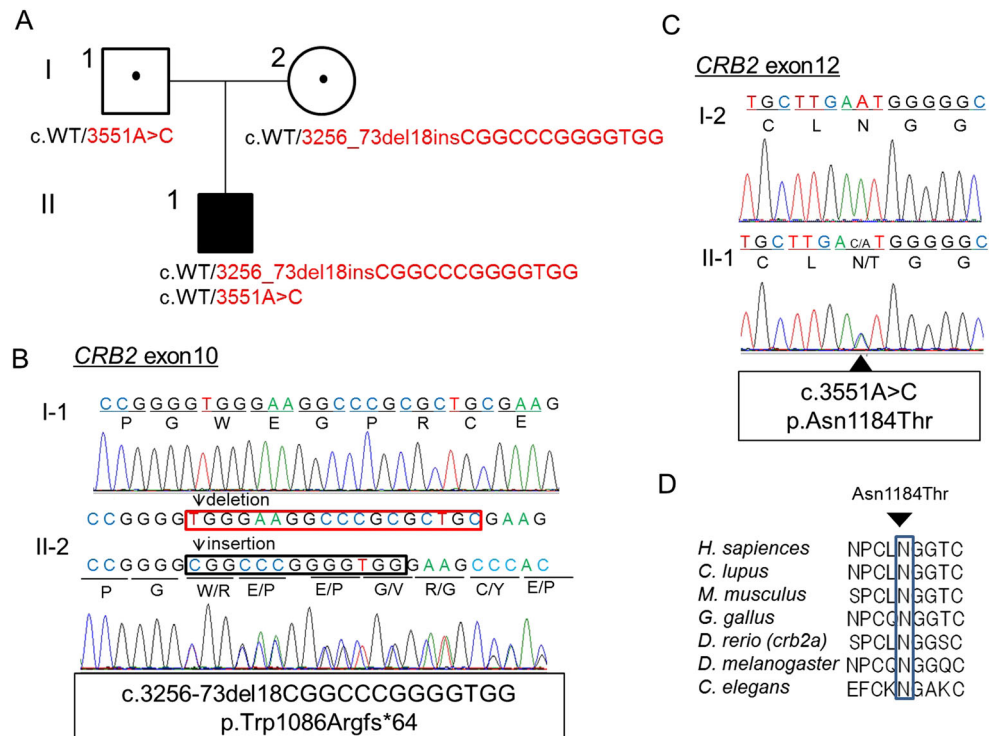
Results

The patient was a 3-year-old girl with fever, edema, and macroscopic hematuria. She had an unremarkable birth and family history and no neurological or cardiac defects had been noted in her past regular medical checkups. On systemic examination, she had generalized edema and a depressed level of consciousness with the Glasgow Coma Scale of 10 (E3, V3, M4). Neck rigidity was present and Kernig’s sign was positive. Examination of the cerebrospinal fluid (CSF) revealed 2,384 cells/mm³; 97 % polymorphs, protein 189 mg/dL and sugar 0 mg/dL. CSF culture showed growth of *Streptococcus*

pneumoniae. She had normal kidney function with blood urea nitrogen of 9.6 mg/dl and creatinine of 0.12 mg/dl. Urinalysis revealed proteinuria at 10.3 g/g creatinine, with urine sediments of 5–9 red blood cells per high power field. She was diagnosed with nephrotic syndrome with bacterial meningitis, and started on antibiotics, which successfully treated her meningitis. Thereafter, she received prednisolone (30 mg/day), but did not respond to a 4-week treatment. Thereafter, immunosuppressive therapy consisting of methylprednisolone pulse therapy and cyclosporine, and finally rituximab did not affect her massive proteinuria. She failed to achieve clinical remission after 5 months’ follow-up.

We hypothesized that this sporadic steroid-resistant NS was caused by mutations in known or novel nonsynonymous coding variants. To identify the causal variant, we then performed exome sequencing using next-generation sequencing for this patient. The mean sequencing coverage was 95 million reads, with 98.8 % of the total bases mapped to the reference genome, which encompassed 89.8 % of the targeted regions with coverage >10×. Among gene mutations reported to cause NS, two heterozygous mutations of *CRB2* were found in exons 10 and 12 (Fig. 1). Direct sequencing of *CRB2* confirmed that the patient had compound heterozygous mutations in *CRB2* (Fig. 1a–c): c.3551A>C (predicting p.Asn1184Thr) was inherited from her healthy father and c.3256_3273del18insCGGCCCGGGGTGG (predicting p.Trp1086ArgfsX64) from her healthy mother. These mutations had not been registered in the database of single-nucleotide polymorphisms (SNPs) of the National Center for

Fig. 1 Genetic analysis of steroid-resistant nephrotic syndrome (SRNS) with *CRB2* mutation. **a** Patient’s familial pedigree. Red: mutant alleles, WT wild-type allele. Sequence chromatograms for portions of **b** exon 10 and **c** 12 of *CRB2* for the patient and her parents. The patient has compound heterozygous mutations c.3256_3273del18insCGGCCCGGGGTGG and c.3551A>C. **d** Protein alignment plot of Crb2 amino acid sequence for residues 1180–1188 in exon 12 of *CRB2* (arrowhead), with complete conservation of the Asn1184 locus



Biotechnology Information (dbSNP, www.ncbi.nlm.nih.gov), in the Exome Aggregation Consortium (ExAC) [14] or in the Japanese SNP control database established by the National Bioscience Data Base Center, which has genome-wide data for a million SNPs from 700 samples (http://gwas.biosciencedbc.jp/snpdb/snp_top.php). Furthermore, the absence of this DNA sequence abnormality in 1,240 alleles from 620 unrelated healthy Japanese individuals indicated that they are mutations and not polymorphisms. Asn1184 is within an extracellular 15th EGF repeat domain, and is highly conserved across various species (Fig. 1d). The functionality of p.As1184Thr was analyzed using the Sorting Intolerant From Tolerant (SIFT) web-based tool (<http://sift.jcvi.org>), the Polymorphism Phenotyping 2 (PolyPhen2) tool (<http://genetics.bwh.harvard.edu/pph2>), and Mutation Taster (<http://www.mutationtaster.org>) by homology modeling and threading. All three models predicted *CRB2* p.As1184Thr to be “damaging.”

A renal biopsy sample of the patient revealed focal segmental glomerulosclerosis (FSGS) by light microscopy (Fig. 2). Segmental sclerosis was evident in the perihilar area of one glomerulus, indicating FSGS, perihilar variant. No specific deposition of IgG, IgA or IgM, or of complement proteins C1q, C3, and C4, was detected by direct immunofluorescence. Electron microscopy revealed that the foot processes of podocytes were well retained, with the effacement of these

processes in only a small area, indicating the secondary form of FSGS.

Next, we investigated Crb2 expression in human kidneys by using polyclonal antibodies against the extracellular part (amino acids 720–802) of human Crb2. Immunohistochemical staining of adult human kidney tissues (donor kidney) revealed intense signals for Crb2 in normal glomeruli along with glomerular capillary loops and parietal glomerular epithelial cells (Fig. 3a, b). These signals disappeared when antibody was pre-absorbed with anti-FLAG immunoprecipitates from cell lysates of HEK293 cells that express FLAG-tagged Crb2 (Fig. 3c–e), indicating the specificity of the signals. To determine the localization of Crb2 in glomeruli, paraffin-embedded sections of the adult human kidney were double-labeled with Crb2 and ZO-1, a podocyte marker. Intense signals for Crb2 in normal glomeruli were observed along with glomerular capillary loops, partially colocalizing with ZO-1 (Fig. 4). Notably, Crb2 staining was also observed outside the linear staining area marked by ZO-1. Next, we analyzed expressions of Crb2, ZO-1, synaptopodin, nephrin, and podocin in kidneys from the patient with *Crb2* mutations and compared with those from control samples. Staining of Crb2 was undetected in glomeruli of the SRNS patient with *CRB2* mutations (Fig. 4), but expressions of ZO-1, synaptopodin, and slit diaphragm proteins (nephrin and podocin) were retained in her podocytes (Figs. 4, 5). We also

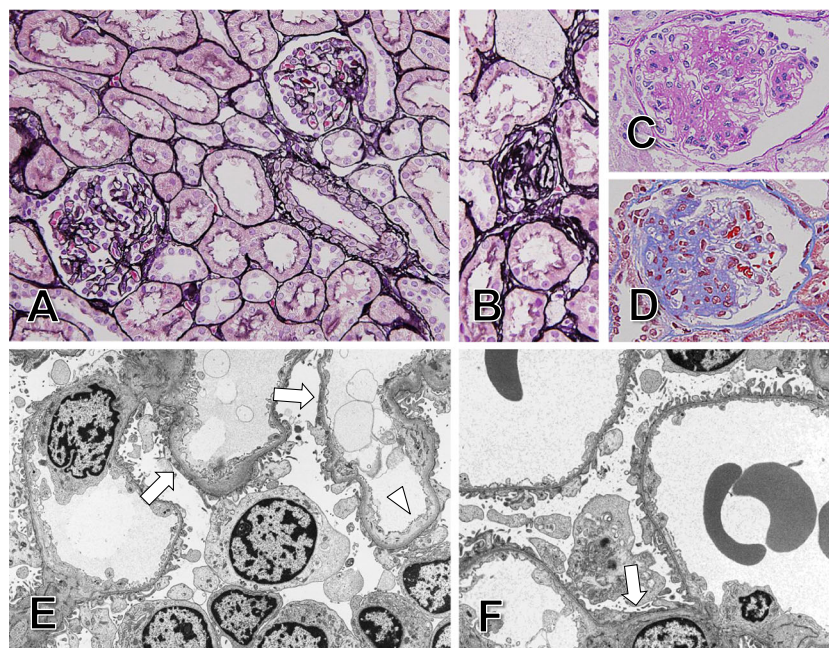


Fig. 2 Kidney histopathology of the affected individual with biallelic *CRB2* mutation. **a** On observation using light microscopy, the biopsy specimen included 21 glomeruli, many of which showed minor glomerular abnormalities (PAM stain, $\times 200$). **b** Two glomeruli were obsolete (PAM stain, $\times 600$), and **c** three glomeruli showed expansion of mesangial areas with accumulation of matrix (PAS stain, $\times 600$). **d** The perihilar type of segmental sclerosis was noted in one

glomerulus (Masson stain, $\times 600$), indicating the perihilar variant of focal segmental glomerulosclerosis. In podocytes, electron microscopy showed relatively well preserved foot processes, with the effacement of these processes in small areas (arrows in **e**, $\times 5,000$, and **f**, $\times 8,000$), indicating the secondary form of focal segmental glomerulosclerosis. Focal widening of subendothelial spaces was shown in the segmental capillary wall (arrowhead in **e**)

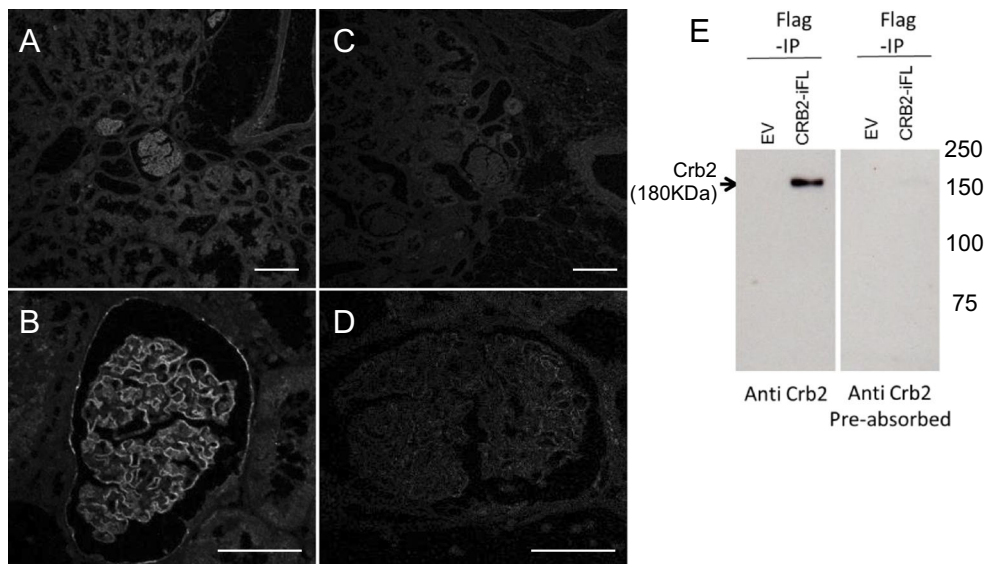


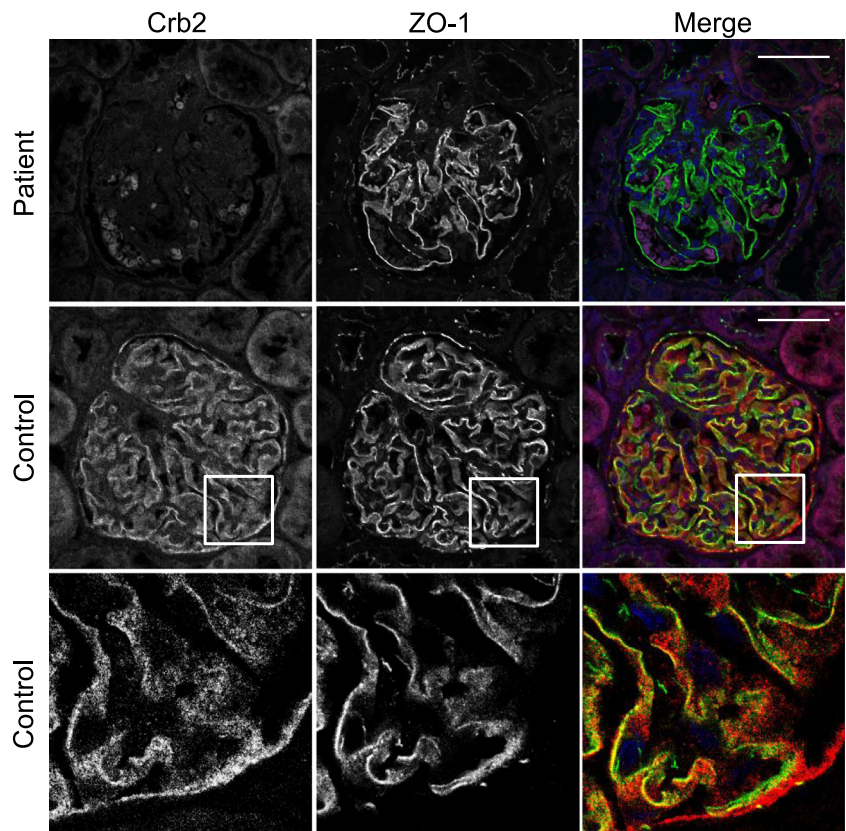
Fig. 3 Crb2 expression in the kidney cortex. Human kidney sections were stained with anti-Crb2 antibody pre-adsorbed with anti-myc immunoprecipitates from lysates of HEK293T cells that expressed **a, c** control vector or **b, d** myc-tagged Crb2. Strong Crb2 signals were detected along glomerular capillary loops and in parietal epithelial cells (**a** and **c**), with

specific signals detected in the vascular endothelium (**e**). Scale bar: 50 μ m. **e** Lysates of HEK293T cells expressing control vector or Crb2 vector were immunoprecipitated with anti-FLAG antibody and analyzed by western blot with indicated antibodies. These immunoprecipitates were used for antibody absorption (**a–d**)

analyzed Crb2 expression in two congenital nephrotic syndrome (CNS) patients with *NPHS1* mutations (CNS1: heterozygous missense mutation [P676R]; CNS2: homozygous

mutation [Q839RfsX849]) [13]. Clear signals for Crb2 that demarcated glomerular capillaries were observed in glomeruli from the CNS patients with *NPHS1* mutations (Fig. 6).

Fig. 4 Expression of Crb2 in the patient with *CRB2* mutations. Dual-labeling immunofluorescence of Crb2 (red) and ZO-1 (green). Strong Crb2 signals were partially colocalized with ZO-1 in the control specimen. However, Crb2 expression was diminished in the patient’s glomeruli. Scale bar: 50 μ m



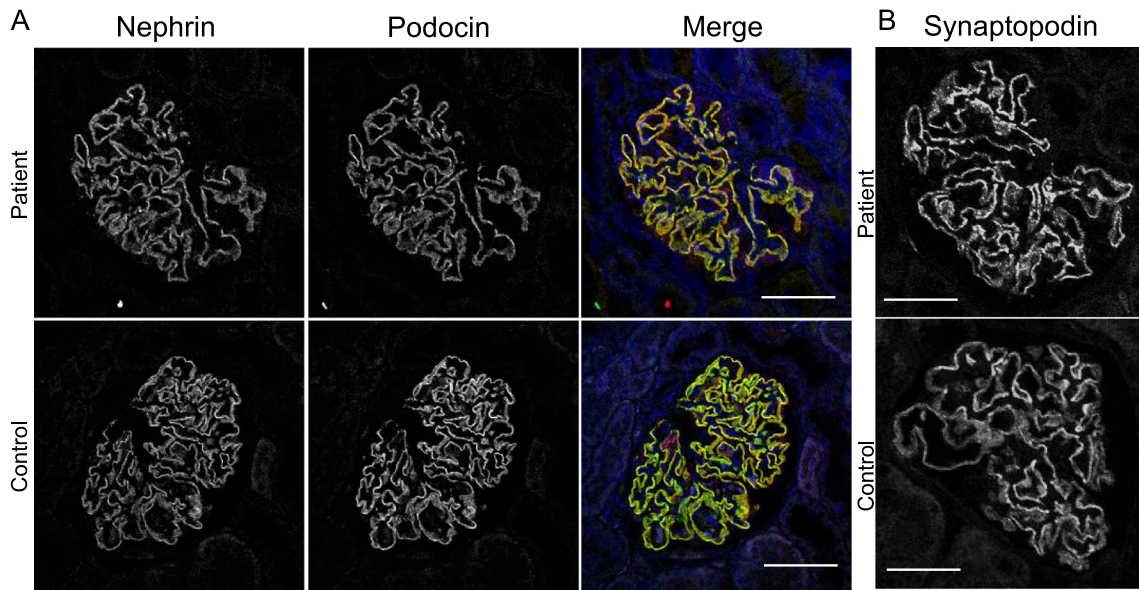


Fig. 5 Expression of nephrin, podocin, and synaptopodin in the patient with *CRB2* mutations. Immunofluorescence is shown for **a** nephrin and podocin and **b** synaptopodin in the control case and the patient with *CRB2*

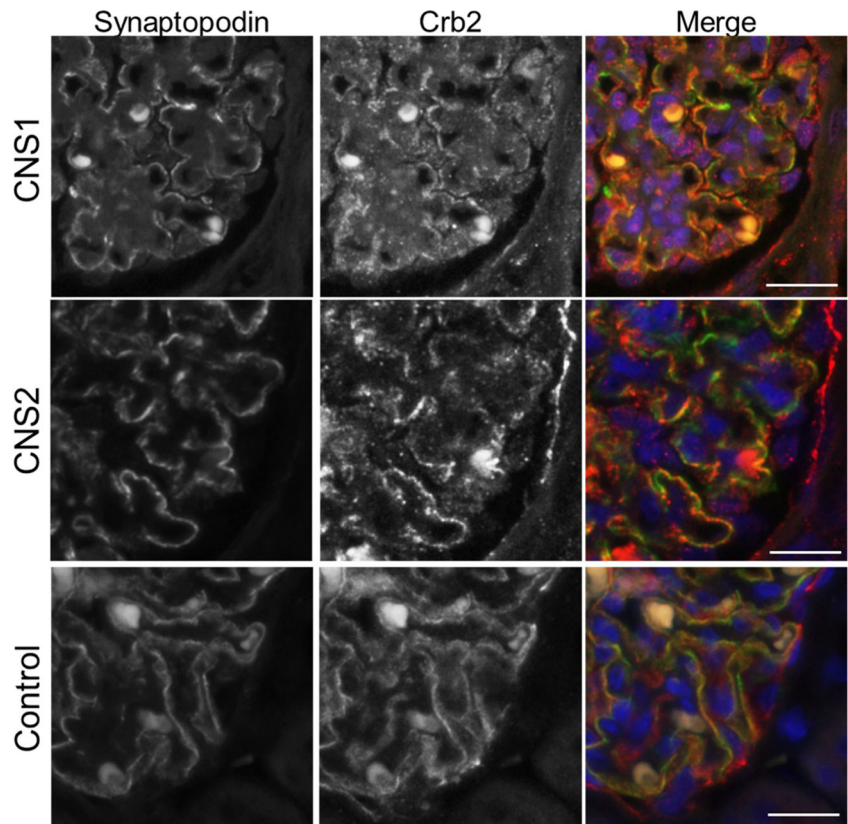
mutations. Signals for nephrin, podocin, and synaptopodin were not altered in the patient

These results support the pathogenic role of *CRB2* mutations in exons 10 and 12 in the patient, and imply that specific disruption of *Crb2* expression causes podocyte dysfunction, which leads to massive proteinuria.

Discussion

In the present study, we identified novel *CRB2* mutations in a girl with SRNS that was resistant to cyclosporine and

Fig. 6 *Crb2* expression in patients with *NPHS1* mutations, showing immunofluorescence for synaptopodin and *Crb2* in congenital nephrotic syndrome (CNS) patients with *NPHS1* mutations. Note that both patients retained *Crb2* expression in podocytes and parietal epithelial cells



rituximab. Immunohistochemical studies showed specific reduced expression of Crb2 in the patient’s podocytes, indicating the pathogenic role of the mutations. After identifying the genetic cause, immunosuppressive therapy was discontinued and supportive treatment was continued.

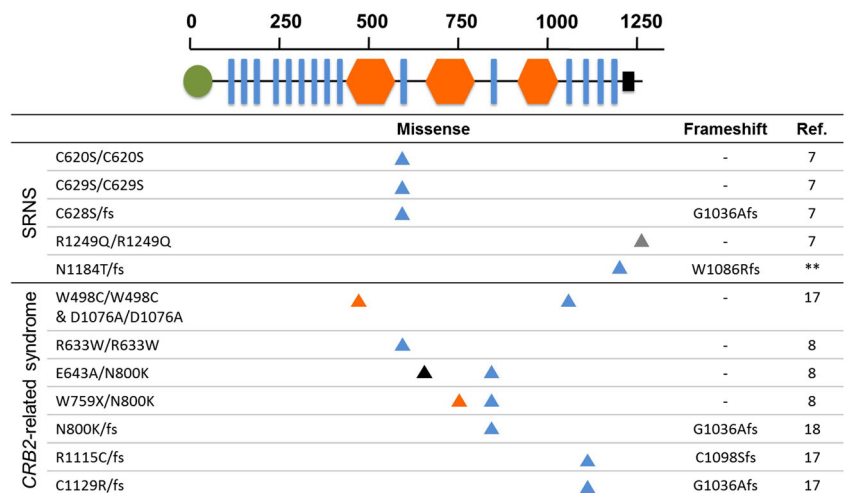
Recently, large international cohorts were studied for monogenic causes of childhood SRNS, in which single-gene mutations associated with SRNS were identified in ~25–33 % of all families with SRNS [4, 5, 15, 16]. The earlier the age at onset, the more likely the causative mutations can be detected: single-gene causes of SRNS were detected in 61 % of the families of patients studied whose onset occurred in the first 12 months of life, compared with 25.3 % of families of patients whose disease began at age 1–6 years [4]. Although mutations in dominant genes such as *INF2* and *TRPC6* are more frequently found in early adulthood [4], mutations of recessive genes (*NPHS1*, *LAMB2*, and *PLCE1*) often manifest as SRNS in early childhood. Recessive mutations in *CRB2* have been found in four different families affected by SRNS. Onset of SRNS due to *CRB2* mutations was reported from the age 9 months to 6 years. Three of the four missense mutations (p.Cys620Ser, p.Arg628Cys, and p.Cys629Ser) previously found in *CRB2*-associated SRNS were clustered within the extracellular tenth EGF-like domain of this protein, and one mutation was in the cytoplasmic tail (p.Arg1249Gln) [7]. However, as p.Arg1249Gln has been reported in a homozygous state in two individuals who were not known to have renal or cerebral defects, the significance of this mutation is unclear [17]. One of the mutations found in the present case is in the 15th EGF-like domain, and the other was a frame-shift mutation. The present case demonstrated that even a mutation outside the tenth EGF-like domain can cause the SRNS phenotype; the association of mutations in the tenth EGF-like domain with SRNS was weakened by the present case.

Biallelic *CRB2* mutations not only cause isolated early-onset SRNS [7], but also severe phenotypes that manifest congenital nephrotic syndrome, showing renal microcysts

complicated with marked cerebral ventriculomegaly, gray matter heterotopias, and elevated maternal serum alpha-fetoprotein and amniotic fluid alpha-fetoprotein. Recent analysis also identified patients with obstructive congenital hydrocephalus, urinary tract anomalies and lung hypoplasia, features clinically consistent with a ciliopathy [18]. All the mutations reported in the present study and previous reports [7, 8, 17, 18] are shown in Fig. 7. The mechanisms leading to these different phenotypes caused by *CRB2* mutations are unknown. With regard to genotype–phenotype correlation, the affected domain does not differentiate the phenotype per se. For example, homozygous missense mutations in the tenth EGF-like domain (C620S, C629S, R633W) can cause either SRNS or the *CRB2*-related syndrome/ciliopathy phenotype (Fig. 7). However, the missense mutations in SRNS or in pleiotropic phenotype reported so far are mutually exclusive (Fig. 7), raising the possibility of a genotype–phenotype relationship. Besides, the specificity or severity of the organ affected by *CRB2* mutations seems to be complex because the severity of nephropathy is not necessarily parallel to extra-renal phenotypes. For example, a patient reported by Lamont et al. with compound heterozygous missense mutations of *CRB2* (p.E643A and p.N800K) showed cerebral ventriculomegaly during the pregnancy, and a ventriculoperitoneal shunt was placed at 5 days of life to treat hydrocephalus [17]. Notably, she did not exhibit any detectable kidney abnormalities at 6 years of age. Future case series and in vitro or in vivo studies using knock-in mice or cell-specific knock-out models will be needed to determine the tissue-specific pathophysiological mechanisms of each mutation.

Although *crb2* expression in podocytes had been confirmed in zebrafish or rodents [7, 9], expression of *Crb2* in human kidneys has not been reported. We found that *Crb2* is exclusively expressed in podocytes and glomerular parietal epithelial cells in human glomeruli. Podocyte process patterning and cellular junction formation by assembling a protein complex that regulates actin cytoskeletal dynamics are

Fig. 7 Schematic representation of *CRB2* mutation positions. *CRB2* contains large extracellular domains with 15 EGF-like domains (blue) and 3 laminin G-like domains (orange), a single transmembrane domain, and a cytoplasmic tail containing single FERM- and PDZ protein-binding motifs at the C-terminus. Mutations reported in patients with SRNS (above) or *CRB2*-related syndrome/ciliopathy phenotype (below) are shown. Double asterisk refers to this case. Ref indicates reference



influenced by slit diaphragm (SD) proteins such as nephrin and Neph1 [19]. By gene knock-down using morpholinos, *Crb2b* was found to be required for the morphological differentiation of podocyte foot processes [9, 20] as *crb2b* morphants had grossly disorganized the podocyte foot process architecture. While nephrin protein in zebrafish is present along the basal aspect of podocyte cell bodies, nephrin is apically mislocalized in podocytes in *crb2b* morphants, which suggests that *crb2b* might be required for the proper protein trafficking of nephrin [9]. In zebrafish morphants with stable heritable loss-of-function mutation in *crb2b* [7], expression of ZO-1, another component of slit diaphragm, is decreased, also suggesting that protein trafficking might be affected in *crb2b* mutants. In the present patient with decreased *Crb2* expression, expression of nephrin, podocin, and ZO-1 was preserved. Furthermore, effacement of podocyte foot processes was observed in only a small area of the capillary wall. It should be noted that expression of *Crb2* was maintained in the CNS patients with *NPHS1* mutations. These data suggest that whereas *Crb2* in zebrafish may participate in the upstream SD cascade by regulating expression and the proper targeting of SD proteins, the modality of regulation by *Crb2* of the maintenance of the glomerular filtration barrier in human podocytes may differ from that of other species. There is also a possibility that the residual *CRB2* mutant in the patient may cause differences in the expression of slit diaphragm molecules in podocytes in the patient and that in zebrafish *crb2*^{-/-} mutants.

The specific loss of *Crb2* expression in this patient's podocytes indicates that SRNS of the present case is caused by novel compound heterozygous mutations of *CRB2*, expanding the genetic spectrum of *CRB2*-related diseases. The advance of the clinical and genetic characterization of the disease caused by *CRB2* mutations will have important implications for the clinical evaluation and management of patients.

Acknowledgments The authors thank Dr. Masaki Nishimura (Shiga University of Medical Science) for providing *Crb2* plasmid constructs.

Compliance with ethical standards Informed consent for DNA analysis was obtained from the parents. The study was performed with approval from the Ethics Committee of the University of Tokyo.

Conflicts of interest The authors declare that they have no conflicts of interest.

References

- Eddy AA, Symons JM (2003) Nephrotic syndrome in childhood. *Lancet* 362:629–639
- Benoit G, Machuca E, Antignac C (2010) Hereditary nephrotic syndrome: a systematic approach for genetic testing and a review of associated podocyte gene mutations. *Pediatr Nephrol* 25:1621–1632
- Saleem MA (2013) New developments in steroid-resistant nephrotic syndrome. *Pediatr Nephrol* 28:699–709
- Sadowski CE, Lovric S, Ashraf S, Pabst WL, Gee HY, Kohl S, Engelmann S, Vega-Warner V, Fang H, Halbritter J, Somers MJ, Tan W, Shril S, Fessi I, Lifton RP, Bockenhauer D, El-Desoky S, Kari JA, Zenker M, Kemper MJ, Mueller D, Fathy HM, Soliman NA, Hildebrandt F, Group SS (2015) A single-gene cause in 29.5% of cases of steroid-resistant nephrotic syndrome. *J Am Soc Nephrol* 26:1279–1289
- Giglio S, Provenzano A, Mazzinghi B, Becherucci F, Giunti L, Sansavini G, Ravaglia F, Roperto RM, Farsetti S, Benetti E, Rotondi M, Murer L, Lazzeri E, Lasagni L, Materassi M, Romagnani P (2015) Heterogeneous genetic alterations in sporadic nephrotic syndrome associate with resistance to immunosuppression. *J Am Soc Nephrol* 26:230–236
- Büscher AK, Beck BB, Melk A, Hoefele J, Kranz B, Bamborschke D, Baig S, Lange-Sperandio B, Jungraithmayr T, Weber LT, Kemper MJ, Tönshoff B, Hoyer PF, Konrad M, Weber S, (GPN) GPNA (2016) Rapid response to cyclosporin A and favorable renal outcome in nongenetic versus genetic steroid-resistant nephrotic syndrome. *Clin J Am Soc Nephrol* 11:245–253
- Ebarasi L, Ashraf S, Bierzynska A, Gee HY, McCarthy HJ, Lovric S, Sadowski CE, Pabst W, Vega-Warner V, Fang H, Koziell A, Simpson MA, Dursun I, Serdaroglu E, Levy S, Saleem MA, Hildebrandt F, Majumdar A (2015) Defects of *CRB2* cause steroid-resistant nephrotic syndrome. *Am J Hum Genet* 96:153–161
- Slavotinek A, Kaylor J, Pierce H, Cahr M, DeWard SJ, Schneidman-Duhovny D, Alsadah A, Salem F, Schmajuk G, Mehta L (2015) *CRB2* mutations produce a phenotype resembling congenital nephrosis, Finnish type, with cerebral ventriculomegaly and raised alpha-fetoprotein. *Am J Hum Genet* 96:162–169
- Ebarasi L, He L, Hultenby K, Takemoto M, Betsholtz C, Tryggvason K, Majumdar A (2009) A reverse genetic screen in the zebrafish identifies *crb2b* as a regulator of the glomerular filtration barrier. *Dev Biol* 334:1–9
- Li H, Durbin R (2009) Fast and accurate short read alignment with Burrows-Wheeler transform. *Bioinformatics* 25:1754–1760
- Li H, Handsaker B, Wysoker A, Fennell T, Ruan J, Homer N, Marth G, Abecasis G, Durbin R, Subgroup GPD (2009) The sequence alignment/map format and SAMtools. *Bioinformatics* 25:2078–2079
- Harita Y, Kurihara H, Kosako H, Tezuka T, Sekine T, Igarashi T, Ohsawa I, Ohta S, Hattori S (2009) Phosphorylation of nephrin triggers Ca²⁺ signaling by recruitment and activation of phospholipase C- γ 1. *J Biol Chem* 284:8951–8962
- Kajiho Y, Harita Y, Kurihara H, Horita S, Matsunaga A, Tsurumi H, Kanda S, Sugawara N, Miura K, Sekine T, Hattori S, Hattori M, Igarashi T (2012) SIRPalpha interacts with nephrin at the podocyte slit diaphragm. *FEBS J* 279:3010–3021
- Lek M, Karczewski KJ, Minikel EV, Samocha KE, Banks E, Fennell T, O'Donnell-Luria AH, Ware JS, Hill AJ, Cummings BB, Tukiainen T, Birnbaum DP, Kosmicki JA, Duncan LE, Estrada K, Zhao F, Zou J, Pierce-Hoffman E, Berghout J, Cooper DN, Deflaux N, DePristo M, Do R, Flannick J, Fromer M, Gauthier L, Goldstein J, Gupta N, Howrigan D, Kiezun A, Kurki MI, Moonshine AL, Natarajan P, Orozco L, Peloso GM, Poplin R, Rivas MA, Ruano-Rubio V, Rose SA, Ruderfer DM, Shakir K, Stenson PD, Stevens C, Thomas BP, Tiao G, Tusie-Luna MT, Weisburd B, Won HH, Yu D, Altshuler DM, Ardissino D, Boehnke M, Danesh J, Donnelly S, Elosua R, Florez JC, Gabriel SB, Getz G, Glatt SJ, Hultman CM, Kathiresan S, Laakso M, McCarrroll S, McCarthy MI, McGovern D, McPherson R, Neale BM, Palotie A, Purcell SM, Saleheen D, Scharf JM, Sklar P, Sullivan PF, Tuomilehto J, Tsuang MT, Watkins HC, Wilson JG, Daly MJ, MacArthur

- DG, Consortium EA (2016) Analysis of protein-coding genetic variation in 60,706 humans. *Nature* 536:285–291
15. Lovric S, Fang H, Vega-Warner V, Sadowski CE, Gee HY, Halbritter J, Ashraf S, Saisawat P, Soliman NA, Kari JA, Otto EA, Hildebrandt F (2014) Rapid detection of monogenic causes of childhood-onset steroid-resistant nephrotic syndrome. *Clin J Am Soc Nephrol* 9:1109–1116
 16. McCarthy HJ, Bierzynska A, Wherlock M, Ognjanovic M, Kerecuk L, Hegde S, Feather S, Gilbert RD, Krischock L, Jones C, Sinha MD, Webb NJ, Christian M, Williams MM, Marks S, Koziell A, Welsh GI, Saleem MA, Group RtUSS (2013) Simultaneous sequencing of 24 genes associated with steroid-resistant nephrotic syndrome. *Clin J Am Soc Nephrol* 8:637–648
 17. Lamont RE, Tan WH, Innes AM, Parboosingh JS, Schneidman-Duhovny D, Rajkovic A, Pappas J, Altschwager P, DeWard S, Fulton A, Gray KJ, Krall M, Mehta L, Rodan LH, Saller DN, Steele D, Stein D, Yatsenko SA, Bernier FP, Slavotinek AM (2016) Expansion of phenotype and genotypic data in CRB2-related syndrome. *Eur J Hum Genet* 24:1436–1444
 18. Jaron R, Rosenfeld N, Zahdeh F, Carmi S, Beni-Adani L, Doviner V, Picard E, Segel R, Zeligson S, Carmel L, Renbaum P, Levy-Lahad E (2016) Expanding the phenotype of CRB2 mutations—a new ciliopathy syndrome? *Clin Genet*. doi:10.1111/cge.12764
 19. Garg P, Holzman LB (2012) Podocytes: gaining a foothold. *Exp Cell Res* 318:955–963
 20. Dreyer SD, Morello R, German MS, Zabel B, Winterpacht A, Lunstrum GP, Horton WA, Oberg KC, Lee B (2000) LMX1B transactivation and expression in nail-patella syndrome. *Hum Mol Genet* 9:1067–1074

Early RAAS Blockade Exerts Renoprotective Effects in Autosomal Recessive Alport Syndrome

Nao Uchida,¹ Naonori Kumagai,¹ Kandai Nozu,² Xue Jun Fu,² Kazumoto Iijima,² Yoshiaki Kondo³ and Shigeo Kure¹

¹Department of Pediatrics, Tohoku University School of Medicine, Sendai, Miyagi, Japan

²Department of Pediatrics, Kobe University School of Medicine, Kobe, Hyogo, Japan

³Department of Healthcare Services Management, Nihon University School of Medicine, Tokyo, Japan

Alport syndrome is a progressive renal disease caused by mutations in *COL4A3*, *COL4A4*, and *COL4A5* genes that encode collagen type IV alpha 3, alpha 4, and alpha 5 chains, respectively. Because of abnormal collagen chain, glomerular basement membrane becomes fragile and most of the patients progress to end-stage renal disease in early adulthood. *COL4A5* mutation causes X-linked form of Alport syndrome, and two mutations in either *COL4A3* or *COL4A4* causes an autosomal recessive Alport syndrome. Recently, renin-angiotensin-aldosterone system (RAAS) blockade has been shown to attenuate effectively disease progression in Alport syndrome. Here we present three Japanese siblings and their father all diagnosed with autosomal recessive Alport syndrome and with different clinical courses, suggesting the importance of the early initiation of RAAS blockade. The father was diagnosed with Alport syndrome. His consanguineous parents and his wife were healthy. All three siblings showed hematuria since infancy. Genetic analysis revealed that they shared the same gene mutations in *COL4A3* in a compound heterozygous state: c.2330G>A (p.Gly777Ala) from the mother and c.4354A>T (p.Ser1452Cys) from the father. Although RAAS blockade was initiated for the older sister and brother when their renal function was already impaired, it did not attenuate disease progression. In the youngest brother, RAAS blockade was initiated during normal renal function stage. After the initiation, his renal function has been normal with the very mild proteinuria to date at the age of 17 years. We propose that in Alport syndrome, RAAS blockade should be initiated earlier than renal function is impaired.

Keywords: autosomal recessive Alport syndrome; *COL4A3*; end-stage renal disease; proteinuria; renin-angiotensin-aldosterone system blockade

Tohoku J. Exp. Med., 2016 November, 240 (3), 251-257. © 2016 Tohoku University Medical Press

Introduction

Alport syndrome (AS) is a progressive renal disease caused by mutations in *COL4A3*, *COL4A4*, and *COL4A5* genes that encode collagen type IV alpha 3, alpha 4, and alpha 5 chains, respectively. Because of abnormal collagen chain, glomerular basement membrane (GBM) becomes fragile and most patients progress to end-stage renal disease in early adulthood. Approximately 85% of cases were caused by *COL4A5* mutation transmitted in X-linked dominant form, whereas 15% of cases were caused by two pathogenic mutations in either *COL4A3* or *COL4A4* on chromosome 2q 35-37 in an autosomal recessive fashion. Rare cases have autosomal dominant inheritance of mutation in *COL4A3* or *COL4A4*.

No curative therapy for AS has been reported; thus, clinicians have been investigating therapies to delay AS

progression. Callis et al. (1999) reported the beneficial effect of cyclosporine on AS progression, although recent reports suggest that the effect is limited and also associated with nephrotoxicity (Charbit et al. 2007; Massella et al. 2010). Recently, the renoprotective effect of renin-angiotensin-aldosterone system (RAAS) blockade by angiotensin-converting enzyme inhibition (ACEi) in AS has become evident (Gross et al. 2012), and there is increasing evidence that angiotensin II receptor blocker (ARB) (Webb et al. 2011) and aldosterone inhibitor (Kaito et al. 2006) are anti-proteinuric and renoprotective. Here we report the cases of three Japanese siblings and their father with autosomal recessive AS. The siblings shared the same genetic mutations in *COL4A3* in a compound heterozygous state and exhibited diverse clinical courses depending on the disease stage at which RAAS blockade was initiated.

Methods

Calculation of estimated glomerular filtration rate (eGFR)

eGFR was calculated using the Shwartz Formula from the age of 4 to 21 years and the Japanese Equation for estimating GFR when they were older than 21 years (Matsuo et al. 2009). The formulae (Shwartz Formula) are as follows: $eGFR \text{ (mL/min/1.73 m}^2\text{)} = k^* \times \text{body height (m)} \times 100/\text{serum creatinine (mg/dL)}$; $k^* = 0.55$ (age 2-12), 0.70 (male, age 13-21), 0.55 (female, age 13-21); and (Japanese Equation for estimating GFR) $eGFR \text{ (mL/min/1.73 m}^2\text{)} = 194 \times (\text{serum creatinine})^{-1.094} \times (\text{Age})^{-0.287}$ ($\times 0.739$, if female).

Mutation analysis

The genetic analysis was performed as previously described (Oka et al. 2014). Genomic DNA was isolated from peripheral blood. All exons and exon boundaries of *COL4A3* and *COL4A4* were amplified using polymerase chain reaction (PCR). PCR products were purified and subjected to direct sequencing.

Immunofluorescent staining

Immunofluorescent staining for collagen IV $\alpha 5$ was performed as previously described (Oka et al. 2014). Rat monoclonal antibodies $\alpha 5$ (IV) chains were used that is already conjugated by secondary antibody (H52; Shigei Medical Research Institute, Okayama, Japan).

Ethics

This study was approved by the Ethics Committee of the Tohoku University School of Medicine and Kobe University Graduate School of Medicine. Informed consent was obtained from all patients

and their mother.

Case Presentation

We report three Japanese siblings and their father with autosomal recessive AS (Fig. 1). The relevant data from the three siblings were published in a previous report (Oka et al. 2014).

Father

The father was diagnosed with AS and had impaired hearing. He underwent maintenance dialysis in his 30s and died at the age of 47 years (Fig. 1). His consanguineous parents and his wife (mother of the siblings) were healthy. Continuous hematuria was not evident in his parents and wife.

Patient 1 (Eldest sister)

At the age of 7 years, the eldest sister was referred to our hospital because of familial hematuria. Her laboratory findings were as follows: blood urea nitrogen (BUN), 8 mg/dL; serum creatinine (sCre), 0.3 mg/dL; total protein, 6.0 g/dL; albumin (ALB), 3.6 g/dL; uric acid (UA), 4.1 mg/dL; hematuria, 3+; and urine protein, negative. She showed neither edema nor hypertension. Her physical and mental developments were normal. Renal biopsy revealed irregular thickening and thinning of the glomerular basement membrane (GBM). The lamina densa was irregularly lamellated (Fig. 2A). According to the additional immuno-

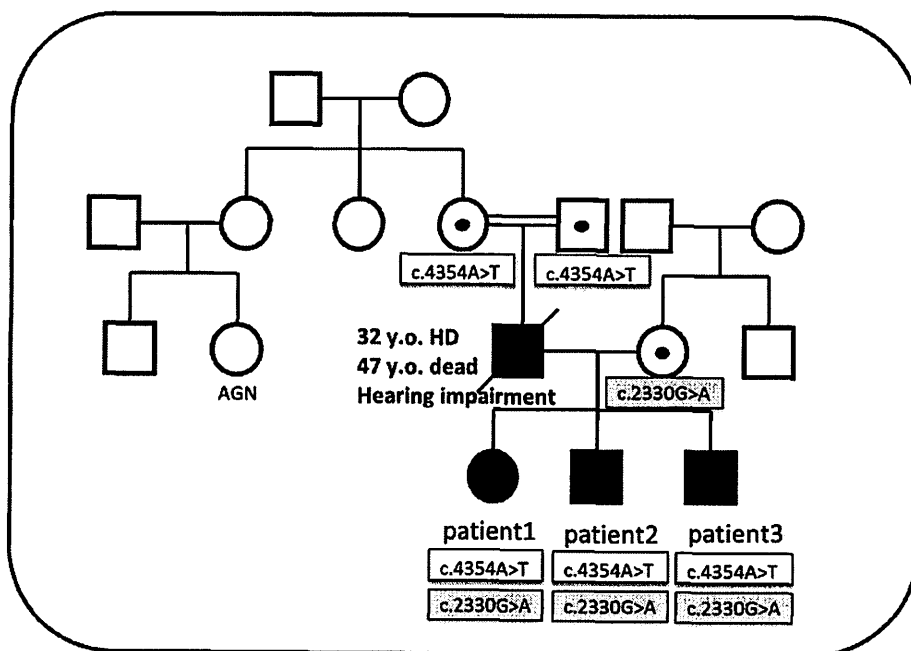


Fig. 1. Family tree showing the distribution of genetic mutations.

The father underwent hemodialysis (HD) at the age of 32 years and died at the age of 47 years. All three siblings share the same gene mutations *c.2330G>A* and *c.4354A>T* in *COL4A3* in a compound heterozygous state. *c.2330G>A* was transmitted from their mother. DNA from their deceased father was unavailable. Their paternal grandparents are expected to have *c.4354A>T* in a heterozygous state; hence, the father is expected to have *c.4354A>T* in the homozygous state. HD, hemodialysis; AGN, Acute Glomerulonephritis.

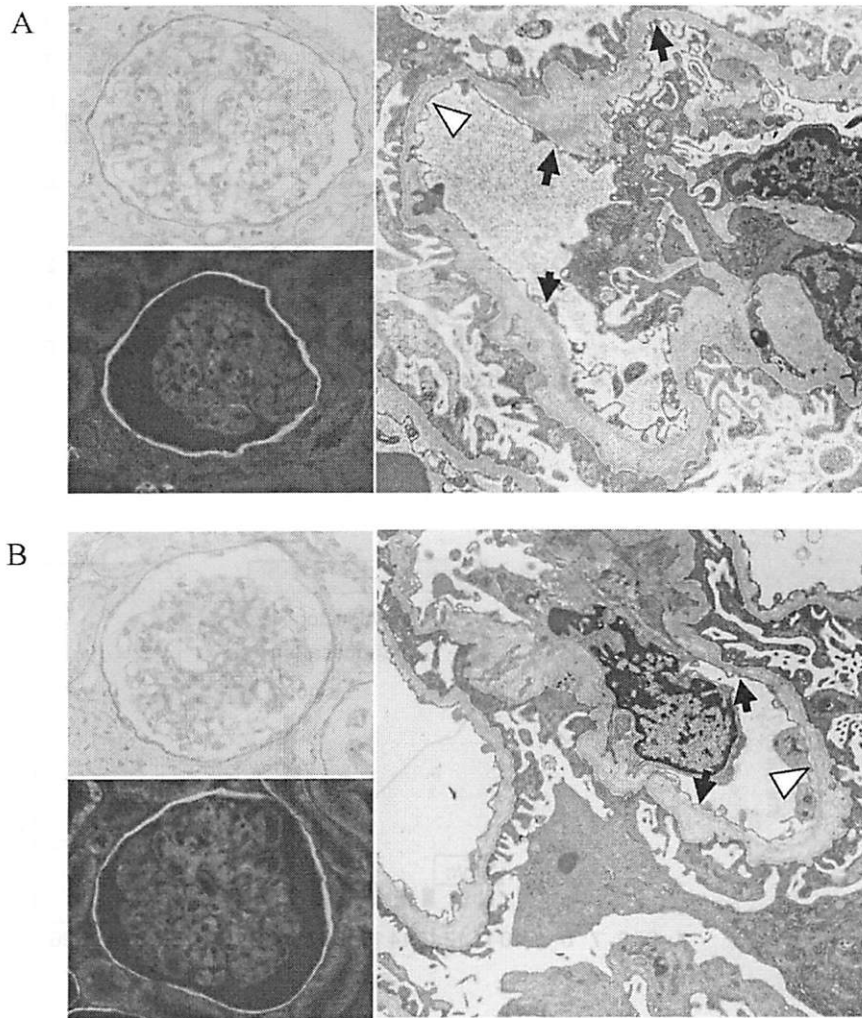


Fig. 2. Morphological analysis of the renal biopsy specimens. The renal biopsy specimens were obtained from patient 1 (A) and patient 2 (B). Light microscopy with Periodic Acid-Schiff (PAS) stain (left upper) shows mild mesangial proliferation. Immunostaining for collagen 4 α 5 (left lower) reveals that collagen 4 α 5 is only distributed on the Bowman's capsule but absent in the GBM, suggesting the autosomal recessive AS. Electron microscopy (right) shows irregular thickening and thinning of GBM (black arrow). The lamina densa is irregularly lamellated (white arrow).

histochemistry performed 15 years later, collagen 4 α 5 was absent in the GBM and present only on the Bowman's capsule (Fig. 2A), indicating that she had autosomal recessive AS (Kashtan 2005). No effective AS treatment was available in the 1990s; hence, she was initially followed up annually without any therapy. Subsequently, cyclosporine was administered when she was at 12, 15, and 18 years of age, with the expectation of renoprotective effect. Trough value of cyclosporine was mostly kept within 50-70 ng/mL; maximum value was 83.5 ng/mL during follow up. It was partially effective in decreasing proteinuria; however, decline in renal function progressed. At the age of 17 years, her laboratory findings were as follows: BUN 17 mg/dL; sCr, 0.8 mg/dL; hematuria, 2+; eGFR, 86.9 mL/min/1.73 m²; and urine protein creatinine ratio (Up/c), 1.8 g/gCr. At

the age of 19 years (BUN, 33 mg/dL; sCr, 1.2 mg/dL; eGFR, 62.4 mL/min/1.73 m²; hematuria, 2+; and Up/c, 1.9 g/gCr), RAAS blockade including lisinopril, candesartan, and aldactone was initiated. However, her renal function continued to decline. At the age of 27 years, she was diagnosed with stage 4 chronic kidney disease (Fig. 3A). Mild retinopathy was observed on follow up. Hearing impairment has not been observed.

Patient 2 (Elder brother)

The elder brother was referred to our hospital along with patient 1 for familial hematuria at the age of 6 years. His laboratory findings were as follows: BUN 13 mg/dL; sCr, 0.4 mg/dL; hematuria, 3+; eGFR, 107.2 mL/min/1.73 m²; and urine protein, 1+. He had shown normal develop-

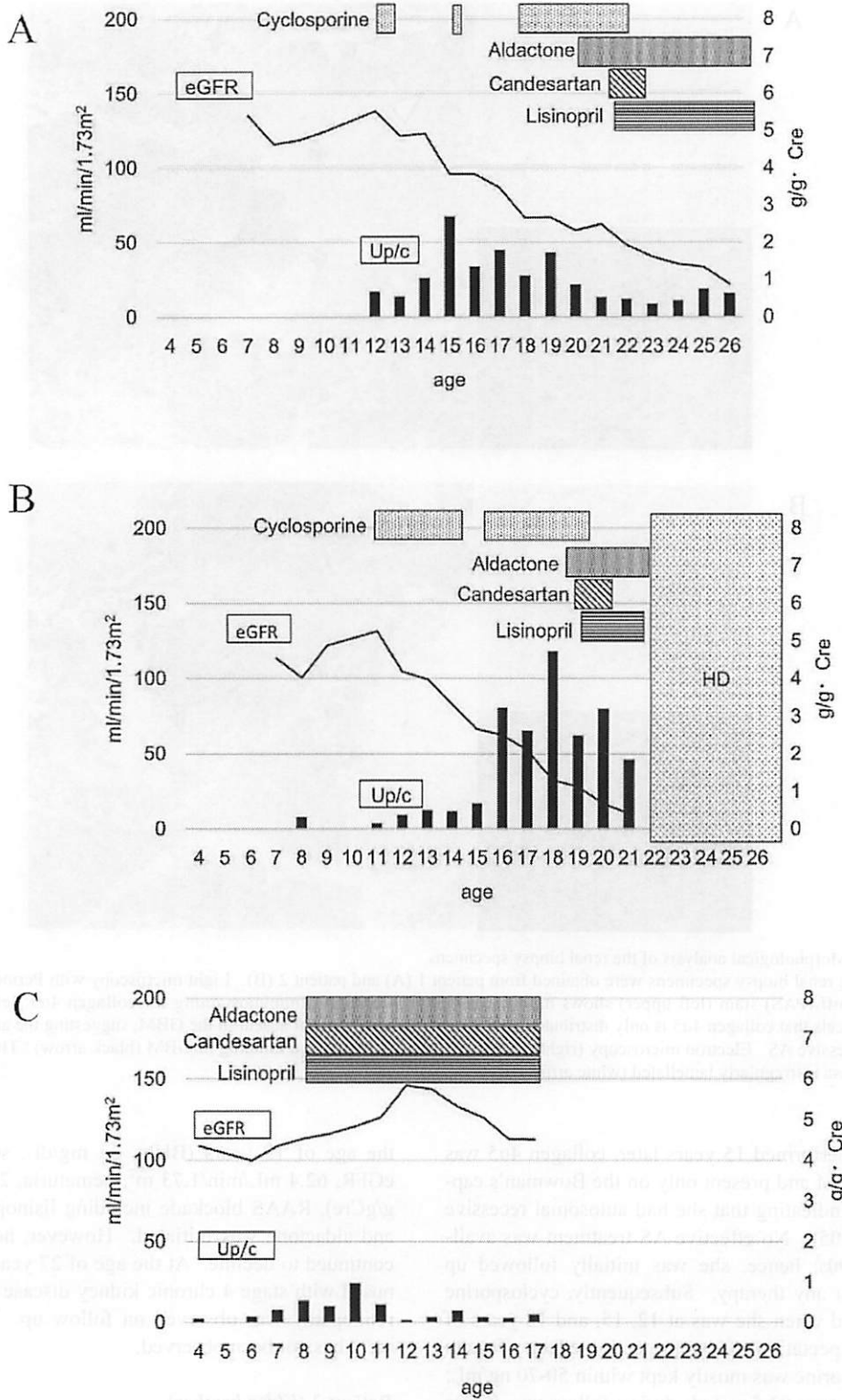


Fig. 3. Clinical courses of the three siblings.

A) Patient 1: Cyclosporine was administered with the expectation of renoprotective effect, but could not attenuate disease progression. Despite the initiation of RAAS blockade including Aldactone, Candesartan and Lisinopril during the renal impairment stage, her renal function was deteriorated. B) Patient 2: Cyclosporine could not stop the deterioration of renal function. RAAS blockade was initiated during the renal impairment stage, but he has already progressed to end-stage renal disease. C) Patient 3: RAAS blockade was started earlier than the other siblings, before the onset of renal impairment, and he has normal eGFR. His urine protein level has been low after the initiation of RAAS blockade.

ment. His renal biopsy was also consistent with autosomal recessive AS (Fig. 2B). At the age of 11 and 15 years, cyclosporine was administered and seemed to be partially effective in reducing proteinuria, although the decline in renal function was not terminated. Trough value of cyclosporine was mostly kept within 50-70 ng/mL; maximum value was 84.4 ng/mL during follow up. At the age of 17 years, his laboratory findings were as follows: sCr, 1.6 mg/dL; hematuria, 2+; eGFR, 52.5 mL/min/1.73 m²; and Up/c, 2.6 g/gCr. At the age of 19 years (sCr, 3.0 mg/dL; eGFR, 27.8 mL/min/1.73 m²; hematuria, 2+; and Up/c, 4.7 g/gCr), RAAS blockade was initiated but was ineffective. At the age of 22 years, he underwent maintenance dialysis (Fig. 3B). Ocular and hearing impairment has not been observed thus far.

Patient 3 (Youngest brother)

Patient 3 was born 10 years after his siblings. Hematuria was noted from infancy. At the age of 9 years (with sCr, 0.4 mg/dL; eGFR 121 mL/min/1.73 m²; hematuria, 3+; and Up/c, 0.98 g/gCr), RAAS blockade was initiated because proteinuria emerged. Renal biopsy was not performed, although genetic analysis revealed that he has the same mutations on *COL4A3* as his siblings, suggesting he has autosomal recessive AS. After treatment initiation, his urine protein levels returned to normal. At the age of 17 years, he has not yet shown any decline in renal function and his laboratory findings were as follows: sCr, 0.8 mg/dL; eGFR 112.9 mL/min/1.73 m²; hematuria, 3+; and Up/c, 0.20 g/gCr (Fig. 3C) at the last follow-up. No ocular or hearing impairment has developed so far. No adverse event has been observed related to RAAS blockade, including hyperkalemia, hypotension, and dry cough.

Genetic analysis

Genetic analysis revealed that all three siblings shared the same gene mutation c.2330G>A (p.Gly777Ala) in exon 30 and c.4354A>T (p.Ser1452Cys) in exon 48 in *COL4A3* in a compound heterozygous state (Fig. 1). Both mutations were novel and were not single-nucleotide polymorphisms (Oka et al. 2014). c.2330G>A was transmitted from their mother. DNA from their deceased father was unavailable. Both of their paternal grandparents had c.4354A>T in the heterozygous state; hence, the father was expected to have c.4354A>T in the homozygous state.

Discussion

AS has been an untreatable disease for the past 90 years, and thus, effective therapies have been investigated. Although cyclosporine was reported to have an anti-proteinuric and renoprotective effect in AS patients during the late 1990s (Callis et al. 1999), recent reports showed that its anti-proteinuric effects are transient (Massella et al. 2010), and the prolonged use of cyclosporine results in nephrotoxicity (Charbit et al. 2007). At the beginning of the 2010s, RAAS blockade was shown to delay renal replacement

therapy in AS patients (Gross et al. 2012). Our patients were representative of the transition in therapies for AS; there was no effective treatment when the first case (Father) was diagnosed with AS, and he started maintenance hemodialysis in his 30s and died in his 40s. When patients 1 and 2 were diagnosed, there was still no treatment available. Later, cyclosporine was administered to both of them with the expectation of renoprotective effect; however, its anti-proteinuric effect was transient, and it did not stop renal function deterioration. Although it was unclear how the administration of cyclosporine affected the decline of renal function in patients 1 and 2 (re-biopsy has not been performed), prolonged use of cyclosporine might affect their renal function. During the impaired renal function stage, patients 1 and 2 started RAAS blockade treatment, but they inevitably experienced renal failure. The effect of RAAS blockade on the reduction of proteinuria was also unclear. Patient 3 was born 10 years after his siblings. When his proteinuria emerged, the renoprotective effect of ACEi and ARB on AS progression had been verified by a number of studies (Webb et al. 2011; Gross et al. 2012). In addition, aldosterone inhibitor had been reported to effectively reduce proteinuria in AS patients who showed persistent proteinuria despite of initiation of ACEi and ARB (Kaito et al. 2006). RAAS blockade, including lisinopril, candesartan, and aldosterone, was immediately started before his renal function deteriorated. To date, at the age of 17 years, his renal function is within the normal range with the very mild proteinuria. Oka et al. reported the median age of end-stage renal disease in autosomal recessive AS to be 21.0 years (Oka et al. 2014). In our cases, the older sister and brother progressed to stage 4 chronic kidney disease and end-stage renal disease at the ages of 26 and 22 years, respectively, which were consistent with those in the previous report. Compared with the siblings and the other patients with autosomal recessive AS, the youngest brother has shown a much better clinical course so far (Oka et al. 2014).

To evaluate the effectiveness of AS treatment is difficult because ESRD develops after 10-20 years of age, and the disease phenotype varies depending on the individuals' genotype. Because our cases were siblings sharing the same gene mutations, they should have developed the same phenotype. However, they showed diverse clinical courses depending on the time at which RAAS blockade was initiated which is consistent with the previous report (Gross et al. 2012).

Genetic analysis revealed our cases to have autosomal recessive AS. Autosomal recessive AS consecutively developed in the father and the three siblings, despite the father and his wife not being consanguineous (Fig. 1). To the best of our knowledge, there are no previous reports on such a hereditary form in autosomal recessive AS.

The three siblings shared compound heterozygous mutation, c.2330G>A in exon 30 and c.4354A>T in exon 48 on *COL4A3*. Collagen type IV alpha 3 has a 28-amino-acid leucine-rich signal peptide, followed by a 1,410-

amino-acid collagenous domain, and a 232-amino-acid C-terminal NC1 domain. GBM consists of triple helix of collagen type IV alpha 3, alpha 4, and alpha 5. C-terminal NC1 domain is involved in the alignment of individual alpha chains into a triple-helical structure. c.2330G>A from their mother encodes collagenous domain, and c.4354A>T from their father encodes C-terminal NC1 domain. Thus, the former mutation was expected to cause malformation of the collagen monomer itself and the later was expected to impair to form triple helix of collagen type IV. To confirm that these mutations cause the structural change, future study using in silico three-dimensional structural analysis would be needed.

Impaired hearing is a common extra-renal feature of AS. The rate of hearing impairment in autosomal recessive AS varies from 40 % to 100 % (Oka et al. 2014; Wang et al. 2014). In our cases, the father experienced hearing impairment, while none of the siblings have had difficulty in hearing so far. It was reported that the occurrence and progression of hearing impairment in AS varied depending on the mutations (Barker et al. 1996). It is possible that c.4354A>T mutation, which the father was expected to have in a homozygous form, was strongly related to hearing impairment but c.2330G>A was not. This might be the reason why the siblings who shared the mutations, c.4354A>T and c.2330G>A in a compound heterozygous form, have not developed hearing impairment.

Gross et al. (2012) reported that RAAS blockade with ACEi delayed dialysis in AS patients, regardless of disease stage at which RAAS blockade was initiated. However, the best effect was obtained when the treatment was initiated before proteinuria developed (Gross et al. 2012). Proteinuria is known to accelerate kidney disease progression (Abbate et al. 2006). Excessive protein in the glomerular filtrate activates proinflammatory and profibrotic signaling pathway in proximal tubular epithelial cells, leading to deterioration in renal function. Proteinuria is caused by alterations in glomerular membrane permeability and selectivity due to several mechanisms, including mechanical injury induced by glomerular hypertension (Remuzzi and Bertani 1990). ACEi reduces intra-glomerular pressure not only through inhibition of intra-renal angiotensin II generation but also through a bradykinin-mediated action (Salveti et al. 1999). ARB blocks angiotensin II receptor and lowers intra-glomerular pressure. Reducing intra-glomerular pressure, RAAS blockade is expected to exert renoprotective effects by an anti-proteinuric pathway (Noone and Licht 2013). In addition, angiotensin II has been shown to be profibrotic, behaving as a cytokine, activating mononuclear cells, and increasing proinflammatory mediators (Mezzano et al. 2001). ACEi is expected to be renoprotective by blocking conversion of angiotensin I to angiotensin II (Gross et al. 2003). Consistent with the above findings, the youngest brother (patient 3), whose urine protein level remained to be low after the initiation of RAAS blockade, has not shown any deterioration of renal function so far.

Our cases suggest that the initiation of RAAS blockade earlier than decline of renal function is critical for instigating sufficient renoprotective effect of RAAS blockade. Nowadays, ACEi and ARB/aldosterone inhibitor are the first- and second-line agents for AS because the effectiveness of RAAS blockade has been strongly suggested by retrospective observational study (Gross et al. 2012). However, there remain some clinical questions, such as when RAAS blockade should be initiated and whether it could be done without severe adverse effect if initiated earlier. Ongoing large prospective study (The EARLY PROTECT STUDY) would answer some of these questions (Savva et al. 2016). We think our cases are clinically important because of the rareness of their hereditary form and the efficacy of RAAS blockade on the youngest brother despite of the severe clinical courses of his siblings. We hope that the initiation of RAAS blockade with no delay would improve the prognosis of AS by early diagnosis and careful monitoring in entire pediatric population with AS.

Conflict of Interest

The authors declare no conflict of interest.

References

- Abbate, M., Zoja, C. & Remuzzi, G. (2006) How does proteinuria cause progressive renal damage? *J. Am. Soc. Nephrol.*, **17**, 2974-2984.
- Barker, D.F., Pruchno, C.J., Jiang, X., Atkin, C.L., Stone, E.M., Denison, J.C., Fain, P.R. & Gregory, M.C. (1996) A mutation causing Alport syndrome with tardive hearing loss is common in the western United States. *Am. J. Hum. Genet.*, **58**, 1157-1165.
- Callis, L., Vila, A., Carrera, M. & Nieto, J. (1999) Long-term effects of cyclosporine A in Alport's syndrome. *Kidney Int.*, **55**, 1051-1056.
- Charbit, M., Gubler, M.C., Dechaux, M., Gagnadoux, M.F., Grunfeld, J.P. & Niaudet, P. (2007) Cyclosporin therapy in patients with Alport syndrome. *Pediatr. Nephrol.*, **22**, 57-63.
- Gross, O., Beirowski, B., Koepke, M.L., Kuck, J., Reiner, M., Addicks, K., Smyth, N., Schulze-Lohoff, E. & Weber, M. (2003) Preemptive ramipril therapy delays renal failure and reduces renal fibrosis in COL4A3-knockout mice with Alport syndrome. *Kidney Int.*, **63**, 438-446.
- Gross, O., Licht, C., Anders, H.J., Hoppe, B., Beck, B., Tonshoff, B., Hocker, B., Wygoda, S., Ehrich, J.H., Pape, L., Konrad, M., Rascher, W., Dotsch, J., Muller-Wiefel, D.E., Hoyer, P., et al. (2012) Early angiotensin-converting enzyme inhibition in Alport syndrome delays renal failure and improves life expectancy. *Kidney Int.*, **81**, 494-501.
- Kaito, H., Nozu, K., Iijima, K., Nakanishi, K., Yoshiya, K., Kanda, K., Przybyslaw Krol, R., Yoshikawa, N. & Matsuo, M. (2006) The effect of aldosterone blockade in patients with Alport syndrome. *Pediatr. Nephrol.*, **21**, 1824-1829.
- Kashtan, C.E. (2005) The nongenetic diagnosis of thin basement membrane nephropathy. *Semin. Nephrol.*, **25**, 159-162.
- Massella, L., Muda, A.O., Legato, A., Di Zazzo, G., Giannakakis, K. & Emma, F. (2010) Cyclosporine A treatment in patients with Alport syndrome: a single-center experience. *Pediatr. Nephrol.*, **25**, 1269-1275.
- Matsuo, S., Imai, E., Horio, M., Yasuda, Y., Tomita, K., Nitta, K., Yamagata, K., Tomino, Y., Yokoyama, H. & Hishida, A. (2009) Revised equations for estimated GFR from serum creatinine in Japan. *Am. J. Kidney Dis.*, **53**, 982-992.

- Mezzano, S.A., Ruiz-Ortega, M. & Egido, J. (2001) Angiotensin II and renal fibrosis. *Hypertension*, **38**, 635-638.
- Noone, D. & Licht, C. (2013) An update on the pathomechanisms and future therapies of Alport syndrome. *Pediatr. Nephrol.*, **28**, 1025-1036.
- Oka, M., Nozu, K., Kaito, H., Fu, X.J., Nakanishi, K., Hashimura, Y., Morisada, N., Yan, K., Matsuo, M., Yoshikawa, N., Vorechovsky, I. & Iijima, K. (2014) Natural history of genetically proven autosomal recessive Alport syndrome. *Pediatr. Nephrol.*, **29**, 1535-1544.
- Remuzzi, G. & Bertani, T. (1990) Is glomerulosclerosis a consequence of altered glomerular permeability to macromolecules? *Kidney Int.*, **38**, 384-394.
- Salvetti, A., Mattei, P. & Sudano, I. (1999) Renal protection and antihypertensive drugs: current status. *Drugs*, **57**, 665-693.
- Savva, I., Pierides, A. & Deltas, C. (2016) RAAS inhibition and the course of Alport syndrome. *Pharmacol. Res.*, **107**, 205-210.
- Wang, Y., Sivakumar, V., Mohammad, M., Colville, D., Storey, H., Flinter, F., Dagher, H. & Savige, J. (2014) Clinical and genetic features in autosomal recessive and X-linked Alport syndrome. *Pediatr. Nephrol.*, **29**, 391-396.
- Webb, N.J., Lam, C., Shahinfar, S., Strehlau, J., Wells, T.G., Gleim, G.W. & Le Bailly De Tillegem, C. (2011) Efficacy and safety of losartan in children with Alport syndrome—results from a subgroup analysis of a prospective, randomized, placebo- or amlodipine-controlled trial. *Nephrol. Dial. Transplant.*, **26**, 2521-2526.
-



OPEN ACCESS

EXTENDED REPORT

GWAS of clinically defined gout and subtypes identifies multiple susceptibility loci that include urate transporter genes

Akiyoshi Nakayama,¹ Hirofumi Nakaoka,² Ken Yamamoto,³ Masayuki Sakiyama,^{1,4} Amara Shaukat,⁵ Yu Toyoda,⁶ Yukinori Okada,^{7,8,9} Yoichiro Kamatani,⁸ Takahiro Nakamura,¹⁰ Tappei Takada,⁶ Katsuhisa Inoue,¹¹ Tomoya Yasujima,¹² Hiroaki Yuasa,¹² Yuko Shirahama,³ Hiroshi Nakashima,¹³ Seiko Shimizu,¹ Toshihide Higashino,¹ Yusuke Kawamura,¹ Hiraku Ogata,¹ Makoto Kawaguchi,¹ Yasuyuki Ohkawa,¹⁴ Inaho Danjoh,¹⁵ Atsumi Tokumasu,¹⁶ Keiko Ooyama,¹⁶ Toshimitsu Ito,¹⁷ Takaaki Kondo,¹⁸ Kenji Wakai,¹⁹ Blanka Stiburkova,^{20,21} Karel Pavelka,²¹ Lisa K Stamp,²² Nicola Dalbeth,²³ Eurogout Consortium Yutaka Sakurai,¹³ Hiroshi Suzuki,⁶ Makoto Hosoyamada,²⁴ Shin Fujimori,²⁵ Takashi Yokoo,²⁶ Tatsuo Hosoya,^{26,27} Ituro Inoue,² Atsushi Takahashi,^{8,28} Michiaki Kubo,²⁹ Hiroshi Ooyama,¹⁶ Toru Shimizu,^{30,31} Kimiyoshi Ichida,^{27,32} Nariyoshi Shinomiya,¹ Tony R Merriman,⁵ Hirotaka Matsuo¹

Handling editor Tore K Kvien

► Additional material is published online only. To view please visit the journal online (<http://dx.doi.org/10.1136/annrheumdis-2016-209632>).

For numbered affiliations see end of article.

Correspondence to

Dr Hirotaka Matsuo, Department of Integrative Physiology and Bio-Nano Medicine, National Defense Medical College, 3-2 Namiki, Tokorozawa, Saitama 359-8513, Japan; hmatsuo@ndmc.ac.jp

AN, HNakaoka, KY, MS, AS and YT contributed equally.

Received 29 March 2016
Revised 4 November 2016
Accepted 5 November 2016
Published Online First
29 November 2016



CrossMark

To cite: Nakayama A, Nakaoka H, Yamamoto K, et al. *Ann Rheum Dis* 2017;**76**:869–877.

ABSTRACT

Objective A genome-wide association study (GWAS) of gout and its subtypes was performed to identify novel gout loci, including those that are subtype-specific.

Methods Putative causal association signals from a GWAS of 945 clinically defined gout cases and 1213 controls from Japanese males were replicated with 1396 cases and 1268 controls using a custom chip of 1961 single nucleotide polymorphisms (SNPs). We also first conducted GWASs of gout subtypes. Replication with Caucasian and New Zealand Polynesian samples was done to further validate the loci identified in this study.

Results In addition to the five loci we reported previously, further susceptibility loci were identified at a genome-wide significance level ($p < 5.0 \times 10^{-8}$): urate transporter genes (*SLC22A12* and *SLC17A1*) and *HIST1H2BF-HIST1H4E* for all gout cases, and *NIPAL1* and *FAM35A* for the renal underexcretion gout subtype. While *NIPAL1* encodes a magnesium transporter, functional analysis did not detect urate transport via *NIPAL1*, suggesting an indirect association with urate handling. Localisation analysis in the human kidney revealed expression of *NIPAL1* and *FAM35A* mainly in the distal tubules, which suggests the involvement of the distal nephron in urate handling in humans. Clinically ascertained male patients with gout and controls of Caucasian and Polynesian ancestries were also genotyped, and *FAM35A* was associated with gout in all cases. A meta-analysis of the three populations revealed *FAM35A* to be associated with gout at a genome-wide level of significance ($p_{meta} = 3.58 \times 10^{-8}$).

Conclusions Our findings including novel gout risk loci provide further understanding of the molecular pathogenesis of gout and lead to a novel concept for the therapeutic target of gout/hyperuricaemia.

INTRODUCTION

Gout is a common disease characterised by acute painful arthritis, and its global burden continues to rise with the increasingly ageing population.¹ Gout is caused by hyperuricaemia, and can be classified according to patients' clinical parameters reflecting its causes^{2,3} as renal overload (ROL) gout and renal underexcretion (RUE) gout. As shown in online supplementary figure S1, patients with gout with increased urinary excretion of urate due to overproduction and/or decreased extra-renal underexcretion of urate are classified as having ROL gout, whereas those with decreased renal excretion of urate are defined as having RUE gout.² Reflecting their causes, almost all patients with gout are divided into those two subtypes. Although these subtypes are important from both genetic and pathophysiological points of view,^{2,4} genome-wide association studies (GWASs) of gout subtypes have never been performed, partly due to the difficulty in assembling sufficient gout cases with requisite clinical data, including data from a time-consuming urinary collection examination.

We and other groups^{5–9} recently reported gout/hyperuricaemia to have relatively strong genetic risk factors. More recently, and for the first time, we performed a GWAS with only clinically defined Japanese male gout cases in which 16 single nucleotide polymorphisms (SNPs) were replicated, and five gout-risk loci were identified including two novel loci (*MYL2-CUX2* and *CNIH-2*).¹⁰ In the present study (see online supplementary figure S2), we extended our analysis to identify novel susceptibility loci for gout by replicating approximately 2000 SNPs top-ranked in the GWASs of all gout and/or its subtypes. In addition, for the first time, we performed GWASs of gout subtypes to identify

subtype-specific (cause-specific) risk loci. Furthermore, we conducted a replication study with independent Caucasian and Polynesian populations to validate loci.

METHODS

Subjects and genotyping

Genome-wide genotyping was performed with the Illumina HumanOmniExpress-12 v1.0 (Illumina) platform using 946 clinically defined gout cases and 1213 controls, all Japanese males. Detailed methods of genotyping and quality control are previously described.¹⁰ Ultimately, 570 442 SNPs passed filters for 945 cases and 1213 controls. At the replication stage, 1246 cases were genotyped with a custom genotype platform using iSelect HD Custom Genotyping BeadChips (Illumina) on 1961 SNPs, as described in online supplementary methods and supplementary figure S3, and 150 gout cases were genotyped with the Illumina HumanOmniExpress-24 v1.0 (Illumina) platform. For controls, 1268 Japanese males with a serum uric acid (SUA) level ≤ 7.0 mg/dL and without gout history were recruited from BioBank Japan^{11 12} and genotyped with the Illumina HumanOmniExpress-12 v1.0 (Illumina) platform. Finally, 1961 SNPs with 1396 gout cases and 1268 controls were successfully genotyped (see online supplementary table S1). A genome-wide significance threshold was set to be $\alpha=5.0 \times 10^{-8}$ to claim evidence of a significant association.

GWASs of the two subtypes of gout, ROL gout and RUE gout (see online supplementary figure S1), were also performed, followed by replication studies with a custom SNP chip (see online supplementary figure S3) and a subsequent meta-analysis. As described previously,^{2 10} and shown in online supplementary figure S1 and supplementary methods, ROL gout and RUE gout are defined when patients' urinary urate excretion is over 25.0 mg/hour/1.73 m² (600 mg/day/1.73 m²) and patients' urate clearance (urate clearance/creatinine clearance ratio, FE_{UA}) is under 5.5%, respectively. For GWASs of gout subtypes, 1178 cases were classified as ROL gout (560 cases at GWAS stage and 618 cases at replication stage) and 1315 cases as RUE gout (619 cases at GWAS stage and 696 cases at replication stage), respectively (see online supplementary table S2).

A replication study with independent Caucasian and New Zealand (NZ) Polynesian sample sets was also performed to validate the genetic risk loci identified in the present study. This replication was done in a data set recruited from New Zealand¹³ and from Europe by the Eurogout Consortium¹⁴ comprising 1319 male cases and 514 male controls of European ancestry and 971 male cases and 565 male controls of NZ Polynesian ancestry. SNPs were genotyped by an allelic discrimination assay (TaqMan) with a LightCycler 480 Real-Time PCR (RT-PCR) System (Roche Applied Science, Indianapolis, Indiana, USA). Detailed information of clinical characteristics and genetic analysis is shown in online supplementary methods and tables S1–S3.

Statistical analyses

The inverse-variance fixed-effects model was used for meta-analysis. In the meta-analysis with Japanese, Caucasian and NZ Polynesian populations or in the presence of heterogeneity ($p_{\text{het}} < 0.05$ or $I^2 > 50\%$), we implemented the DerSimonian and Laird random-effects model for meta-analysis.¹⁵ For the replication analysis with Caucasian and NZ Polynesian sample sets, ORs were adjusted by age and ancestral group. All the meta-analyses were performed using the R V3.1.1 and 3.2.2 (R Development Core Team, R: a language and environment for statistical computing, Vienna: R. Foundation for Statistical

Computing, 2006) with meta package. All calculations of linkage disequilibrium (LD, measured in r^2) were conducted using the Japanese population. The detailed information for statistical analyses is described in online supplementary methods.

Functional and localisation analyses

Urate transport analysis of NIPAL1 was performed with an oocyte expression system^{16 17} with high potassium (HK) buffer or HK buffer without magnesium. For immunohistochemical analysis, the human kidney sections (3 μ m) incubated with anti-human NIPAL1 antibody (1:50) (LS-C164878; LifeSpan BioSciences, Washington, USA) or with anti-human FAM35A antibody (1:75) (HPA036582; Sigma-Aldrich, Missouri, USA) were used, and then visualised with diaminobenzidine (0.8 mM).^{18 19} Intracellular localisation of NIPAL1 was also studied in *Xenopus* oocytes and Madin-Darby canine kidney II (MDCKII) cells. Detailed information for the functional and localisation analyses is described in online supplementary methods.

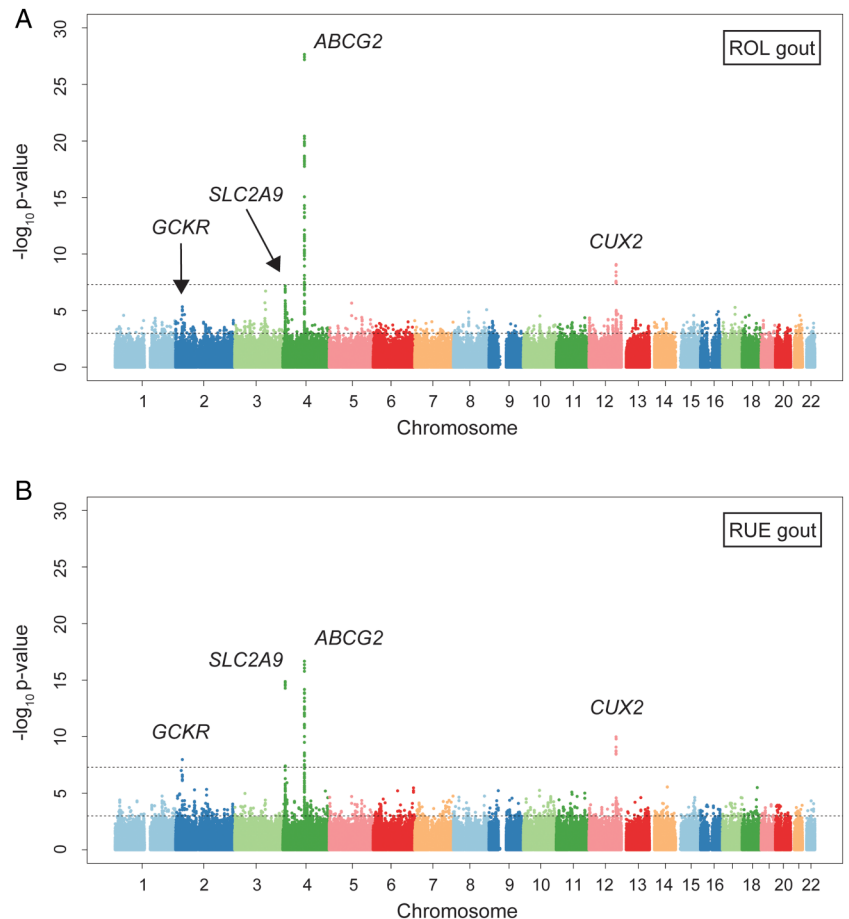
RESULTS

GWAS of all gout and its subtypes

In addition to the GWAS stage previously performed with 945 patients with clinically defined gout and 1213 controls, all Japanese males¹⁰ (see online supplementary figure S4), the replication stage for all cases of gout was carried out by genotyping 1961 SNPs (see online supplementary figure S3 and supplementary note) in a further 1396 male patients and 1268 male controls, and a meta-analysis then conducted (see online supplementary figure S2). Furthermore, GWASs of two subtypes of gout, ROL gout (figure 1A) and RUE gout (figure 1B), were also performed in the present study, followed by replication studies with a custom SNP chip and a subsequent meta-analysis.

Meta-analysis of both the GWAS and the replication study for all gout cases (table 1) identified eight loci which showed evidence for associations at the genome-wide significance level: rs3114020 of *ABCG2* ($p_{\text{meta}}=8.66 \times 10^{-35}$; OR=1.89), rs1014290 of *SLC2A9* ($p_{\text{meta}}=6.50 \times 10^{-26}$; OR=1.57), rs4766566 of *CUX2* ($p_{\text{meta}}=4.03 \times 10^{-20}$; OR=1.51), rs2285340 of *SLC22A12* ($p_{\text{meta}}=4.61 \times 10^{-11}$; OR=1.40), rs1260326 of *GCKR* ($p_{\text{meta}}=7.19 \times 10^{-11}$; OR=1.31), rs1165176 of *SLC17A1* ($p_{\text{meta}}=1.47 \times 10^{-9}$; OR=1.42), rs11758351 of *HIST1H2BF-HIST1H4E* ($p_{\text{meta}}=1.63 \times 10^{-8}$; OR=1.40) and rs4073582 of *CNIH-2* ($p_{\text{meta}}=3.56 \times 10^{-8}$; OR=1.58). Among these eight loci, *SLC22A12*, *SLC17A1* and *HIST1H2BF-HIST1H4E* (figure 2A–C) were first identified as gout-risk loci by the GWAS approach at the genome-wide significance level. *SLC17A1* was identified here by the GWAS approach for the first time, while Hollis-Moffatt *et al*²⁰ reported that rs1183201, another SNP of *SLC17A1*, is strongly associated with gout in Caucasians and NZ Polynesian sample sets by the candidate gene approach. While rs11758351 of *HIST1H2BF-HIST1H4E* is located 374 kb downstream from rs1165176 of *SLC17A1*, they are not in LD with each other ($r^2=0.03$), demonstrating them to be independent susceptibility loci for gout. There was also a significant signal from rs2532941 of *VARS2* ($p_{\text{meta}}=2.74 \times 10^{-8}$; OR=1.32), which is located downstream of *HIST1H2BF-HIST1H4E* by 4.7 Mb, and is reported to be associated with mitochondrial respiration.²¹ Since rs2532941 of *VARS2* showed mild LD with rs11758351 of *HIST1H2BF-HIST1H4E* ($r^2=0.37$), its significance did not remain for the GWAS stage samples after adjustment with rs11758351 of *HIST1H2BF-HIST1H4E* ($p=0.08$), or with both rs1165176 of *SLC17A1* and rs11758351 ($p=0.11$).

Figure 1 Manhattan plots of GWASs of subtypes of gout. Manhattan plots of GWASs of (A) ROL gout subtype and (B) RUE gout subtype. X-axis shows chromosomal positions. Y-axis shows $-\log_{10}$ p values. The upper and lower dotted lines indicate the genome-wide significance threshold ($p=5.0 \times 10^{-8}$) and the cut-off level for selecting single nucleotide polymorphisms for replication study ($p=0.001$), respectively. GWAS, genome-wide association study; ROL, renal overload; RUE, renal underexcretion.



For GWASs of gout subtypes, 1178 cases were classified as ROL gout (560 cases at GWAS stage and 618 cases at replication stage) and 1315 cases as RUE gout (619 cases at GWAS stage and 696 cases at replication stage), respectively (see online supplementary table S2). The meta-analysis of a GWAS of the ROL gout subtype and a replication study revealed significant SNPs in the following four loci: rs2728104 of *ABCG2* ($p_{meta}=5.08 \times 10^{-33}$; OR=1.84), rs4766566 of *CUX2* ($p_{meta}=8.14 \times 10^{-17}$; OR=1.59), rs3733589 of *SLC2A9* ($p_{meta}=2.25 \times 10^{-13}$; OR=1.47) and rs1260326 of *GCKR* ($p_{meta}=5.39 \times 10^{-9}$; OR=1.35).

Another subtype analysis, that is, the meta-analysis of a GWAS of RUE gout and a replication study (table 1) demonstrated significant SNPs in the following seven loci: rs1014290 of *SLC2A9* ($p_{meta}=8.71 \times 10^{-25}$; OR=1.69), rs1871744 of *ABCG2* ($p_{meta}=2.49 \times 10^{-22}$; OR=1.81), rs4766566 of *CUX2* ($p_{meta}=2.17 \times 10^{-18}$; OR=1.60), rs2285340 of *SLC22A12* ($p_{meta}=8.79 \times 10^{-10}$; OR=1.44), rs780094 of *GCKR* ($p_{meta}=1.62 \times 10^{-9}$; OR=1.35), rs11733284 of *NIPAL1* ($p_{meta}=1.13 \times 10^{-8}$; OR=1.34) and rs7903456 of *FAM35A* ($p_{meta}=4.29 \times 10^{-8}$; OR=1.34). The latter two loci, *NIPAL1* and *FAM35A*, were novel risk loci by the GWAS of the RUE gout subtype (figure 2D, E). In total, 10 loci were identified from the present GWAS of gout and its subtypes (table 1 and see online supplementary table S4).

Of the seven loci newly identified by GWAS of the RUE gout subtype, only *NIPAL1* and *FAM35A* had not been implicated previously in the GWASs of SUA levels or gout. Analysis with data from previously reported GWAS²² of SUA in Caucasians revealed the association with *NIPAL1* and *FAM35A* loci (see online supplementary figure S5).

Urate transport analysis of *NIPAL1* transporter

NIPAL1 and *FAM35A* were revealed to be associated with RUE gout in the present study. *NIPAL1* has been reported to be a magnesium transporter,²³ which has nine transmembrane domains (figure 3A), whereas *FAM35A* is predicted to be a soluble protein. In this context, we hypothesised that *NIPAL1* could be involved in the regulation of urate handling as a renal urate efflux transporter. However, our functional analysis using *Xenopus* oocytes did not show urate transport via *NIPAL1*, regardless of the presence of magnesium (figure 3B).

Localisation analysis of *NIPAL1* and *FAM35A*

By immunohistochemical analysis, *NIPAL1* and *FAM35A* showed cytosolic expression in the renal distal tubules of human kidney (figure 4A, B). Both proteins were also weakly detected in the cytoplasm of collecting ducts. *NIPAL1*-expressing *Xenopus* oocytes and MDCKII cells also showed intracellular localisation of *NIPAL1* (see online supplementary figure S6).

Replication study of all gout cases with Caucasian and Polynesian populations

A replication study for the discovered loci (*SLC22A12*, *SLC17A1*, *HIST1H2BF-HIST1H4E*, *NIPAL1* and *FAM35A*) was performed for all gout cases with males drawn from Caucasian (1319 cases and 514 controls) and NZ Polynesian populations (971 cases and 565 controls). Because a gain-of-function SNP of *SLC17A1*, rs1165196 (Ile269Thr),¹⁶ was in strong LD with rs1165176 ($r^2=0.99$), we performed the following analyses using rs1165196, assuming that the causal SNP in this locus was rs1165196 of *SLC17A1*. Among these five loci, the

Table 1 Single nucleotide polymorphisms (SNPs) associated with gout and its subtypes at a genome-wide level of significance in the Japanese population

| Gout types | SNP* | Chr. | Position (bp)† | Gene‡ | A1/A2§ | GWAS¶ | | | | Replication study** | | | | Meta-analysis†† | | Heterogeneity | |
|------------|------------|-----------|----------------|---------------------------|--------|-------|---------------------|------------------------|------------------------|---------------------|---------------------|-----------------------|------------------------|------------------------|------------------------|---------------|--------------------|
| | | | | | | Cases | Controls | OR (95% CI) | p Value | Cases | Controls | OR (95% CI) | p Value | OR (95% CI) | p Value | Cochran's Q | I ² (%) |
| All gout | rs1260326 | 2 | 27730940 | <i>GCKR</i> | T/C | 0.616 | 0.535 | 1.39 (1.23 to 1.57) | 1.34×10 ⁻⁷ | 0.611 | 0.557 | 1.25 (1.12 to 1.39) | 6.10×10 ⁻⁵ | 1.31 (1.21 to 1.42) | 7.19×10 ⁻¹¹ | 0.20 | 38.2 |
| | rs1014290 | 4 | 10001861 | <i>SLC2A9</i> | T/C | 0.678 | 0.564 | 1.63 (1.44 to 1.85) | 1.75×10 ⁻¹⁴ | 0.673 | 0.576 | 1.51 (1.35 to 1.69) | 2.97×10 ⁻¹³ | 1.57 (1.44 to 1.70) | 6.50×10 ⁻²⁶ | 0.39 | 0.0 |
| | rs3114020 | 4 | 89083666 | <i>ABCG2</i> | C/T | 0.842 | 0.724 | 2.03 (1.75 to 2.37) | 1.17×10 ⁻²⁰ | 0.844 | 0.752 | 1.78 (1.55 to 2.04) | 7.74×10 ⁻¹⁷ | 1.89 (1.71 to 2.09) | 8.66×10 ⁻³⁵ | 0.20 | 38.9 |
| | rs1165176 | 6 | 25830298 | <i>SLC17A1</i> | G/A | 0.874 | 0.834 | 1.38 (1.16 to 1.64) | 2.89×10 ⁻⁴ | 0.872 | 0.824 | 1.46 (1.25 to 1.69) | 1.08×10 ⁻⁶ | 1.42 (1.27 to 1.59) | 1.47×10 ⁻⁹ | 0.63 | 0.0 |
| | rs11758351 | 6 | 26203910 | <i>HIST1H2BF-HIST1H4E</i> | G/T | 0.158 | 0.121 | 1.37 (1.15 to 1.63) | 4.22×10 ⁻⁴ | 0.158 | 0.116 | 1.43 (1.22 to 1.67) | 1.01×10 ⁻⁵ | 1.40 (1.25 to 1.57) | 1.63×10 ⁻⁸ | 0.72 | 0.0 |
| | rs2285340 | 11 | 64435906 | <i>SLC22A12</i> | A/G | 0.228 | 0.174 | 1.40 (1.21 to 1.63) | 1.09×10 ⁻⁵ | 0.227 | 0.174 | 1.40 (1.22 to 1.61) | 9.96×10 ⁻⁷ | 1.40 (1.27 to 1.55) | 4.61×10 ⁻¹¹ | 1.00 | 0.0 |
| | rs4073582 | 11 | 66050712 | <i>CNIH-2</i> | C/T | 0.950 | 0.915 | 1.78 (1.39 to 2.29) | 4.32×10 ⁻⁶ | 0.943 | 0.920 | 1.44 (1.16 to 1.79) | 8.47×10 ⁻⁴ | 1.58 (1.34 to 1.86) | 3.56×10 ⁻⁸ | 0.21 | 36.1 |
| rs4766566 | 12 | 111706877 | <i>CUX2</i> | T/C | 0.735 | 0.633 | 1.60 (1.41 to 1.83) | 1.22×10 ⁻¹² | 0.741 | 0.665 | 1.44 (1.28 to 1.62) | 2.07×10 ⁻⁹ | 1.51 (1.38 to 1.65) | 4.03×10 ⁻²⁰ | 0.22 | 33.8 | |
| ROL gout | rs1260326 | 2 | 27730940 | <i>GCKR</i> | T/C | 0.611 | 0.535 | 1.36 (1.18 to 1.58) | 2.43×10 ⁻⁵ | 0.626 | 0.557 | 1.33 (1.16 to 1.53) | 6.12×10 ⁻⁵ | 1.35 (1.22 to 1.49) | 5.39×10 ⁻⁹ | 0.81 | 0.0 |
| | rs3733589 | 4 | 9987324 | <i>SLC2A9</i> | G/A | 0.662 | 0.570 | 1.48 (1.28 to 1.71) | 2.00×10 ⁻⁷ | 0.668 | 0.580 | 1.46 (1.26 to 1.68) | 2.05×10 ⁻⁷ | 1.47 (1.32 to 1.63) | 2.25×10 ⁻¹³ | 0.88 | 0.0 |
| | rs2728104 | 4 | 88973006 | <i>ABCG2</i> | C/T | 0.505 | 0.346 | 1.93 (1.67 to 2.23) | 3.28×10 ⁻¹⁹ | 0.496 | 0.359 | 1.75 (1.53 to 2.01) | 1.56×10 ⁻¹⁵ | 1.84 (1.66 to 2.03) | 5.08×10 ⁻³³ | 0.35 | 0.0 |
| | rs4766566 | 12 | 111706877 | <i>CUX2</i> | T/C | 0.737 | 0.633 | 1.62 (1.39 to 1.90) | 8.42×10 ⁻¹⁰ | 0.757 | 0.665 | 1.57 (1.34 to 1.83) | 7.55×10 ⁻⁹ | 1.59 (1.43 to 1.78) | 8.14×10 ⁻¹⁷ | 0.76 | 0.0 |
| RUE gout | rs780094 | 2 | 27741237 | <i>GCKR</i> | T/C | 0.633 | 0.543 | 1.45 (1.26 to 1.67) | 2.43×10 ⁻⁷ | 0.615 | 0.559 | 1.26 (1.10 to 1.44) | 6.47×10 ⁻⁴ | 1.35 (1.22 to 1.48) | 1.62×10 ⁻⁹ | 0.16 | 48.8 |
| | rs1014290 | 4 | 10001861 | <i>SLC2A9</i> | T/C | 0.699 | 0.564 | 1.80 (1.55 to 2.08) | 1.58×10 ⁻¹⁵ | 0.685 | 0.576 | 1.60 (1.39 to 1.84) | 1.72×10 ⁻¹¹ | 1.69 (1.53 to 1.87) | 8.71×10 ⁻²⁵ | 0.26 | 21.8 |
| | rs11733284 | 4 | 48028097 | <i>NIPAL1</i> | A/G | 0.346 | 0.281 | 1.35 (1.17 to 1.57) | 6.48×10 ⁻⁵ | 0.342 | 0.280 | 1.34 (1.16 to 1.54) | 6.36×10 ⁻⁵ | 1.34 (1.21 to 1.49) | 1.13×10 ⁻⁸ | 0.91 | 0.0 |
| | rs1871744 | 4 | 89039629 | <i>ABCG2</i> | T/C | 0.834 | 0.723 | 1.93 (1.62 to 2.29) | 3.85×10 ⁻¹⁴ | 0.824 | 0.733 | 1.71 (1.45 to 2.01) | 7.04×10 ⁻¹¹ | 1.81 (1.60 to 2.04) | 2.49×10 ⁻²² | 0.33 | 0.0 |
| | rs7903456 | 10 | 88919319 | <i>FAM35A</i> | A/G | 0.303 | 0.248 | 1.32 (1.13 to 1.53) | 4.32×10 ⁻⁴ | 0.296 | 0.235 | 1.37 (1.18 to 1.59) | 3.09×10 ⁻⁵ | 1.34 (1.21 to 1.49) | 4.29×10 ⁻⁸ | 0.72 | 0.0 |
| | rs2285340 | 11 | 64435906 | <i>SLC22A12</i> | A/G | 0.236 | 0.174 | 1.47 (1.25 to 1.74) | 8.04×10 ⁻⁶ | 0.228 | 0.174 | 1.41 (1.20 to 1.66) | 4.04×10 ⁻⁵ | 1.44 (1.28 to 1.62) | 8.79×10 ⁻¹⁰ | 0.72 | 0.0 |
| | rs4766566 | 12 | 111706877 | <i>CUX2</i> | T/C | 0.738 | 0.633 | 1.63 (1.40 to 1.89) | 1.58×10 ⁻¹⁰ | 0.759 | 0.665 | 1.58 (1.36 to 1.83) | 9.51×10 ⁻¹⁰ | 1.60 (1.44 to 1.78) | 2.17×10 ⁻¹⁸ | 0.78 | 0.0 |

*dbSNP rs number. SNPs having associations for all gout, ROL gout and RUE gout at the lowest p value in each locus by meta-analysis are shown in this table.

†SNP positions are based on NCBI human genome reference sequence build 37.4.

‡Five discovered loci are shown in bold.

§A1 is risk-associated allele and A2 is non-risk-associated allele.

¶1945 cases for all gout, 560 cases for ROL gout, 619 cases for RUE gout with 1213 controls from Japanese male population.

**1396 cases for all gout, 618 cases for ROL gout, 696 cases for RUE gout with 1268 controls from Japanese male population.

††Meta-analysis of GWAS and replication samples.

Chr., chromosome; GWAS, genome-wide association study; ROL, renal overload; RUE, renal underexcretion; SNP, single nucleotide polymorphism.

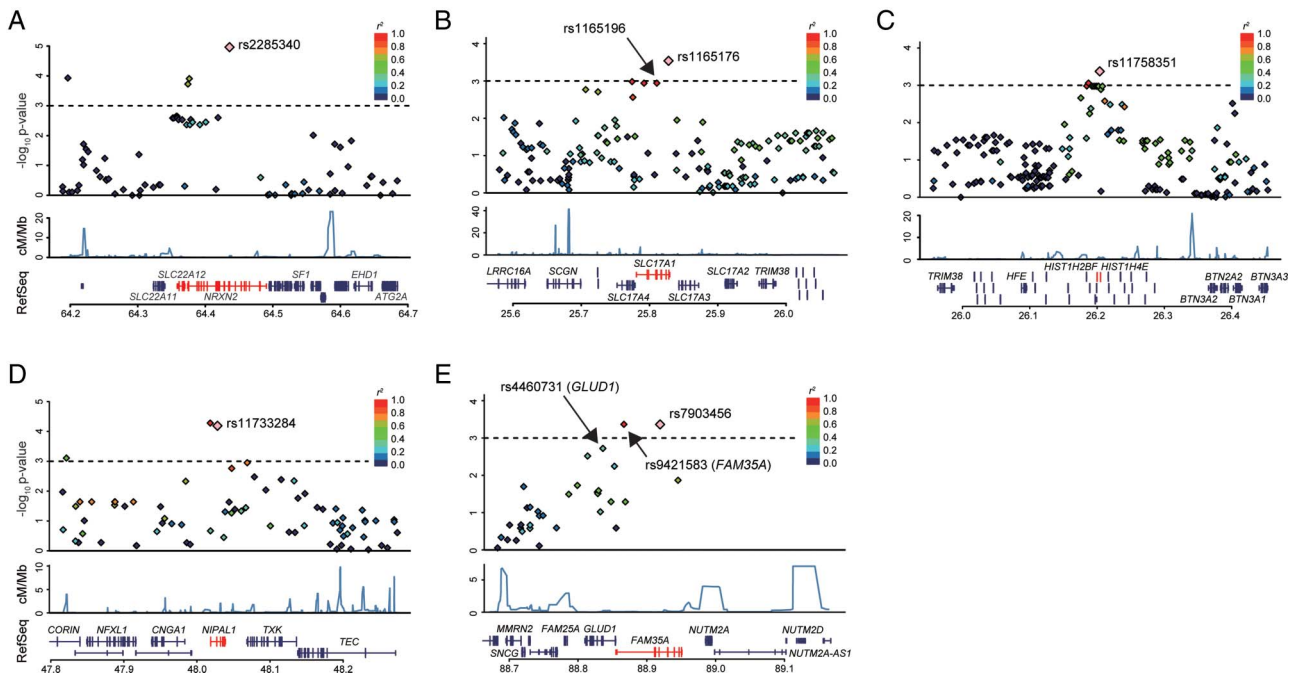
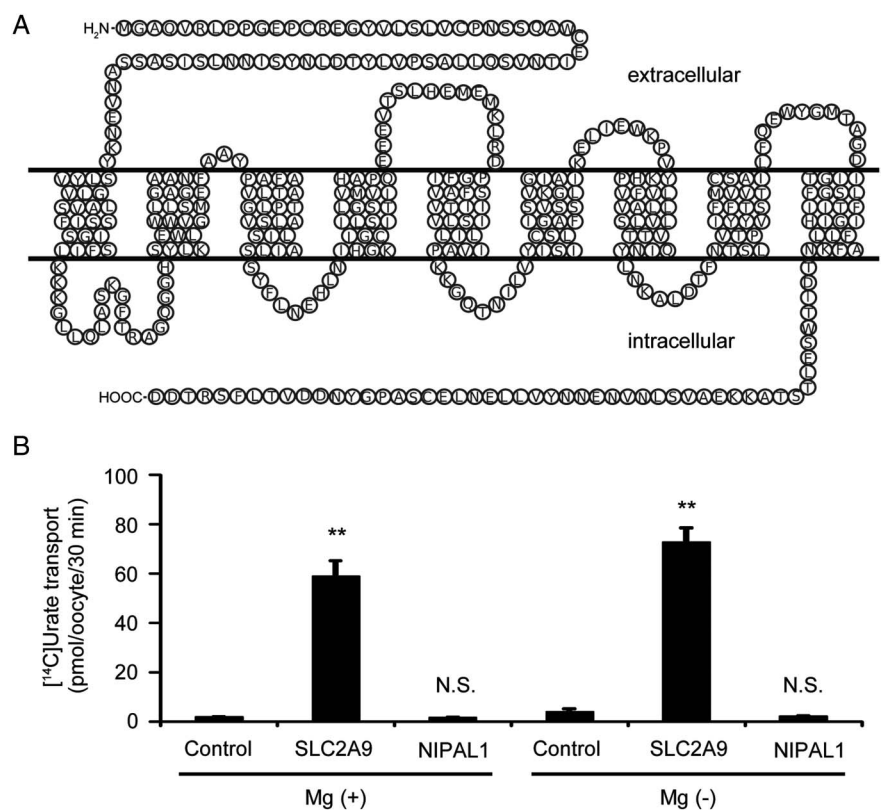


Figure 2 Regional association plots of five discovered loci. Three loci were revealed to exceed the genome-wide significance level from the meta-analysis with all gout cases, and two loci with renal underexcretion (RUE) gout cases. The highest association signal in each panel is located on (A) *SLC22A12*, (B) *SLC17A1* and (C) *HIST1H2BF-HIST1H4E* for all gout cases, and (D) *NIPAL1* and (E) *FAM35A* for RUE gout cases. The region within 250 kb from the single nucleotide polymorphism (SNP) indicating the lowest p value is shown. (Top panel) Plots of $-\log_{10}$ p values for the test of SNP association with gout in the genome-wide association study stage. The SNP showing the lowest p value in the meta-analysis is depicted as a pink diamond. Other SNPs are colour-coded according to the extent of linkage disequilibrium (measured in r^2) with the SNP showing the lowest p value. (Middle panel) Recombination rates (centimorgans per Mb) estimated from HapMap Phase II data are plotted. (Bottom panel) RefSeq genes. Genomic coordinates are based on NCBI human genome reference sequence build 37.

Figure 3 Functional analysis of *NIPAL1* transporter. (A) The topological model of the *NIPAL1* transporter. *NIPAL1* is predicted to have nine transmembrane regions. The amino acid sequences of *NIPAL1* were obtained from GenBank (accession code NM_207330). (B) Urate transport analysis of *NIPAL1*. *SLC2A9* (also known as *GLUT9*) is a renal urate transporter and is used for a positive control for the urate transport analysis. In contrast to *SLC2A9*, urate transport via *NIPAL1* was not detected, regardless of the presence of magnesium. Data are expressed as mean \pm SEM (n=8). Statistical analyses for significant differences were performed according to Student's t-test. (**p<0.01; N.S., not significantly different as compared with control.).



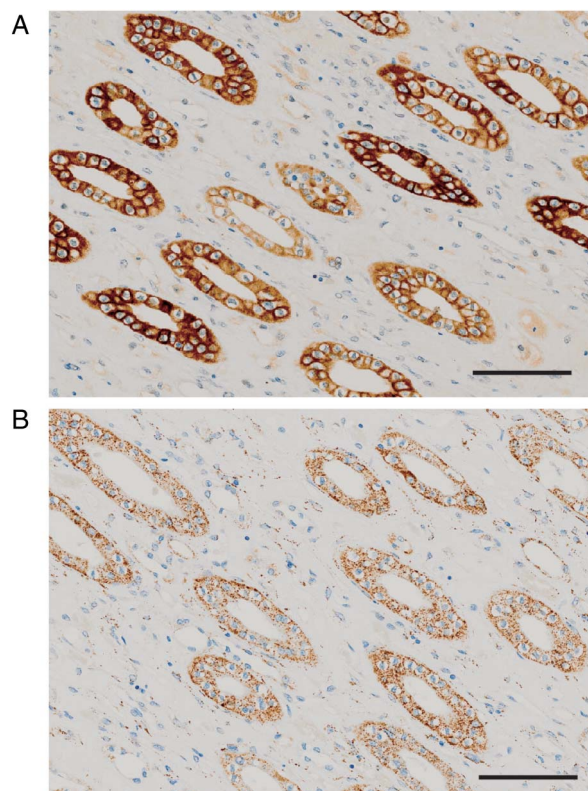


Figure 4 Localisation analysis of NIPAL1 and FAM35A in the human kidney. Cytosolic expression was detected strongly in distal tubules and weakly in collecting ducts in human kidney for (A) NIPAL1 protein and (B) FAM35A protein. Bar=100 μ m.

meta-analysis of those populations for all gout revealed a significant association with rs7903456 of *FAM35A* ($p_{meta}=9.72 \times 10^{-3}$; OR=1.17) (table 2). Although *SLC17A1* did not show significance ($p_{meta}=0.119$) in the present study of those populations (table 2), a previous paper²⁰ revealed a significant association of *SLC17A1* with gout in Caucasian and NZ Polynesian sample sets, indicating the necessity of further replication studies to investigate the ancestral differences in the significance of other genetic loci including *SLC17A1*. Genotyping the *CUX2* and *CNIH-2* loci, which were identified in both our present and previous GWASs of Japanese,¹⁰ was also performed, and the *CUX2* locus was replicated successfully for the first time in other populations (see online supplementary table S5). The results of further association analyses and expression quantitative trait locus (eQTL) analysis are shown in online supplementary note and tables S6 and S7. Significant effects on FE_{UA} were detected in *NIPAL1*, *FAM35A* and *SLC22A12* loci in the Japanese population, and were also observed at *SLC17A1* in NZ Polynesian population.

A further meta-analysis of all gout cases with Japanese, Caucasian and NZ Polynesian populations was performed for *NIPAL1* and *FAM35A*, which were at a genome-wide significance level in the Japanese population only for the RUE gout subtype, and not for all gout cases. rs11733284 of *NIPAL1* was not associated with all gout ($p_{meta}=0.16$; OR=1.11), suggesting the presence of ancestral differences in genetic effects of this locus, or a subtype-specific effect. On the other hand, rs7903456 of *FAM35A* showed an association with all gout at a genome-wide level of significance ($p_{meta}=3.58 \times 10^{-8}$; OR=1.23) (figure 5), indicating that rs7903456 is a susceptibility locus for all gout as well as the RUE gout subtype.

Table 2 Replication study of all gout for five discovered loci in Caucasian and NZ Polynesian sample sets

| SNP* | Chr. | position (bp)† | Gene | Caucasians‡ | | | | NZ Polynesians§ | | | | Meta-analysis** | | | | |
|-------------|------|----------------|---------------------------|-----------------|----------|---------|---------------------|-----------------|----------|---------|---------------------|-----------------|---------------------|-------------------------|------|-----|
| | | | | Frequency of A1 | | p Value | OR (95% CI) | Frequency of A1 | | p Value | OR (95% CI) | Heterogeneity | | | | |
| | | | | Cases | Controls | | | Cases | Controls | | | p Value | Q | I ² (%) | | |
| rs11733284 | 4 | 48028097 | <i>NIPAL1</i> | A/G | 0.362 | 0.356 | 1.01 (0.86 to 1.18) | 0.896 | 0.251 | 0.270 | 0.92 (0.77 to 1.10) | 0.355 | 0.97 (0.86 to 1.09) | 0.603 | 0.43 | 0.0 |
| rs1165196 | 6 | 25813150 | <i>SLC17A1</i> | T/C | 0.614 | 0.583 | 1.11 (0.95 to 1.30) | 0.271 | 0.731 | 0.711 | 1.12 (0.93 to 1.35) | 0.266 | 1.11 (0.98 to 1.25) | 0.119 | 0.88 | 0.0 |
| rs11758351 | 6 | 26203910 | <i>HIST1H2BF-HIST1H4E</i> | G/T | 0.141 | 0.158 | 0.86 (0.70 to 1.07) | 0.173 | 0.192 | 0.199 | 0.90 (0.74 to 1.10) | 0.334 | 0.88 (0.77 to 1.02) | 0.0941 | 0.77 | 0.0 |
| rs7903456 | 10 | 88919319 | <i>FAM35A</i> | A/G | 0.737 | 0.699 | 1.18 (1.00 to 1.40) | 0.0462 | 0.351 | 0.333 | 1.16 (0.98 to 1.38) | 0.0997 | 1.17 (1.04 to 1.32) | 9.72 × 10 ⁻³ | 0.85 | 0.0 |
| rs2285340†† | 11 | 64435906 | <i>SLC22A12</i> | A/G | - | - | - | - | 0.158 | 0.143 | 1.06 (0.84 to 1.35) | 0.634 | - | - | - | - |

*dbSNP rs number.

†SNP positions are based on NCBI human genome reference sequence build 37.4.

‡A1 is risk-associated allele, and A2 is non-risk-associated allele.

§1319 cases for all gout and 514 controls from Caucasian male population.

¶971 cases for all gout and 565 controls from NZ Polynesian male population.

**Meta-analysis of Caucasian and NZ Polynesian samples.

††rs2285340 is monomorphic in Caucasians.

Chr., chromosome; NZ, New Zealand; SNP, single nucleotide polymorphism.

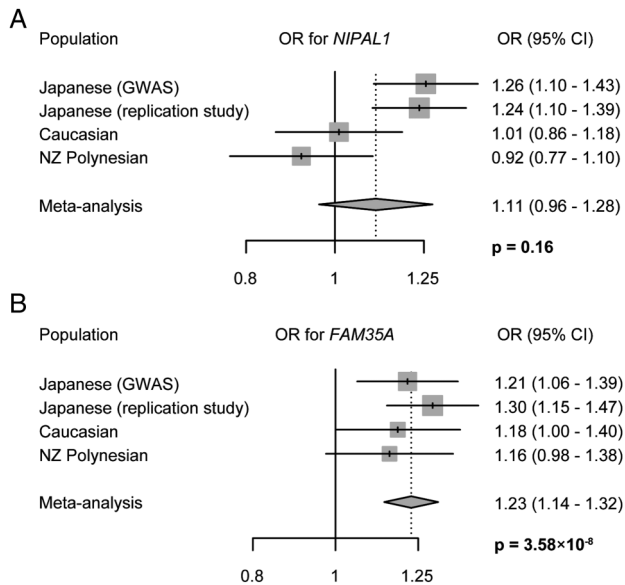


Figure 5 Forest plots for all gout among Japanese, Caucasian and New Zealand (NZ) Polynesian populations. Although rs11733284 of *NIPAL1* (A) did not show significant association with all gout, rs7903456 of *FAM35A* (B) revealed an association with all gout at a genome-wide significance level ($p_{meta}=3.58 \times 10^{-8}$; OR=1.23). GWAS, genome-wide association study.

Meta-analysis of all gout for the other three loci (*SLC22A12*, *SLC17A1* and *HIST1H2BF-HIST1H4E*) was also performed with Japanese, Caucasian and NZ Polynesian populations as shown in online supplementary figure S7. rs11758351 of *HIST1H2BF-HIST1H4E* did not show a significant association with gout ($p_{meta}=0.40$; OR=1.12). rs2285340 of *SLC22A12* and rs1165196 of *SLC17A1* did not reach a genome-wide level of significance ($p_{meta}=2.47 \times 10^{-4}$; OR=1.31; and $p_{meta}=1.28 \times 10^{-3}$; OR=1.25, respectively) partly due to statistical fluctuation in relatively small sample sets, although the effects were consistently in the same direction.

DISCUSSION

With clinically defined gout cases, we previously performed a GWAS¹⁰ and revealed that *ABCG2*, *SLC2A9*, *MYL2-CUX2*, *GCKR* and *CNIH-2* were associated with gout at a genome-wide significance level (see online supplementary figure S4). A more recent GWAS by Li *et al*²⁴ with clinically ascertained gout cases revealed three novel loci (*BCAS3*, *RFX3* and *KCNQ1*) in Han Chinese. In the present study, we performed a gout follow-up study focused on loci not reaching the genome-wide level of significance in the previous GWAS,¹⁰ genotyping 1961 SNPs in an additional 1396 cases and 1268 controls. We revealed a total of eight loci to be associated with all gout cases in Japanese males (table 1). Among them, three loci (*SLC22A12*, *SLC17A1* and *HIST1H2BF-HIST1H4E*) were first identified as gout risk loci at a genome-wide significance level by the present GWAS approach.

Both *SLC22A12* and *SLC17A1* encode urate transporters at the apical side of the renal proximal tubule^{16 25} (see online supplementary figure S8) and are reportedly associated with SUA level in humans by previous GWASs of SUA.^{12 22 26 27} Therefore, it is reasonable that SNPs around these loci would display significant associations with gout or sequelae of hyperuricaemia (see also online supplementary note for detail).

The *HIST1H2BF* and *HIST1H4E* genes encode histone 1 H2bf and histone 1 H4e, respectively, both of which have a role of binding DNA to form a chromatin structure. Both are replication-dependent histone proteins with expression dependent on cell cycle. Therefore, functional SNPs in this locus might affect the stability of the chromatin structure, varying the cell cycle, cell amount or reaction to inflammation by changing the expression level of histones in the kidney and/or intestine. Since it is also possible that rs11758351 is a surrogate marker near these histone genes, further studies concerning this locus will be necessary.

In this study, we first performed GWASs of gout subtypes, that is, RUE gout and ROL gout (figure 1). From the results of meta-analysis for GWASs of both ROL gout and RUE gout, four shared loci of *GCKR*, *SLC2A9*, *ABCG2* and *CUX2* were identified at a genome-wide significance level, showing the importance of these loci for the pathogenesis of both gout subtypes. Especially for RUE gout, three more loci, *SLC22A12*, *NIPAL1* and *FAM35A*, were identified to be associated at a genome-wide significance level. As described above, it is compatible for *SLC22A12* to be associated with RUE gout, because *SLC22A12* (like *SLC2A9*) encodes a renal urate reabsorption transporter.^{25 28}

Of note, *NIPAL1* and *FAM35A* were identified as novel loci by performing GWAS of the RUE gout subtype. Associations with gout and SUA have never been previously reported with *NIPAL1* and *FAM35A*. Furthermore, to our knowledge, there is no study reporting an association between any diseases and *NIPAL1* or *FAM35A*.

NIPAL1, also known as NIPA3, is reportedly expressed on the membrane of some organs including kidney, and to be a magnesium transporter,²³ as another magnesium transporter NIPA2.²³ Because *NIPAL1* was associated with RUE gout (ie, gout with renal urate underexcretion), we hypothesised that *NIPAL1* is a urate transporter in the human kidney. However, our functional study did not show urate transport via *NIPAL1*, regardless of the presence of magnesium (figure 3B). Moreover, localisation to the membrane was not detected for *NIPAL1* protein, which was mainly expressed within the distal tubules of human kidney, as revealed by immunohistochemical analysis (figure 4A). A similar result was obtained in confocal microscopic observation, with *NIPAL1*-expressing oocytes showing intracellular localisation of *NIPAL1* protein (see online supplementary figure S6). These findings suggest that *NIPAL1* is not a urate transporter and that it might be involved in the indirect regulation of urate transport kinetics. Nevertheless, recent studies have revealed associations between hyperuricaemia and magnesium intake,²⁹ serum magnesium level³⁰ and magnesium excretion.³¹ Together with previous reports, our findings support the hypothesis that there could be some relationship between gout and magnesium handling via magnesium transporters including *NIPAL1*, and that the present study could well provide new insights into the genetic background of urate and magnesium handling in patients with gout/hyperuricaemia.

FAM35A is ubiquitously expressed in organs including the kidney, and our immunohistochemical analysis of human kidney also revealed cytosolic immunoreactivity of the *FAM35A* protein mainly in the distal tubules (figure 4B). Our findings from *FAM35A* and *NIPAL1* suggest the involvement of the distal nephron in gout progression as well as dysfunction in urate handling in humans (see online supplementary figure S9). To date, the molecular function of *FAM35A* is totally unknown. Although further studies are necessary to confirm this, it is possible that genes near *FAM35A* including *GLUD1* (figure 2E)

have some relationship with gout (see also online supplementary note for details).

In addition to studying the Japanese population, we performed a replication study with male Caucasian and NZ Polynesian sample sets for the five newly discovered loci. Since they were not divided into subtypes, further evaluations by meta-analysis were conducted with all gout groups. While other loci were not replicated, rs7903456 of *FAM35A* was replicated with a significant association with gout (table 2). *CUX2*, which was reported by both our present and previous gout GWAS in Japanese,¹⁰ was also replicated in these sample sets (see online supplementary table S5).

A meta-analysis of all gout with Japanese, Caucasian and NZ Polynesian populations for these five SNPs revealed *FAM35A* to be associated with all gout at the genome-wide significance level (figure 5B), and that rs2285340 of *SLC22A12* and rs1165196 of *SLC17A1* showed a significant association but did not reach a genome-wide significance level (see online supplementary figure S7). rs11758351 of *HIST1H2BF-HIST1H4E* and rs11733284 of *NIPAL1* were not associated by this meta-analysis, although these loci showed a genome-wide significant association in the Japanese population. Since this might be due to the differences in LD structure among these populations, a replication analysis with East Asian populations will be necessary for these loci. rs2285340 of *SLC22A12* was monomorphic (only G allele) in Caucasians and not associated with NZ Polynesians. Therefore, replication studies of this locus in East Asian populations would also be insightful for future analysis. Although the underlying molecular mechanism of gout by *FAM35A* is unknown, this locus seems to have a common pathophysiological risk of gout for Japanese, NZ Polynesians and Caucasians.

In summary, we performed GWASs of all gout as well as gout subtypes and identified five loci in addition to the five loci that we reported previously.¹⁰ Furthermore, the *FAM35A* locus showed an association with all gout by meta-analysis among the Japanese, Caucasian and NZ Polynesian sample sets at a genome-wide level of significance. Together with their expression in the renal distal tubules, the identification of *NIPAL1* and *FAM35A* as gout loci suggests the involvement of the distal nephron (see online supplementary figure S9) in the urate handling of the human kidney and in the pathogenesis of gout/hyperuricaemia. These findings could well provide a clue leading to a novel concept for the therapeutic target of gout (see online supplementary figure S10).

Author affiliations

- ¹Department of Integrative Physiology and Bio-Nano Medicine, National Defense Medical College, Tokorozawa, Saitama, Japan
- ²Division of Human Genetics, Department of Integrated Genetics, National Institute of Genetics, Mishima, Shizuoka, Japan
- ³Department of Medical Chemistry, Kurume University School of Medicine, Kurume, Fukuoka, Japan
- ⁴Department of Dermatology, National Defense Medical College, Tokorozawa, Saitama, Japan
- ⁵Department of Biochemistry, University of Otago, Dunedin, New Zealand
- ⁶Department of Pharmacy, The University of Tokyo Hospital, Tokyo, Japan
- ⁷Department of Human Genetics and Disease Diversity, Graduate School of Medical and Dental Sciences, Tokyo Medical and Dental University, Tokyo, Japan
- ⁸Laboratory for Statistical Analysis, RIKEN Center for Integrative Medical Sciences, Yokohama, Kanagawa, Japan
- ⁹Department of Statistical Genetics, Osaka University Graduate School of Medicine, Osaka, Japan
- ¹⁰Laboratory for Mathematics, National Defense Medical College, Tokorozawa, Saitama, Japan
- ¹¹Department of Biopharmaceutics, School of Pharmacy, Tokyo University of Pharmacy and Life Sciences, Tokyo, Japan
- ¹²Department of Biopharmaceutics, Graduate School of Pharmaceutical Sciences, Nagoya City University, Nagoya, Aichi, Japan

- ¹³Department of Preventive Medicine and Public Health, National Defense Medical College, Tokorozawa, Saitama, Japan
- ¹⁴Division of Transcriptomics, Research Center for Transomics Medicine, Medical Institute of Bioregulation, Kyushu University, Fukuoka, Japan
- ¹⁵Department of Integrative Genomics, Tohoku Medical Megabank Organization, Tohoku University, Sendai, Miyagi, Japan
- ¹⁶Ryougoku East Gate Clinic, Tokyo, Japan
- ¹⁷Department of Internal Medicine, Self-Defense Forces Central Hospital, Tokyo, Japan
- ¹⁸Program in Radiological and Medical Laboratory Sciences, Pathophysiological Laboratory Sciences, Nagoya University Graduate School of Medicine, Nagoya, Aichi, Japan
- ¹⁹Department of Preventive Medicine, Nagoya University Graduate School of Medicine, Nagoya, Aichi, Japan
- ²⁰First Faculty of Medicine, Charles University in Prague and General University Hospital in Prague, Institute of Inherited Metabolic Disorders, Prague, Czech Republic
- ²¹Institute of Rheumatology, Prague, Czech Republic
- ²²Department of Medicine, University of Otago, Christchurch, New Zealand
- ²³Department of Medicine, University of Auckland, Grafton, Auckland, New Zealand
- ²⁴Department of Human Physiology and Pathology, Faculty of Pharma-Sciences, Teikyo University, Tokyo, Japan
- ²⁵Department of Internal Medicine, Teikyo University School of Medicine, Tokyo, Japan
- ²⁶Division of Kidney and Hypertension, Department of Internal Medicine, Jikei University School of Medicine, Tokyo, Japan
- ²⁷Department of Pathophysiology and Therapy in Chronic Kidney Disease, Jikei University School of Medicine, Tokyo, Japan
- ²⁸Omics Research Center, National Cerebral and Cardiovascular Center, Suita, Osaka, Japan
- ²⁹Laboratory for Genotyping Development, Center for Integrative Medical Sciences, RIKEN, Yokohama, Kanagawa, Japan
- ³⁰Midorigaoka Hospital, Takatsuki, Osaka, Japan
- ³¹Kyoto Industrial Health Association, Kyoto, Japan
- ³²Department of Pathophysiology, Tokyo University of Pharmacy and Life Sciences, Tokyo, Japan

Acknowledgements The authors thank all the participants involved in this study. They are also grateful to members of the BioBank Japan Project for supporting the study. They are indebted to M Watanabe and Y Katsurada (National Defense Medical College) for immunohistochemical analysis; K Gotanda, Y Morimoto, M Miyazawa, T Chiba, Y Utsumi, S Terashige, Y Kato, H Sasaki, Y Takashima, S Tatsukawa, A Akashi, Y Tanahashi, Y Nagao, M Nakajima, H Inoue, S Takeuchi (National Defense Medical College), M Sonoda (Kurume University School of Medicine) and T Tamatsukuri (Jikei University School of Medicine) for genetic analysis; S Ushida (Ikagaku) and H Fujiwara (Midorigaoka Hospital) for Japanese sample collection; R Akuhata, N Aupouri (Ngati Porou Hauora Charitable Trust) and J H Hindmarsh (Research Coordinator, Ngati Porou Hauora Charitable Trust) for NZ Māori (Eastern Polynesian) sample collection from the Rohe (area) of Ngati Porou iwi; Y Oka, S Kanda and C Umatani (the University of Tokyo) for their biomaterial support and technical advice in the oocyte experiment; J Boocock (University of Otago) for eQTL analysis; H Motohashi (Tohoku University), N Hamajima, M Naito (Nagoya University) and H Tanaka (Aichi Cancer Center Research Institute) for helpful discussion.

Collaborators Members of the Eurogout Consortium are: Mariano Andres (Sección de Reumatología, Hospital General Universitario de Alicante, Alicante), Leo A Joosten (Department of Internal Medicine and Radboud Institute of Molecular Life Science, Radboud University Medical Center, The Netherlands), Matthijs Janssen (Department of Rheumatology, Rijnstate Hospital, The Netherlands), Tim L Jansen (Department of IQ HealthCare, VieCuri Medical Centre, The Netherlands), Frederic Lioté (INSERM, UMR-S 1132, Hospital Lariboisière, Paris, University Paris Diderot (UFR de Médecine), Sorbonne Paris Cité, Paris), Timothy R Radstake (Department of Rheumatology and Clinical Immunology, Laboratory of Translational Immunology, University Medical Centre Utrecht, The Netherlands, and Department of Immunology, University Medical Centre Utrecht, The Netherlands), Philip L Riches (Rheumatic Diseases Unit, Institute of Genetics and Molecular Medicine, University of Edinburgh, Edinburgh), Alexander So (DAL, Service of Rheumatology, Laboratory of Rheumatology, University of Lausanne, CHUV, Nestlé), Anne-Kathrin Tausche (Department of Rheumatology, University Clinic 'Carl-Gustav-Carus', Dresden).

Contributors AN, HNakaoka, KY, MS, AS, YT, TT, NS, TRM and HM conceived and designed this study. Y Sakurai, HS, II, ATakahashi and MKubo assisted with research design. AN, HNakaoka, MS, Yokada, YKamatani, THigashino, YKawamura, ATokumasu, KO, TK, KW, BS, KP, ATakahashi, MKubo, HOoyama, TS, KIchida and HM collected and analyzed clinical data of Japanese participants. AS, LKS, ND, Eurogout Consortium and TRM collected and analyzed clinical data of replication participants. AN, KY, MS, AS, YShirahama, SS, THigashino, YKawamura, HOgata, MKawaguchi, ID, NS, TRM and HM performed genetic analysis. AN, HNakaoka, MS,

AS, Yokada, YKamatani, TN, HNAkashima, ATakahashi, TRM and HM performed statistical analysis. AN, YT, TT, KInoue, TYasujima, HY, HS and HM performed functional analysis and localization analysis. AN, HNAkaoka, KY, MS, AS, YT, YOKada, YKamatani, TN, TT, KInoue, TYasujima, HY, YOhkawa, NS, TRM and HM analyzed data. ID, TI, MH, SF, TYokoo, THosoya, KIchida provided intellectual input and assisted with the preparation of the manuscript. AN, HNAkaoka, KY, MS, AS, YT, NS, TRM and HM wrote the manuscript.

Funding This study was supported by grants from the Ministry of Education, Culture, Sports, Science and Technology (MEXT) of Japan, including MEXT KAKENHI (Nos. 25293145 and 15K15227), Grants-in-Aid for Scientific Research on Priority Areas (No. 17015018) and Innovative Areas (Nos. 22150001 and 22150002) and a JSPS KAKENHI Grant (Nos. 16H06277 and 16H06279), the Ministry of Health, Labour and Welfare of Japan, the Ministry of Defense of Japan, the Japan Society for the Promotion of Science, the Kawano Masanori Memorial Foundation for Promotion of Pediatrics, the Gout Research Foundation of Japan and the Health Research Council of New Zealand. The BioBank Japan Project was supported by MEXT of Japan.

Competing interests TT, KIchida, NS and HM have a patent pending based on the work reported in this paper.

Patient consent Obtained.

Ethics approval This study was approved by the institutional ethical committees, and written consent was obtained from all of its participants. All involved procedures were performed in accordance with the Declaration of Helsinki.

Provenance and peer review Not commissioned; externally peer reviewed.

Open Access This is an Open Access article distributed in accordance with the Creative Commons Attribution Non Commercial (CC BY-NC 4.0) license, which permits others to distribute, remix, adapt, build upon this work non-commercially, and license their derivative works on different terms, provided the original work is properly cited and the use is non-commercial. See: <http://creativecommons.org/licenses/by-nc/4.0/>

REFERENCES

- Smith E, Hoy D, Cross M, *et al*. The global burden of gout: estimates from the Global Burden of Disease 2010 study. *Ann Rheum Dis* 2014;73:1470–6.
- Ichida K, Matsuo H, Takada T, *et al*. Decreased extra-renal urate excretion is a common cause of hyperuricemia. *Nat Commun* 2012;3:764.
- Wortmann RL. Disorders of purine and pyrimidine metabolism. In: Fauci AS, Braunwald E, Kasper D, *et al.*, eds. *Harrison's principles of internal medicine*. 17th edn. New York, NY: McGraw-Hill, 2008:2444–9.
- Matsuo H, Nakayama A, Sakiyama M, *et al*. ABCG2 dysfunction causes hyperuricemia due to both renal urate underexcretion and renal urate overload. *Sci Rep* 2014;4:3755.
- Woodward OM, Kottgen A, Coresh J, *et al*. Identification of a urate transporter, ABCG2, with a common functional polymorphism causing gout. *Proc Natl Acad Sci USA* 2009;106:10338–42.
- Matsuo H, Takada T, Ichida K, *et al*. Common defects of ABCG2, a high-capacity urate exporter, cause gout: a function-based genetic analysis in a Japanese population. *Sci Transl Med* 2009;1:5ra11.
- Matsuo H, Ichida K, Takada T, *et al*. Common dysfunctional variants in ABCG2 are a major cause of early-onset gout. *Sci Rep* 2013;3:2014.
- Nakayama A, Matsuo H, Nakaoka H, *et al*. Common dysfunctional variants of ABCG2 have stronger impact on hyperuricemia progression than typical environmental risk factors. *Sci Rep* 2014;4:5227.
- Phipps-Green AJ, Merriman ME, Topless R, *et al*. Twenty-eight loci that influence serum urate levels: analysis of association with gout. *Ann Rheum Dis* 2016;75:124–30.
- Matsuo H, Yamamoto K, Nakaoka H, *et al*. Genome-wide association study of clinically defined gout identifies multiple risk loci and its association with clinical subtypes. *Ann Rheum Dis* 2016;75:652–9.
- Nakamura T, Shi D, Tzetis M, *et al*. Meta-analysis of association between the ASPN D-repeat and osteoarthritis. *Hum Mol Genet* 2007;16:1676–81.
- Kamatani Y, Matsuda K, Okada Y, *et al*. Genome-wide association study of hematological and biochemical traits in a Japanese population. *Nat Genet* 2010;42:210–15.
- Rasheed H, Phipps-Green A, Topless R, *et al*. Association of the lipoprotein receptor-related protein 2 gene with gout and non-additive interaction with alcohol consumption. *Arthritis Res Ther* 2013;15:R177.
- Lioté F, Merriman T, Nasi S, *et al*. Workshop report: 4th European crystal network meeting. *Arthritis Res Ther* 2013;15:304.
- DerSimonian R, Laird N. Meta-analysis in clinical trials. *Control Clin Trials* 1986;7:177–88.
- Chiba T, Matsuo H, Kawamura Y, *et al*. NPT1/SLC17A1 is a renal urate exporter in humans and its common gain-of-function variant decreases the risk of renal underexcretion gout. *Control Clin Trials* 2015;67:281–7.
- Matsuo H, Kanai Y, Kim JY, *et al*. Identification of a novel Na⁺-independent acidic amino acid transporter with structural similarity to the member of a heterodimeric amino acid transporter family associated with unknown heavy chains. *J Biol Chem* 2002;277:21017–26.
- Matsuo H, Tsukada S, Nakata T, *et al*. Expression of a system L neutral amino acid transporter at the blood-brain barrier. *Neuroreport* 2000;11:3507–11.
- Matsuo H, Kanai Y, Tokunaga M, *et al*. High affinity D- and L-serine transporter Asc-1: cloning and dendritic localization in the rat cerebral and cerebellar cortices. *Neurosci Lett* 2004;358:123–6.
- Hollis-Moffatt JE, Phipps-Green AJ, Chapman B, *et al*. The renal urate transporter SLC17A1 locus: confirmation of association with gout. *Arthritis Res Ther* 2012;14:R92.
- Diodato D, Melchionda L, Haack TB, *et al*. VARS2 and TARS2 mutations in patients with mitochondrial encephalomyopathies. *Hum Mutat* 2014;35:983–9.
- Köttgen A, Albrecht E, Teumer A, *et al*. Genome-wide association analyses identify 18 new loci associated with serum urate concentrations. *Nat Genet* 2013;45:145–54.
- Goytain A, Hines RM, Quamme GA. Functional characterization of NIPA2, a selective Mg²⁺ transporter. *Am J Physiol, Cell Physiol* 2008;295:C944–53.
- Li C, Li Z, Liu S, *et al*. Genome-wide association analysis identifies three new risk loci for gout arthritis in Han Chinese. *Nat Commun* 2015;6:7041.
- Enomoto A, Kimura H, Chairoungdua A, *et al*. Molecular identification of a renal urate anion exchanger that regulates blood urate levels. *Nature* 2002;417:447–52.
- Kolz M, Johnson T, Sanna S, *et al*. Meta-analysis of 28,141 individuals identifies common variants within five new loci that influence uric acid concentrations. *PLoS Genet* 2009;5:e1000504.
- Okada Y, Sim X, Go MJ, *et al*. Meta-analysis identifies multiple loci associated with kidney function-related traits in east Asian populations. *Nat Genet* 2012;44:904–9.
- Matsuo H, Chiba T, Nagamori S, *et al*. Mutations in glucose transporter 9 gene SLC2A9 cause renal hypouricemia. *Am J Hum Genet* 2008;83:744–51.
- Wang YL, Zeng C, Wei J, *et al*. Association between dietary magnesium intake and hyperuricemia. *PLoS ONE* 2015;10:e0141079.
- Zeng C, Wang YL, Wei J, *et al*. Association between low serum magnesium concentration and hyperuricemia. *Magnes Res* 2015;28:56–63.
- Kuroczycka-Saniutycz E, Porowski T, Protas PT, *et al*. Does obesity or hyperuricemia influence lithogenic risk profile in children with urolithiasis? *Pediatr Nephrol* 2015;30:797–803.



GWAS of clinically defined gout and subtypes identifies multiple susceptibility loci that include urate transporter genes

Akiyoshi Nakayama, Hirofumi Nakaoka, Ken Yamamoto, Masayuki Sakiyama, Amara Shaukat, Yu Toyoda, Yukinori Okada, Yoichiro Kamatani, Takahiro Nakamura, Tappei Takada, Katsuhisa Inoue, Tomoya Yasujima, Hiroaki Yuasa, Yuko Shirahama, Hiroshi Nakashima, Seiko Shimizu, Toshihide Higashino, Yusuke Kawamura, Hiraku Ogata, Makoto Kawaguchi, Yasuyuki Ohkawa, Inaho Danjoh, Atsumi Tokumasu, Keiko Ooyama, Toshimitsu Ito, Takaaki Kondo, Kenji Wakai, Blanka Stiburkova, Karel Pavelka, Lisa K Stamp, Nicola Dalbeth, Eurogout Consortium, Yutaka Sakurai, Hiroshi Suzuki, Makoto Hosoyamada, Shin Fujimori, Takashi Yokoo, Tatsuo Hosoya, Ituro Inoue, Atsushi Takahashi, Michiaki Kubo, Hiroshi Ooyama, Toru Shimizu, Kimiyoshi Ichida, Nariyoshi Shinomiya, Tony R Merriman and Hirotaka Matsuo

Ann Rheum Dis 2017 76: 869-877 originally published online November 29, 2016
doi: 10.1136/annrheumdis-2016-209632

Updated information and services can be found at:
<http://ard.bmj.com/content/76/5/869>

These include:

References

This article cites 30 articles, 8 of which you can access for free at:
<http://ard.bmj.com/content/76/5/869#BIBL>

Open Access

This is an Open Access article distributed in accordance with the Creative Commons Attribution Non Commercial (CC BY-NC 4.0) license, which permits others to distribute, remix, adapt, build upon this work non-commercially, and license their derivative works on different terms, provided the original work is properly cited and the use is non-commercial. See: <http://creativecommons.org/licenses/by-nc/4.0/>

Email alerting service

Receive free email alerts when new articles cite this article. Sign up in the box at the top right corner of the online article.

Topic Collections

Articles on similar topics can be found in the following collections

[Open access](#) (596)
[Degenerative joint disease](#) (4641)
[Genetics](#) (968)
[Musculoskeletal syndromes](#) (4951)

To request permissions go to:
<http://group.bmj.com/group/rights-licensing/permissions>

To order reprints go to:
<http://journals.bmj.com/cgi/reprintform>

To subscribe to BMJ go to:
<http://group.bmj.com/subscribe/>

Notes

To request permissions go to:
<http://group.bmj.com/group/rights-licensing/permissions>

To order reprints go to:
<http://journals.bmj.com/cgi/reprintform>

To subscribe to BMJ go to:
<http://group.bmj.com/subscribe/>



Patient Reports

Congenital nephrotic syndrome with a novel *NPHS1* mutation

Chikage Yoshizawa,^{1,2} Yasuko Kobayashi,^{1,6} Yuka Ikeuchi,^{1,2} Masahiko Tashiro,² Satoko Kakegawa,^{1,2} Toshio Watanabe,¹ Yoshimitsu Goto,³ Koichi Nakanishi,⁴ Norishige Yoshikawa^{4,5} and Hirokazu Arakawa¹

¹Department of Pediatrics, Gunma University School of Medicine, ²Department of Pediatrics, Gunma Central Hospital, Maebashi, ³Department of Pediatrics, Nagoya Daini Red Cross Hospital, Nagoya, ⁴Department of Pediatrics, Wakayama Medical University, Wakayama, ⁵Center for Clinical Research and Development National Center for Child Health and Development, Tokyo, Japan and ⁶Bristol Renal, University of Bristol, Bristol, UK

Abstract Congenital nephrotic syndrome of the Finnish type (CNF) is a rare autosomal recessive disorder. The incidence of CNF is relatively high in Finland but considerably lower in other countries. We encountered a male newborn with CNF, associated with compound heterozygous mutations in *nephrosis 1, congenital, Finnish type (NPHS1)*. The patient was admitted to hospital as a preterm infant. Physical and laboratory findings fulfilled the diagnostic criteria of nephrotic syndrome, and were compatible with a diagnosis of CNF, but there was no family history of the disease. On genetic analysis of *NPHS1* a paternally derived heterozygous frame-shift mutation caused by an 8 bp deletion, resulting in a stop codon in exon 16 (c.2156-2163 delTGCCTGC causing p.L719DfsX4), and a novel, maternally derived nonsense mutation in exon 15 (c.1978G>T causing p.E660X) were identified. Early genetic diagnosis of CNF is important for proper clinical management and appropriate genetic counseling.

Key words congenital nephrotic syndrome, Finnish type, *NPHS1*.

Congenital nephrotic syndrome (CNS) manifests at birth or within the first 3 months of life. The most common type of CNS is the Finnish type (CNF). CNF is characterized by massive proteinuria, which may even commence *in utero*.¹ Most infants with CNF are born prematurely, with a low birthweight for gestational age. The placenta is enlarged, representing more than 25% of the total birthweight. The course of CNF is progressive, often leading to end-stage renal disease by 2 or 3 years of age.²

Congenital nephrotic syndrome is an autosomal recessive disease caused by mutations in *nephrosis 1, congenital, Finnish type (NPHS1)* encoding nephrin, which is a key component of the podocyte slit diaphragm. These mutations lead to disruption of the filtration barrier and cause massive protein loss into the urine.^{1,2} Thus far, 240 mutations in *NPHS1* have been reported. We encountered a male CNF newborn with compound heterozygous nonsense mutations in *NPHS1* inherited from each parent; one of the mutations was a novel mutation in exon 15. The characteristics of variations in the gene in the Asian population are discussed relative to the Finnish population.

Case report

The patient was admitted to hospital as a preterm infant. He was born at a gestational age of 33 weeks, with a birthweight

of 2180 g. The birthweight and height were appropriate for the gestational age. Neither kidney disease nor consanguineous marriage was noted in his family. The parents and his older brother were all healthy, and the pregnancy was otherwise normal. Apgar scores at 1 and 5 min were 8 and 9 points, respectively. Placental weight was 895 g, which was 41% of the birthweight.

Physical findings on admission showed a soft, flat fontanel, although the anterior fontanel was open wide and joined to the posterior fontanel. Breathing was retracted and a crackle was heard in both lung fields. The extremities were edematous and the ankle joints were hyperdorsiflexed. External genitalia were normal.

Laboratory results indicated low basal serum total protein (total protein, 3.2 g/dL; albumin, 1.2 g/dL) and low IgG. Serum IgG on admission was 294 mg/dL (Table 1). The lowest level was 70 mg/dL at a few days after admission. Total cholesterol was high. Uric albumin and occult blood were 3+. Urinary protein: creatinine ratio was 133, and the selectivity index was 1.6 (Table 1). Pulmonary stenosis was noted on echocardiography. Physical and laboratory findings fulfilled the diagnostic criteria of nephrotic syndrome.

α -Fetoprotein (AFP) in maternal blood was high (AFP, 3680 ng/mL). The index of placental weight/birthweight was also high. The patient had massive proteinuria and hypoalbuminemia. There was no evidence of congenital infection. Malformation was negative. Glomerular filtration rate during the first 6 months of life was normal (serum creatinine, 0.18 mg/dL). The findings were compatible with a diagnosis of CNF, except that there was no family history of the disease. The

Correspondence: Yasuko Kobayashi, MD PhD, Gunma University, 3-39-22 Showa-machi Maebashi, Gunma, 371-8511, Japan. Email: kobayasu@gunma-u.ac.jp

Received 7 May 2015; revised 9 May 2016; accepted 6 June 2016.

doi: 10.1111/ped.13118

patient's and the parents' samples were submitted for genetic analysis. Informed consent for genetic analysis was obtained from the parents of the child.

Polymerase chain reaction and direct sequencing were performed to screen for *NPHS1* mutations in peripheral blood from the patient and his parents, and compound heterozygous nonsense mutations were identified. A paternally derived frame-shift mutation was caused by an 8 bp deletion in exon 16 (c.2156-2163 delTGCAGTGC causing p.L719DfsX4), and a novel, maternally derived nonsense mutation was identified in exon 15 (c.1978G>T causing p.E660X; Fig. 1).

Given the massive proteinuria and hypoalbuminemia noted on laboratory tests, intermittent albumin infusions and

furosemide injection were initiated, but generalized edema worsened with intermittent albumin infusion; hence, this was changed to daily albumin infusion. For hypothyroidism, thyroid auxiliary therapy with levothyroxine sodium was initiated. For hypertension, angiotensin-converting enzyme inhibitor (ACEI) and angiotensin receptor blocker were used. Prior to genetic test, steroid therapy was used in an attempt to reduce proteinuria but was found to be ineffective. Unilateral nephrectomy of the left kidney was required at 5 months of age to control generalized edema by reducing the level of proteinuria and the frequency of albumin infusions. At the same time, peritoneal dialysis was initiated for water removal. Hypoproteinemia, which had required albumin infusion,

Table 1 Results from Blood and Urinary Test

| | | | | | | | |
|---------------------|------------------------------|----------------------------|------------|---------------------------------------|------------------|--------------------------|----------------------------------|
| White blood cells | 11800/ μ L | Aspartate aminotransferase | 99 IU/L | Prothrombin time | 104% | Urinary specific gravity | 1.01 |
| Red blood cells | 628×10^4 / μ L | Alanine aminotransferase | 7 IU/L | Activated partial thromboplastin time | 59.1 s | Proteinuria | (3+) |
| Hemoglobin | 23.0 g/dL | Lactate dehydrogenase | 1350 IU/L | Fibrinogen | 233 mg/dL | Hematuria | (3+) |
| Hematocrit | 64.40% | Total cholesterol | 234 mg/dL | AT-III | 38.90% | U-Red blood cells | 30~49/hpf |
| Platelet | 21.1×10^4 / μ L | Triglycerides | 224 mg/dL | Hepaplastin test | 69.60% | U-protein/ U-creatinine | 133 |
| | | Na | 134 mEq/L | Immunoglobulin G | 294 mg/dL | Urinary β 2-MG | 2060 μ g/L (<4000 μ g/L) |
| Total protein | 3.2 g/dL | K | 4.7 mEq/L | Immunoglobulin A | <6 mg/dL | Urinary NAG | 329 U/g.Cr |
| Albumin | 1.2 g/dL | Cl | 107 mEq/L | Immunoglobulin M | 12 mg/dL | | |
| Blood urea nitrogen | 20.1 mg/dL | Ca | 8.4 mg/dL | Thyroid stimulation hormone | 2.66 μ IU/mL | Selectivity Index | 1.6 |
| Creatinine | 0.70 mg/dL | C-reactive protein | 0.05 mg/dL | Free T4 | 0.59 ng/mL | | |

AT-III, antithrombin-III; U-, urinary-; β 2-MG, β 2-microglobulin; NAG, N-acetyl- β -D-glucosaminidase.

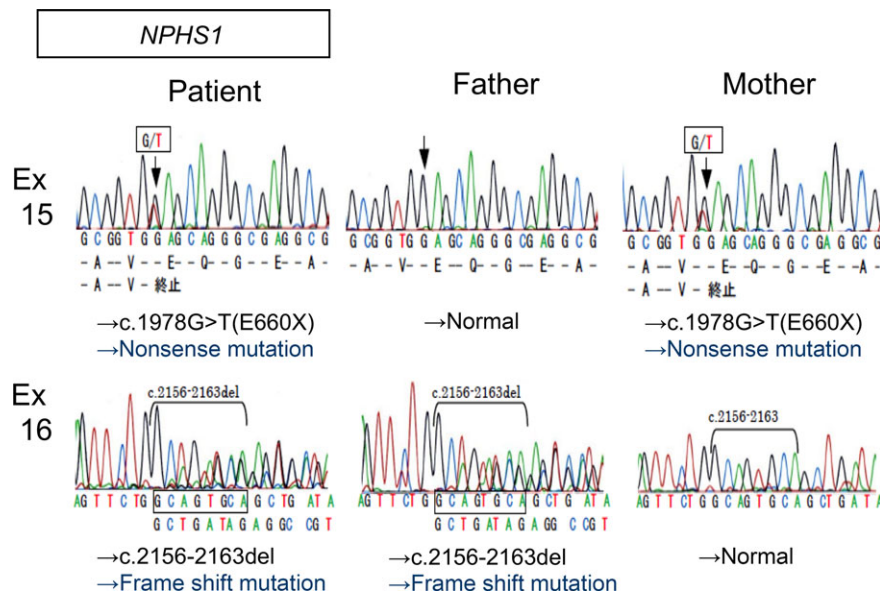


Fig. 1 Compound heterozygous mutation in *nephrosis 1, congenital, Finnish type*: a frame-shift mutation caused by an 8 bp deletion in exon 16 (c.2156-2163 delTGCAGTGC causing p.L719DfsX4) inherited from the father, and a nonsense mutation in exon 15 (c.1978G>T [E660X]) inherited from the mother.

Table 2 *NPHS1* mutations reported in Asia

| Case | Ethnicity | Mutation type | Genotype | | | | Consanguinity | Family history | Age at diagnosis | Reference |
|------|-----------|---------------|---------------------------|-----------------------------|------------------------------|-----|------------------|----------------|------------------|-----------|
| | | | Patient | Father | Mother | | | | | |
| 1 | Japanese | Hom | 447G>A(E447K) | No information | 447G>A(E447K) | Yes | Sibling case | 2 days | (4) | |
| | | Hom | 819A>T (D819V) | No information | 819A>T (D819V) | | | | | |
| 2 | Japanese | Hom | 736G>T (E246X) | Not analyzed | 736G>T (E246X) | No | No | 1 month | (3) | |
| 3 | Japanese | Hom | 2156_2163 del (L719DfsX4) | Not analyzed | Not analyzed | Yes | No | 1 month | (3) | |
| 4 | Japanese | Het | R460Q | Not detected | R460Q | No | No | At birth | (3) | |
| 5 | Japanese | Het | D105N | Not analyzed | Not analyzed | No | No | 1 month | (3) | |
| 6 | Chinese | Cpd het | G928A (D310N) | | G928A(D310N) | ND | Sibling; case 7 | 10 days | (5) | |
| | | | 1893-1900del 8 | 1893-1900del 8 | | | | | | |
| | | | G2869C (V957L) | G2869C (V957L) | | | | | | |
| 7 | Chinese | Cpd het | G928A (D310N) | | G928A(D310N) | ND | Sibling; case 6 | 10 days | (5) | |
| | | | 1893-1900del 8 | 1893-1900del | | | | | | |
| | | | G2869C (V957L) | G2869C (V957L) | | | | | | |
| 8 | Japanese | Cpd het | 479G>C (C160S) | 479G>C (C160S) | | ND | ND | At birth | (6) | |
| | | | 736G>T (E246X) | | 736G>T (E246X) | | | | | |
| 9 | Japanese | Hom | 1135C>T(R379W) | Not analyzed | Not analyzed | ND | ND | | (6) | |
| 10 | Japanese | Cpd het | 2479C>T(R827X) | | 2479C>T (E827X) | ND | ND | | (6) | |
| | | | nt2515delC | Not analyzed | | ND | ND | At birth | | |
| 11 | Japanese | Cpd het | 736G>T (E246X) | 736G>T (E246X) | | ND | ND | At birth | (6) | |
| | | | nt2515delC | | nt2515delC | | | | | |
| 12 | Japanese | Cpd het | 1801G>C (G601R) | | 1801G>C (R601R) | ND | ND | 1 month | (6) | |
| | | | nt2515delC | nt2515delC | | | | | | |
| 13 | Korean | Cpd het | 2156_2163 del (L719DfsX4) | | 2156_2163 del j8 (L719DfsX4) | ND | Sporadic | 2 months | (7) | |
| | | | 3250insG (V1084fsX1095) | 3250_3251insG (V1084GfsX12) | | | | | | |
| 14 | Korean | Cpd het | 1381G>A (R460Q) | | 1381G>A (R460Q) | ND | Sporadic | At birth | (7) | |
| | | | 2442C>G (Y814X) | 2442C>G (Y814X) | | | | | | |
| 15 | Chinese | Cpd het | 2225T>C (I742T) | | 2225T>C(I742T) | | Sibling; case 16 | | (8) | |
| | | | 2783C>A | 2783C>A | | ND | | 10 days | | |
| 16 | Chinese | Cpd het | 2225T>C (I742T) | | 2225T>C(I742T) | | Sibling; case 15 | | (8) | |
| | | | 2783C>A | 2783C>A | | ND | | 20 days | | |
| 17 | Chinese | Hom | 3250insG(V1084fsX1095) | | | | Sporadic | 6 days | (9) | |
| 18 | Japanese | Cpd het | c.1978G>T causing p.E660X | | c.1978G>T causing p.E660X | No | Sporadic | At birth | Present case | |
| | | | 2156_2163 del (L719DfsX4) | 2156_2163 del (L719DfsX4) | | | | | | |

Cpd het, compound heterozygous mutation; het, heterozygous mutation; hom, homozygous mutation; ND, not described; NPHS1, nephrosis 1, congenital, Finnish type.

improved but was still present given that serum albumin was 1.5 g/dL and total protein was 4 g/dL. At 9 months of age, peritoneal dialysis was stopped and the dialysis catheter decannulated because of peritoneal infection. Poor weight gain was observed, likely as a result of low protein levels. Therefore, indomethacin was initiated from the age of 1 year 3 months to reduce proteinuria and to increase the serum protein level. At 1 year 5 months, the right kidney was removed and peritoneal dialysis was re-initiated. At that time, serum albumin was 1.5 g/dL and total protein was 4.2 g/dL. After bilateral nephrectomy, serum protein improved to the normal range. The patient gained weight and height, even though the calorie intake did not increase (335–628 kJ/kg/day). At the age of 3 years, the patient received a kidney transplant from his grandfather.

Discussion

Congenital nephrotic syndrome was diagnosed on identification of *NPHS1* mutations. On genetic analysis the patient had compound heterozygous mutations in *NPHS1* derived from each parent. Although the frame-shift mutation in exon 16 was previously reported by Sako *et al.*,³ the nonsense mutation in exon 15 has not previously been reported in PubMed or on the Human Gene Mutation Database (HGMD[®] Professional 2014.4). The nephrin protein consists of eight extracellular immunoglobulin-like domains numbered 1–8, a fibronectin type III-like module, a transmembrane domain, and an intracellular domain. The mutation sites and the stop codon generated by the mutations in this case lay between the sixth and seventh Ig-like domain coding sites.

Eighteen cases of CNF have been reported from East Asia, including the present one (Table 2), with 21 mutations in *NPHS1* identified. Five patients (28%) carried a homozygous mutation, and 13 (72%) carried heterozygous or compound heterozygous mutations. Six of the 21 mutations were common to two or three non-related patients. In contrast, CNF caused by a homozygous mutation of *NPHS1* is the common form of CNS in the Finnish population. In total, 65% of Finnish patients are homozygous for the Fin-major mutation and 8% carry a Fin-minor mutation, whereas 16% of patients are compound heterozygous.¹⁰ Thus, in the Asian population, compound heterozygous mutations are more common than homozygous mutations, and no hot spot mutations have been reported.

Accurate and early identification of known pathogenic variants in CNF is important for proper clinical management and guidance of therapeutic approach to avoid unnecessary immunosuppression, for supporting therapeutic decisions including whether or not to use aggressive and invasive treatment, for helping to predict outcome even after renal transplantation, and for indicating additional therapeutic possibilities. Traditional CNS treatment includes aggressive supportive care such as massive i.v. albumin infusions and early nephrectomy. Recent developments have allowed patients to avoid dialysis prior to transplantation with a medical regimen of ACEI and prostaglandin synthesis inhibition to reduce glomerular blood flow and filtration, plus minimal

supportive infusion therapy with or without unilateral nephrectomy.

In the present case, conservative medical therapy including steroid treatment was carried out during the early stage of the clinical course because the association between response to pharmacotherapy and *NPHS1* mutation genotype was not clear clinically. Furthermore, bilateral nephrectomy was required for the patient to gain weight and height, possibly as a result of improved serum total protein and albumin after the second nephrectomy, despite the lack of change in caloric intake after the first nephrectomy.

Prospective analyses that include clinical outcome and genetic analysis of CNS are needed to support and strengthen diagnostic and prognostic accuracy.

In conclusion, compound heterozygous mutations predominate in CNF among East Asian patients; the present patient carried a novel mutation in *NPHS1*.

Acknowledgment

We thank Ms Agnieszka Bierzynska at the University of Bristol for assistance with the search for reported *NPHS1* mutations by HGMD[®] Professional 2014.4.

Disclosure

The authors declare no conflicts of interest.

Author contributions

C.Y. and Y.K. designed the study and wrote the manuscript; C.Y., Y.K., Y.I., S.K., T.W., M.T. and Y.G. examined the patient and collected clinical data; K.N. and N.Y. performed the genetic analysis; H.A. gave conceptual advice and supervised the whole study. All authors read and approved the final manuscript.

References

- 1 Kestilä M, Lenkkeri U, Männikkö M *et al.* Positionally cloned gene for a novel glomerular protein – nephrin – is mutated in congenital nephrotic syndrome. *Mol. Cell* 1998; **1**: 575–82.
- 2 Heeringa SF, Vlangos CN, Chernin G *et al.* Thirteen novel *NPHS1* mutations in a large cohort of children with congenital nephrotic syndrome. *Nephrol. Dial. Transplant.* 2008; **23**: 3527–33.
- 3 Sako M, Nakanishi K, Obana M *et al.* Analysis of *NPHS1*, *NPHS2*, *ACTN4*, and *WT1* in Japanese patients with congenital nephrotic syndrome. *Kidney Int.* 2005; **67**: 1248–55.
- 4 Aya K, Tanaka H, Seino Y. Novel mutation in the nephrin gene of a Japanese patient with congenital nephrotic syndrome of the Finnish type. *Kidney Int.* 2000; **57**: 401–4.
- 5 Shi Y, Ding J, Liu JC, Wang H, Bu DF. *NPHS1* mutations in a Chinese family with congenital nephrotic syndrome. *Zhonghua Er Ke Za Zhi* 2005; **43**: 805–9.
- 6 Aya K, Shimizu J, Ohtomo Y *et al.* *NPHS1* gene mutation in Japanese patients with congenital nephrotic syndrome. *Nephrol. Dial. Transplant.* 2009; **24**: 2411–4.

- 7 Lee BH, Ahn YH, Choi HJ *et al.* Two Korean infants with genetically confirmed congenital nephrotic syndrome of Finnish type. *J. Korean Med. Sci.* 2009; **24**: S210–4.
- 8 Wu LQ, Hu JJ, Xue JJ, Liang DS. Two novel NPHS1 mutations in a Chinese family with congenital nephrotic syndrome. *Genet. Mol. Res.* 2011; **10**: 2517–22.
- 9 Yu ZH, Wang DJ, Meng DC, Huang J, Nie XJ. Mutations in NPHS1 in a Chinese child with congenital nephrotic syndrome. *Genet. Mol. Res.* 2012; **11**: 1460–4.
- 10 Patrakka J, Kestila M, Wartiovaara J *et al.* Congenital nephrotic syndrome (NPHS1): Features resulting from different mutations in Finnish patients. *Kidney Int.* 2000; **58**: 972–80.

Familial acute necrotizing encephalopathy without *RANBP2* mutation: Poor outcome

Naoko Nishimura,^{1,2} Yoshihisa Higuchi,² Nobusuke Kimura,² Fumihito Nozaki,³ Tomohiro Kumada,³ Ai Hoshino,⁴ Makiko Saitoh⁴ and Masashi Mizuguchi⁴

¹Division of Endocrinology and Metabolism, Aichi Children's Health and Medical Center, Aichi, ²Department of Pediatrics, Otsu Red Cross Hospital, ³Department of Pediatrics, Shiga Medical Center for Children, Shiga and ⁴Department of Developmental Medical Sciences, Graduate School of Medicine, University of Tokyo, Tokyo, Japan

Abstract Most childhood cases of acute necrotizing encephalopathy (ANE) involve neither family history nor recurrence. ANE occasionally occurs, however, as a familial disorder or recurs in Caucasian patients. A mutation of *RAN-binding protein 2 (RANBP2)* has been discovered in more than one half of familial or recurrent ANE patients. In contrast, there has been no report of this mutation in East Asia. Here, we report the first sibling cases of typical ANE in Japan, with poor outcome. DNA analysis of genes associated with ANE or other encephalopathies, including *RANBP2* and *carnitine palmitoyl transferase II (CPT2)*, indicated neither mutations nor disease-related polymorphisms. On literature review, recurrent or familial ANE without the *RANBP2* mutation has a more severe outcome and greater predilection for male sex than that with the *RANBP2* mutation. This suggests that there are unknown gene mutations linked to ANE.

Key words acute necrotizing encephalopathy, carnitine palmitoyl transferase II, familial acute necrotizing encephalopathy, RAN-binding protein 2.

Acute necrotizing encephalopathy (ANE) is a type of acute encephalopathy characterized by symmetric brain lesions on computed tomography or magnetic resonance imaging (MRI). It progresses rapidly to coma within days after viral infection, mainly influenza.¹ Most cases are sporadic, but some familial or recurrent cases have been reported from North America and Europe. Heterozygous missense mutations of *RAN-binding protein 2 (RANBP2)* are found in approximately a half of these cases; this variant of ANE is called ANE1.^{1–6} Although ANE predominantly affects children in Asia, no ANE1 patients have been reported.^{3,4} Here, we report the first sibling cases of typical ANE in Asia along with a literature review.

Correspondence: Naoko Nishimura, MD, Division of Endocrinology and Metabolism, Aichi Children's Health and Medical Center, 7-426, Morioka-cho, Obu, Aichi 474-8710, Japan. Email: naoko246ra@yahoo.co.jp

Received 4 December 2014; revised 29 April 2016; accepted 7 June 2016.

doi: 10.1111/ped.13119

Case reports

Case 1

A Japanese boy was born uneventfully, and was healthy until the onset of ANE. He had microcephaly, with head circumference <3.0 SD and height <1.8 SD. Psychomotor development was normal. At 3 years 5 months of age, he had fever for 6 days, and was suspected to have viral bronchitis. He then developed generalized tonic-clonic convulsions, followed by coma with decorticate posture. Twelve hours later, MRI showed bilateral lesions in the thalami and basal ganglia with patchy subcortical white matter lesions (Fig. 1a). Electroencephalography showed diffuse, slow basic activity without epileptiform discharge. Laboratory blood examination showed mildly elevated transaminases and normal ammonia (Table 1). Despite intensive care, including steroid pulse therapy, he died 18 days after the onset of ANE.

Case 2

The younger sibling of patient 1 was born with low birth-weight (2158 g). He had short stature (<2.9 SD at 3 years of

Female X-linked Alport syndrome with somatic mosaicism

Kana Yokota¹ · Kandai Nozu¹ · Shogo Minamikawa¹ · Tomohiko Yamamura¹ · Keita Nakanishi¹ · Hisashi Kaneda² · Riku Hamada³ · Yoshimi Nozu¹ · Akemi Shono¹ · Takeshi Ninchoji¹ · Naoya Morisada¹ · Shingo Ishimori¹ · Junya Fujimura¹ · Tomoko Horinouchi¹ · Hiroshi Kaito¹ · Koichi Nakanishi⁴ · Ichiro Morioka¹ · Mariko Taniguchi-Ikeda¹ · Kazumoto Iijima¹

Received: 18 August 2016 / Accepted: 16 October 2016
© Japanese Society of Nephrology 2016

Abstract

Background X-linked Alport syndrome (XLAS) is a progressive, hereditary nephropathy. Although males with XLAS usually develop end-stage renal disease before 30 years of age, some men show a milder phenotype and possess somatic mosaic variants of the type IV collagen $\alpha 5$ gene (*COL4A5*), with severity depending on variant frequencies. In females, somatic mosaic variants are rarely reported in XLAS, and it is not clear what determines severity.

Methods Two females with somatic mosaic mutations in *COL4A5* with variant frequencies of 17.9 and 22.1% were detected using the next-generation sequencing. One patient only had hematuria. The other, however, had moderate proteinuria, which is a severe phenotype for a female XLAS patient of her age. The molecular mechanisms for the severe phenotype were investigated by examining variant frequencies in urinary sediment cells and X chromosome inactivation patterns, and by looking for modifier variants in podocyte-related genes using the next-generation sequencing.

Results The severe phenotype patient had a variant frequency of 36.6% in urinary sediment cells, which is not markedly high, nor did she show skewed X chromosome inactivation. However, she did have the heterozygous variant in *COL4A3*, which can affect severity.

Conclusion Factors determining severity in female XLAS patients remain unclear. One studied patient with the somatic variant in *COL4A5* showed a severe phenotype without skewed X chromosome inactivation, which might be derived from digenic variants in *COL4A3* and *COL4A5*. Further studies are required to determine molecular mechanisms behind female XLAS resulting in the severe phenotype.

Keywords Somatic mosaic variants · Female · Next-generation sequencing · X chromosome inactivation · Modifier gene

Introduction

Alport syndrome is a hereditary disorder of type IV collagen, characterized by chronic kidney disease progressing to end-stage renal disease, sensorineural hearing loss, and ocular abnormalities. Approximately 80% of Alport syndrome patients show X-linked inheritance (XLAS) (OMIM301050) and variants in *COL4A5*, which encodes the type IV collagen $\alpha 5$ chain. *COL4A5* variants result in abnormal type IV collagen $\alpha 5$ expression, typically with the complete absence of type IV collagen $\alpha 5$ in the glomerular basement membrane and Bowman's capsule in men, and a mosaic expression pattern in women [1].

Male patients with XLAS usually develop end-stage renal disease by the age of 30 [2]. We recently reported that some male cases tend to show a milder phenotype, because

✉ Kandai Nozu
nozu@med.kobe-u.ac.jp

¹ Department of Pediatrics, Kobe University Graduate School of Medicine, 7-5-1 Kusunoki-cho, Chuo, Kobe 6500017, Japan

² Department of Pediatrics, Komatsu Municipal Hospital, Komatsu, Ishikawa, Japan

³ Department of Nephrology, Tokyo Metropolitan Children's Medical Center, Fuchu, Tokyo, Japan

⁴ Department of Pediatrics, Wakayama Medical University, Wakayama, Japan

they possess somatic mosaic variants in *COL4A5* [3, 4]. We previously examined four male cases with somatic mosaic variants using the next-generation sequencing and determined allele frequency. Interestingly, the two patients whose variant frequency was greater than 50% showed hematuria and moderate proteinuria; however, the two patients whose frequency was less than 50% were asymptomatic or only had hematuria. This suggests that the low variant frequency results in a milder phenotype in male cases of XLAS with somatic mosaic variants [4].

The molecular mechanisms affecting severity in female cases are unclear. This study discusses two female cases of XLAS with somatic mosaic variants in *COL4A5*, one in which showed a severe phenotype. In the severe phenotype case, we examined variant frequency, X chromosome inactivation pattern, and influence of modifier genes.

Materials and methods

Targeted resequencing

Genomic DNA was isolated from peripheral blood leukocytes from the patients and their family members using the Quick Gene Mini 80 system (Wako Pure Chemical Industries, Ltd., Tokyo, Japan) according to the manufacturer's instructions. Genomic DNA from urinary sediment was isolated using a Quick-DNA urine kit (Zymo Research, Orange, CA, USA). The next-generation sequencing samples were prepared using a HaloPlex target enrichment system kit (Agilent Technologies, Santa Clara, CA, USA) according to the manufacturer's instructions. Briefly, digested genomic DNA (225 ng) was hybridized at 54 °C for 16 h with custom-designed next-generation sequencing probes to capture 45 genes, including *COL4A3*, *COL4A4*, and *COL4A5*, and other focal segmental glomerulosclerosis causative genes to search for modifier genes [5]. Amplified target libraries were sequenced with 150-base pair-end reads using the MiSeq platform (Illumina, San Diego, CA, USA), followed by variant analysis using SureCall 3.0 (Agilent Technologies, Santa Clara, CA, USA).

Mutational analyses using Sanger sequencing

For genomic DNA analysis, exon 30 and exon 32 of *COL4A5* were amplified by PCR. PCR-amplified products were purified and subjected to direct sequencing using a dye terminator cycle sequencing kit (Amersham Biosciences, Piscataway, NJ, USA) and an automatic DNA sequencer (ABI Prism 3130; Perkin Elmer Applied Biosystems, Foster City, CA, USA). For variant descriptions, reference sequences were NC_000023.9 and

NM_000495.3. Exons were numbered according to a previous report [6].

PCR-based X chromosome inactivation analysis

To assess X chromosome inactivation patterns in the affected females, a PCR-based *HUMARA* assay (i.e., digestion with methylation-sensitive restriction endonuclease Hpa II for the human androgen receptor gene (*HUMARA*) followed by PCR amplification and fragment analysis) was performed. Briefly, HpaII digestion results in the cleavage of the non-methylated *HUMARA* template DNA. As *HUMARA* contains variable numbers of CAG repeats between different alleles, PCR results in two peaks, corresponding to the maternal and paternal X chromosomes, which can be identified and quantified. This method was established by Allen et al. [7]. They calculated the activity ratio on the basis of Southern blotting, reading the density of bands for the maternal and paternal alleles. This method was modified by Kubota et al. with the use of GeneScan (ABI Prism 3130; Perkin Elmer Applied Biosystems, Foster City, CA, USA) to improve the quantification of the PCR product [8]. Genomic DNA (200 ng) was digested at 37 °C for 16 h using 5 units of the restriction enzyme Dde I with or without 25 units of Hpa II (New England BioLabs, Inc., Ipswich, MA) in a total volume of 20 µL followed by heat-inactivation at 80 °C for 20 min. Dde I is a restriction enzyme of which recognition sites are randomly distributed over genomic DNA. It cuts DNA into small pieces, resulting in improved efficiency in digestion by Hpa II and the following PCR amplification. The PCR reaction mixture contained 1 µL of digested products, 10 µL of HotStarTaq plus Master Mix (2×) (Qiagen, Inc., Valencia, CA, USA), and 0.5 µL each of 10 µM primers (FAM-labeled forward primer: 5'-TCCAGAATCTGT TCCAGAGCGTGC-3'; and reverse primer: 5'-GCT GTGAAGGTTGCTGTTCCCTCAT-3') in a total volume of 20 µL. PCR was performed as follows: first denaturation at 95 °C for 5 min, 35 cycles at 94 °C for 30 s, 62 °C for 30 s, and 72 °C for 30 s, and final extension at 72 °C for 5 min. Amplified products were run on an ABI PRISM® 310 genetic analyzer (ThermoFisher Scientific, Waltham, MA, USA), and the fragments were analyzed using GeneMapper® software (ThermoFisher Scientific).

Skewed X chromosome inactivation was evaluated by calculating a corrected ratio compensating for amplification bias of the shorter allele. The corrected ratio was obtained by dividing the peak height of the shorter allele over the longer allele of the double-digested sample by the peak height of the shorter allele over the longer allele of the single-digested sample. Results showing a corrected ratio of 80:20–100:0 were determined as having a skewed X chromosomal inactivation pattern.

Ethical considerations

All procedures were reviewed and approved by the Institutional Review Board of Kobe University School of Medicine. Informed consent was obtained from all patients or their parents.

Results (Table 1)

Case presentations

Case 1 was an adult woman. Her family tree is shown in Fig. 1a. Her son was diagnosed with Alport syndrome by kidney biopsy. She had had hematuria from 10 years old, but had not displayed proteinuria until recently. It was determined that her son had a missense mutation of c.2405G>T (p.Gly802Val) at exon 30 of *COL4A5* by targeted sequencing using the next-generation sequencing; the variant has been reported as pathogenic [9]. We conducted Sanger sequencing for Case 1 to confirm that she had the same variant with heterozygosity; however, the chromatogram showed a very small T peak, suggesting that she had the variant with a somatic mosaic state (Fig. 2a; confirmed using Sanger sequencing). Therefore, we conducted the next-generation sequencing and determined a variant frequency of 17.9% with a read depth of 190.

Case 2 was an 11-year-old girl. Her family tree is shown in Fig. 1b. No family member had urinary abnormalities. She had had hematuria and proteinuria from the age of 1. Her urinary protein/creatinine was 1.0 g/g-Cr, although she was taking angiotensin receptor blockers. Kidney biopsy revealed a thin basement membrane. Her kidney function

was within the normal range. Case 2 had a kidney biopsy conducted at 11 years of age, which revealed a basket weave change in the GBM. Based on our clinical experience, the presence of this histological phenotype, as well as moderate proteinuria, indicates that the case should be diagnosed as severe, although there is no widely accepted index for determining severity in female XLAS cases.

The next-generation sequencing revealed c.2732G>A (p.Gly911Glu) at exon 32 of *COL4A5* (Fig. 2b; confirmed using Sanger sequencing of all family members). The variant allele frequency was 22.1% with the read depth of 149.

From genetic analyses, it was determined that Case 1 had a very mild phenotype of XLAS, which is consistent with female cases which have a somatic mosaic variant in *COL4A5*; however, Case 2 had an unexpectedly severe phenotype on the same genetic background. Therefore, further studies were conducted for Case 2 to uncover the molecular background of the severe phenotype.

Comparison of variant frequencies between kidney biopsies and urinary sediment

We previously reported that urinary sediment could be used as an alternative cell source to kidney biopsies [10, 11]. In this study, we compared allele frequencies between DNA extracted from two sources of leukocytes and urinary sediment for Case 2 and found 22.1% in leukocytes with a read depth of 149 and 36.6% in urinary sediment with a read depth of 216. Urine sediment showed the higher percentage for the variant but was much less than 50%, meaning that she should have shown the milder phenotype when compared with typical heterozygous female XLAS patients (50%).

Table 1 Clinical and genetic characteristics of the two cases with somatic mosaic variants

| Case | Case 1: adult female | Case 2: 11-year-old girl |
|---|----------------------|--|
| Kidney symptoms | Hematuria | Hematuria Moderate Proteinuria |
| Pathological findings | Not conducted | Thin basement membrane |
| <i>COL4A5</i> gene variant | | |
| Exon | 30 | 32 |
| Nucleotide change | c.2405G>T | c.2732G>A |
| Amino acid change | p.Gly802Val | p.Gly911Glu |
| Variant frequency (%) | | |
| Leukocytes | 17.9 | 22.1 |
| Urinary sediment | Not conducted | 36.6 |
| X chromosome inactivation (maternal:paternal) | | |
| Leukocytes | Not conducted | 42:58 |
| Urinary sediment | | 34:66 |
| Modifier gene variant | Not detected | <i>COL4A3</i> Exon 42 c.3691G>A (p.Gly1231Ser) |

Fig. 1 Patient pedigrees. **a** Case 1 possessing the *COL4A5* variant c.2405G>T in exon 30. This patient showed only hematuria. The patient's son had hematuria and mild proteinuria and possessed the same variant. **b** Case 2 possessing the *COL4A5* variant c.2732G>A at exon 32. No other family member had hematuria

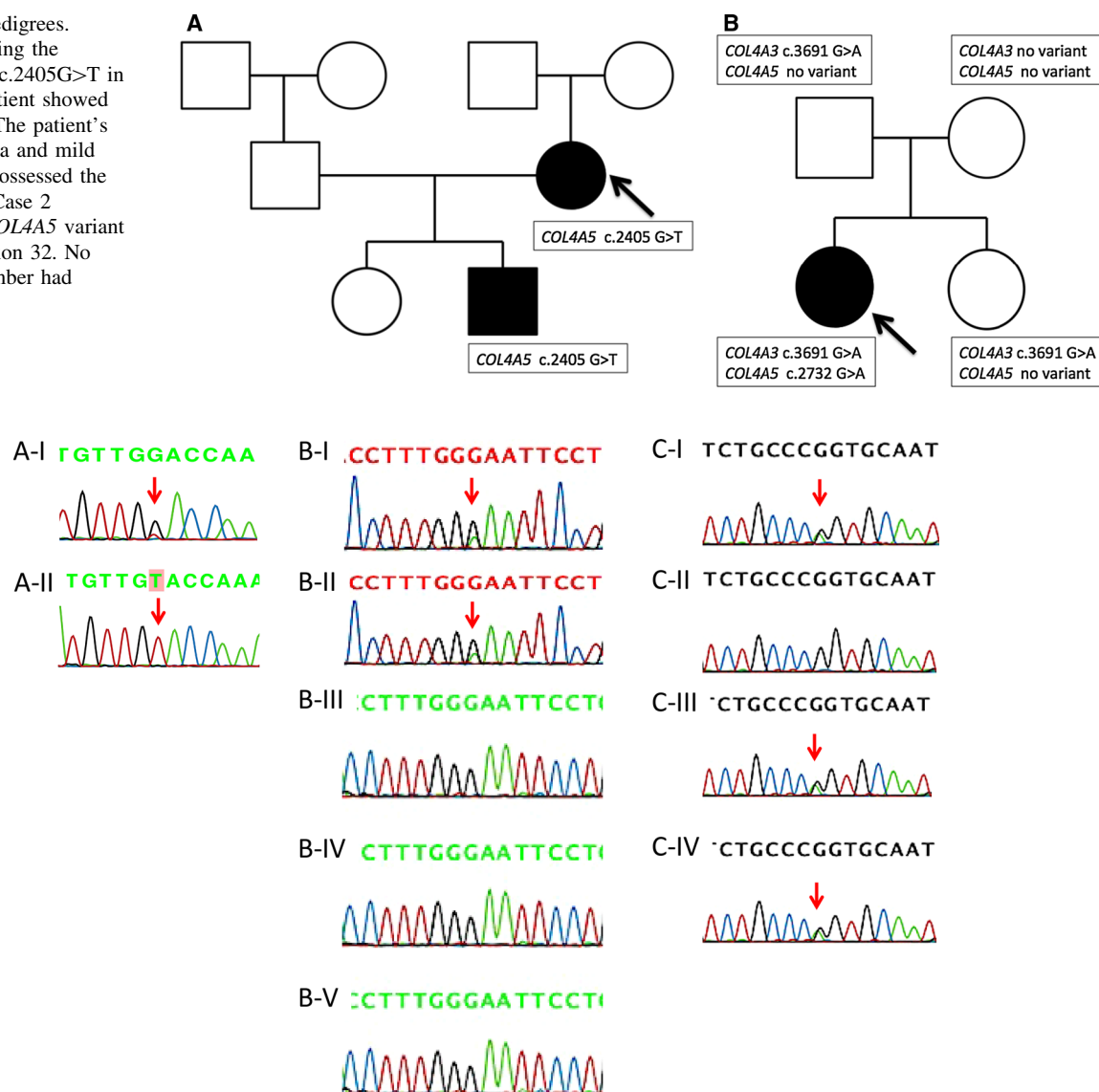


Fig. 2 Direct sequencing of Case 2 with the somatic mosaic variant in *COL4A5* and of family members. **A-I** Case 1 with c.2405G>T (p.Gly802Val) at exon 30 of *COL4A5*. The next-generation sequencing revealed a variant allele frequency of 17.9% in leukocytes. **A-II** son of Case 1. He had the same variant in the hemizygous state. **B-I** Case 2 with c.2732G>A (p.Gly911Glu) at exon 32 of *COL4A5* with genomic DNA extracted from leukocytes. The next-generation sequencing revealed a variant allele frequency of 22.1%. **B-II**

genomic DNA extracted from urinary sediment. The next-generation sequencing revealed a variant allele frequency of 36.6%. The variant was not observed in the mother (**B-III**), father (**B-IV**), or sister (**B-V**). Direct sequencing of *COL4A3* for Case 2 and family members is shown in Fig. 2c. Case 2 (**C-I**), father (**C-III**), and sister (**C-IV**) had the variant c.3691G>A (p.Gly1231Ser) in *COL4A3*, and the mother (**C-II**) did not

X chromosome inactivation pattern in leukocytes and urinary sediment

The activity ratios of the maternal and paternal alleles were 42:58 in leukocytes and 34:66 in urinary sediment (Fig. 3). Case 2 was a sporadic case, and it is not known which allele the variant derived from. The result, however, did not show the skewed X inactivation pattern and, therefore, did not influence severity.

Modifier gene search

For the search of modifier genes, ideally whole exome sequencing should be conducted. However, because only podocyte-related genes have been identified previously as modifiers of this disease, we selected 45 podocyte-related genes, as shown in Table 2 [5, 12, 13]. In targeted sequence analysis for 45 podocyte-related genes, we detected c.3691G>A (p.Gly1231Ser) in *COL4A3*. This is a

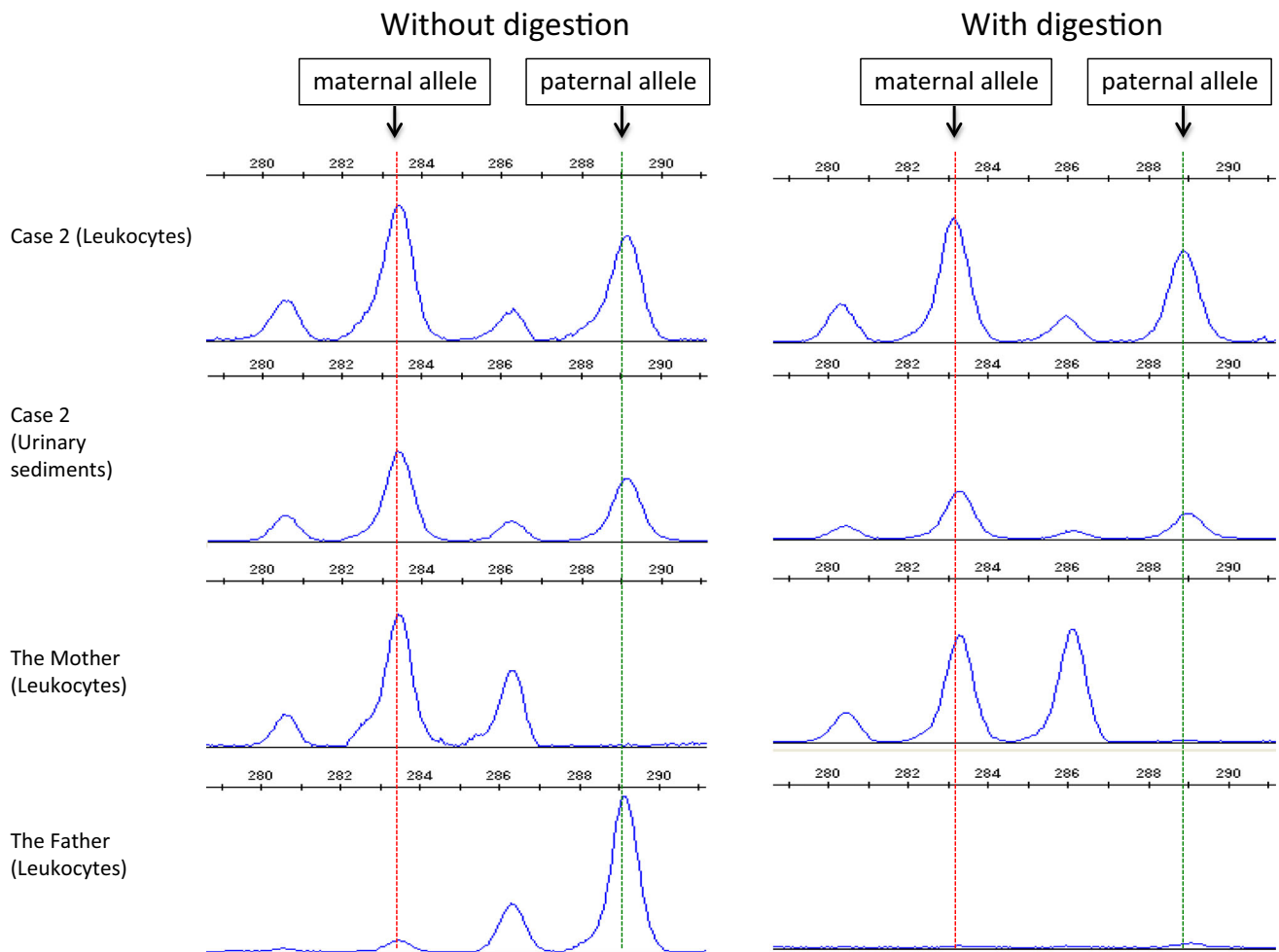


Fig. 3 X chromosome inactivation pattern study results. Results of methylation-specific PCR assay. *Left panels* show PCR assay results without digestion. *Right panels* show results after digestion. The activity ratios of maternal and paternal alleles were 42:58 in leukocytes and 34:66 in urinary sediment. This result did not show

novel variant. The father and sister of Case 2 possessed the same variant, but both did not have urinary abnormalities (Fig. 2c; confirmed using Sanger sequencing of all family members). Predicting software revealed that the amino acid substitution affecting protein function was probably damaging (polymorphism phenotyping v2) and damaging (sorting intolerant from tolerant).

Discussion

The next-generation sequencing analysis has seen a rapid increase in use in many areas of genetic research. Low frequencies of mosaic variants are very difficult to detect using Sanger sequencing. The next-generation sequencing is far more sensitive for these kinds of variants [4, 14].

the skewed X inactivation pattern and did not influence severity. The father's results show no peak after digestion, meaning that digestion was complete, because, generally, the male X chromosome has 100% activity which will result in complete disappearance of the peak after digestion

We previously reported four male XLAS patients with somatic *COL4A5* variants who showed milder phenotypes than normal male XLAS patients [4]. Interestingly, patients with low variant allele frequencies show a milder phenotype. Frequency differs in different organs, and, in severe cases, variant frequency can be high in kidney cells. A recent study by Beicht et al. described a female XLAS patient with a somatic mosaic variant who had variant allele frequencies of 14, 7, 4, and 7% in leukocytes, urinary sediment, hair roots, and oral mucosa, respectively, determined using the next-generation sequencing [14].

Female cases of XLAS can show variety in severity even among members of the same family [15]. Factors that affect severity in females are not clear. Some studies have reported that skewed X chromosome inactivation may determine the clinical phenotype [16, 17]; however, no large-scale studies have been performed. A recent study

Table 2 Gene list for the search of modifier genes

| | Gene name | | Gene name |
|----|-----------|----|-----------|
| 1 | ACTN4 | 24 | KANK4 |
| 2 | ADCK4 | 25 | LAMB2 |
| 3 | ANLN | 26 | LMX1B |
| 4 | ARHGAP24 | 27 | MYH9 |
| 5 | ARHGDI1 | 28 | MYO1E |
| 6 | CD2AP | 29 | NPHS1 |
| 7 | COL4A3 | 30 | NPHS2 |
| 8 | COL4A4 | 31 | NUP107 |
| 9 | COL4A5 | 32 | NUP205 |
| 10 | COQ2 | 33 | NUP93 |
| 11 | COQ6 | 34 | PAX2 |
| 12 | CRB2 | 35 | PDSS2 |
| 13 | CUBN | 36 | PLCE1 |
| 14 | DGKE | 37 | PTPRO |
| 15 | EMP2 | 38 | SCARB2 |
| 16 | FAT1 | 39 | SMARCAL1 |
| 17 | GLEPP1 | 40 | TRPC6 |
| 18 | HNF1B | 41 | TTC21B |
| 19 | INF2 | 42 | UMOD |
| 20 | ITGA3 | 43 | WDR73 |
| 21 | ITGB4 | 44 | WT1 |
| 22 | KANK1 | 45 | XPO5 |
| 23 | KANK2 | | |

reported that Alport syndrome patients with digenic variants in two of either *COL4A3*, *COL4A4*, or *COL4A5* showed a more severe clinical course than patients with single gene variants [13]. Another study reported that digenic variants in both *COL4A5* and *MYO1E* resulted in the most severe symptoms and the development of end-stage renal disease in a girl aged 8 and in a boy aged 3 [12]. These studies suggest the existence of modifier genes that can result in the more severe phenotypes in female patients with XLAS. Currently, no common mechanism for the development of severe XLAS in females has been determined. No genotype–phenotype correlation has been demonstrated [15]. The contributions of skewed X chromosome inactivation or modifier genes have been reported based on a small number of cases [12, 13, 17]. This suggests that the underlying mechanism may be heterogeneous for each individual. Another possibility is the influence of disease- or kidney function-related susceptibility genes that can be determined by genome-wide association [18]. Further investigation, including a genome-wide association study (GWAS), should be conducted for female XLAS cases. As a result, we detected a *COL4A5* variant with somatic mosaic and a *COL4A3* missense variant. Together, they result in a severe phenotype in Case 2.

In this study, we describe two female XLAS patients with mosaic variants in *COL4A5*. Case 1 showed a very mild phenotype of hematuria without proteinuria. Case 2, an 11-year-old girl, showed a severe phenotype of moderate proteinuria, although she had a mosaic variant with a frequency of 22.1% in leukocytes.

For the two *COL4A5* variants, p.Gly802Val and p.Gly911Glu, that were detected in this study, the first is a novel variant, although a different amino acid substitution at the same position (p.Gly802Arg) has been reported, and the second variant has been reported previously [9, 19]. Generally, missense variants result in milder phenotypes than nonsense mutations. In addition, these two cases exhibited variants expressed in a mosaic manner. Therefore, they would be predicted to show mild phenotypes. As expected, Case 1 showed a very mild phenotype of only hematuria; however, Case 2 exhibited a severe phenotype. The difference of the severity in these two cases prompted us to investigate the molecular mechanisms of the development of a severe phenotype in female XLAS cases.

To investigate the molecular mechanisms in Case 2 resulting in the severe phenotype, we examined three factors: (1) differences in variant frequency between leukocytes and urinary sediment; (2) the X chromosome inactivation pattern; and (3) possible modifier gene variants. These studies revealed no contribution by variant frequency or X chromosome inactivation, but we did identify a *COL4A3* pathogenic variant that may have had an effect on the phenotype. Although the variant c.3691G>A in *COL4A3* is novel and the father and the sister, who possessed the same variant, did not show urinary abnormalities, predicting software recognized this variant as pathogenic. It is, therefore, suggested that this variant affected severity in this particular case.

The next-generation sequencing is an important tool for the diagnosis of Alport syndrome [5]. This study suggests the use of the next-generation sequencing for detecting mosaic variants even in female cases, including detection of variant frequency, which helps estimate clinical severity. It should be noted that in females, other factors can influence severity, such as a skewed X chromosome inactivation pattern or the existence of modifier genes [12, 13]. However, in most cases, the mechanism for developing a severe phenotype is still unclear. Therefore, a search for additional disease- or kidney function-related susceptibility genes using GWAS should be conducted.

Conclusion

The next-generation sequencing was used to identify two female cases of XLAS with somatic mosaic variants in *COL4A5*. Phenotype severity in females could be affected by modifier gene variants.

Acknowledgements This study was supported by a Grant from the Ministry of Health, Labor and Welfare of Japan for Research on Rare Intractable Diseases in Kidney and Urinary Tract (H24-nanchitou (nan)-ippan-041 to Kazumoto Iijima) in the “Research on Measures for Intractable Diseases” Project; a Grant-in-Aid for Scientific Research (KAKENHI) from the Ministry of Education, Culture, Sports, Science and Technology of Japan (Subject ID: 25893131 to Kandai Nozu and 26293203 to Kazumoto Iijima).

Compliance with ethical standards

Conflict of interest Kandai Nozu received lecture fees from Novartis Pharma K.K. and Taisho Pharm. Co. Kazumoto Iijima has received grants from Daiichi Sankyo Co., Ltd., Japan Blood Product Organization, Miyarisan Pharmaceutical Co., Ltd., AbbVie LLC, CSL Behring, JCR Pharmaceuticals Co., Ltd., Teijin Pharma Ltd., Novo Nordisk Pharma Ltd., AIR WATER MEDICAL Inc., Astellas Pharma Inc., Takeda Pharmaceutical Company Ltd. and Taisho Toyama Pharmaceutical Co., Ltd. and lecture fees from Meiji Seika Pharma Co., Ltd., Novartis Pharma K.K., Zenyaku Kogyo Co., Ltd., Chugai Pharmaceutical Co., Ltd., Daiichi Sankyo, Co., Ltd., Springer Japan, Asahi Kasei Pharma Corp, Boehringer Ingelheim, Medical Review Co., Ltd., NIKKEI RADIO BROADCASTING CORPORATION, Japan Blood Product Organization and CSL Behring and manuscript fees from Chugai Pharmaceutical Co., Ltd., and consulting fees from Zenyaku Kogyo Co., Ltd., Chugai Pharmaceutical Co., Ltd., Astellas Pharma Inc., Takeda Pharmaceutical Company Ltd., Ono Pharmaceutical Co., Ltd. and Kyowa Hakko Kirin Co. Ltd.

Ethical consideration and informed consent All procedures performed in studies involving human participants were in accordance with the ethical standards of the Institutional Review Board of Kobe University School of Medicine (IRB approval number 301) and with the 1964 Helsinki declaration and its later amendments or comparable ethical standards. Informed consent was obtained from all individual participants included in the study.

References

- Kashtan CE, Ding J, Gregory M, Gross O, Heidt L, Knebelmann B, Rheault M, Licht C. Alport syndrome research C: clinical practice recommendations for the treatment of Alport syndrome: a statement of the Alport syndrome research collaborative. *Pediatr Nephrol.* 2013;28(1):5–11.
- Jais JP, Knebelmann B, Giatras I, De Marchi M, Rizzoni G, Renieri A, Weber M, Gross O, Netzer KO, Flinter F, et al. X-linked Alport syndrome: natural history in 195 families and genotype-phenotype correlations in males. *J Am Soc Nephrol.* 2000;11(4):649–57.
- Krol RP, Nozu K, Nakanishi K, Iijima K, Takeshima Y, Fu XJ, Nozu Y, Kaito H, Kanda K, Matsuo M, et al. Somatic mosaicism for a mutation of the COL4A5 gene is a cause of mild phenotype male Alport syndrome. *Nephrol Dial Transplant.* 2008;23(8):2525–30.
- Fu XJ, Nozu K, Kaito H, Ninchoji T, Morisada N, Nakanishi K, Yoshikawa N, Ohtsubo H, Matsunoshita N, Kamiyoshi N, et al. Somatic mosaicism and variant frequency detected by next-generation sequencing in X-linked Alport syndrome. *Eur J Hum Genet.* 2016;24(3):387–91.
- Kamiyoshi N, Nozu K, Fu XJ, Morisada N, Nozu Y, Ye MJ, Imafuku A, Miura K, Yamamura T, Minamikawa S, et al. Autosomal Dominant Alport Syndrome. *Clin J Am Soc Nephrol.* 2016;11(8):1441–9.
- International Human Genome Sequencing. C: finishing the euchromatic sequence of the human genome. *Nature.* 2004;431(7011):931–45.
- Allen RC, Zoghbi HY, Moseley AB, Rosenblatt HM, Belmont JW. Methylation of HpaII and HhaI sites near the polymorphic CAG repeat in the human androgen-receptor gene correlates with X chromosome inactivation. *Am J Hum Genet.* 1992;51(6):1229–39.
- Kubota T, Nonoyama S, Tonoki H, Masuno M, Imaizumi K, Kojima M, Wakui K, Shimadzu M, Fukushima Y. A new assay for the analysis of X-chromosome inactivation based on methylation-specific PCR. *Hum Genet.* 1999;104(1):49–55.
- Knebelmann B, Breillat C, Forestier L, Arrondel C, Jacassier D, Giatras I, Drouot L, Deschenes G, Grunfeld JP, Broyer M, et al. Spectrum of mutations in the COL4A5 collagen gene in X-linked Alport syndrome. *Am J Hum Genet.* 1996;59(6):1221–32.
- Kaito H, Nozu K, Fu XJ, Kamioka I, Fujita T, Kanda K, Krol RP, Suminaga R, Ishida A, Iijima K, et al. Detection of a transcript abnormality in mRNA of the SLC12A3 gene extracted from urinary sediment cells of a patient with Gitelman’s syndrome. *Pediatr Res.* 2007;61(4):502–5.
- Nozu K, Iijima K, Kawai K, Nozu Y, Nishida A, Takeshima Y, Fu XJ, Hashimura Y, Kaito H, Nakanishi K, et al. In vivo and in vitro splicing assay of SLC12A1 in an antenatal salt-losing tubulopathy patient with an intronic mutation. *Hum Genet.* 2009;126(4):533–8.
- Lennon R, Stuart HM, Bierzynska A, Randles MJ, Kerr B, Hillman KA, Batra G, Campbell J, Storey H, Flinter FA, et al. Coinheritance of COL4A5 and MYO1E mutations accentuate the severity of kidney disease. *Pediatr Nephrol.* 2015;30(9):1459–65.
- Mencarelli MA, Heidt L, Storey H, van Geel M, Knebelmann B, Fallerini C, Miglietti N, Antonucci MF, Cetta F, Sayer JA, et al. Evidence of digenic inheritance in Alport syndrome. *J Med Genet.* 2015;52(3):163–74.
- Beicht S, Strobl-Wildemann G, Rath S, Wachter O, Alberer M, Kaminsky E, Weber LT, Hinrichsen T, Klein HG, Hoefele J. Next generation sequencing as a useful tool in the diagnostics of mosaicism in Alport syndrome. *Gene.* 2013;526(2):474–7.
- Jais JP, Knebelmann B, Giatras I, De Marchi M, Rizzoni G, Renieri A, Weber M, Gross O, Netzer KO, Flinter F, et al. X-linked Alport syndrome: natural history and genotype-phenotype correlations in girls and women belonging to 195 families: a “European Community Alport Syndrome Concerted Action” study. *J Am Soc Nephrol.* 2003;14(10):2603–10.
- Iijima K, Nozu K, Kamei K, Nakayama M, Ito S, Matsuoka K, Ogata T, Kaito H, Nakanishi K, Matsuo M. Severe Alport syndrome in a young woman caused by a t(X;1)(q22.3;p36.32) balanced translocation. *Pediatr Nephrol.* 2010;25(10):2165–70.
- Guo C, Van Damme B, Vanrenterghem Y, Devriendt K, Cassiman JJ, Marynen P. Severe alport phenotype in a woman with two missense mutations in the same COL4A5 gene and preponderant inactivation of the X chromosome carrying the normal allele. *J Clin Invest.* 1995;95(4):1832–7.
- Okada Y, Sim X, Go MJ, Wu JY, Gu D, Takeuchi F, Takahashi A, Maeda S, Tsunoda T, Chen P, et al. Meta-analysis identifies multiple loci associated with kidney function-related traits in east Asian populations. *Nat Genet.* 2012;44(8):904–9.
- Cheong HI, Park HW, Ha IS, Choi Y. Mutational analysis of COL4A5 gene in Korean Alport syndrome. *Pediatr Nephrol.* 2000;14(2):117–21.